INCREASING POWER OUTPUT OF A SHOE-BASED PIEZOELECTRIC ENERGY HARVESTER WITHIN A USER BURDEN-FIRST DESIGN PERSPECTIVE

by

Issak Allaire-MacDonald

A thesis submitted to the faculty of
The University of Utah
in partial fulfillment of the requirements for the degree of

Master of Science

Department of Mechanical Engineering

The University of Utah

May 2022

The University of Utah Graduate School

STATEMENT OF THESIS APPROVAL

The thesis of **type your name here**

has been approved by the following supervisory committee members:

type the name of your chair here	, Chair	**date approved** Date Approved
type the name of a committee member here	, Member	**date approved** Date Approved
type the name of a committee member here	, Member	**date approved** Date Approved

and by **type the name of the chair of your department here** , Chair/Dean of

the Department/College/School of **type the name of your department here**

and by David B. Kieda, Dean of The Graduate School.

ABSTRACT

This work proposes a design perspective and benchmarks for shoe-based energy harvester (SBEH) development in which power output is maximized without increasing user burden relative to a normal shoe. Two piezoelectric SBEH are then developed, the first to illustrate the feasibility of frequency up-conversion as a mechanism to achieve power output, and the second as a full-fledged practical implementation maximizing power output with a user burden-first design perspective.

The latter SBEH design is based on a ball screw and cam (BSC) mechanism to increase the frequency of force input to the piezoelectric transduction mechanism from the footfall's 1 Hz up to 8-60 Hz. A maximum output power of 9.9 mW was measured at a 1 Hz input displacement (representing normal walking speed), which resulted in up-conversion to 18 Hz. This device exhibits energy input requirements and an equivalent spring constant similar to that of normal shoes. Using configurations with higher levels of frequency up-conversion has the potential to substantially increase power output and potentially decrease user burden.

TABLE OF CONTENTS

ABSTRACT 4

LIST OF TABLES vii

LIST OF FIGURES viii

ACKNOWLEDGMENTS xi

INTRODUCTION 12

THEORY AND REVIEW OF SHOE-BASED ENERGY HARVESTING 15

2.1 Why harvest energy from walking? 16
2.1.1 Approaches to harvesting energy from human sources 16
2.1.2 Target motions for human-based energy harvesting 17
2.1.3 Parameters of walking relevant to energy harvesting 19
2.2 Shoe-based energy harvesting 22
2.2.1 Integrating harvesters into shoes 22
2.2.2 Shoe mechanical & energetic behavior 24
2.3 Evaluating user burden 29
2.4 Kinetic energy harvesting mechanisms & review of shoe-based energy harvesters 32
2.4.1 Piezoelectric energy harvesting 33
2.4.2 Electromagnetic energy harvesting 49
2.4.3 Electrostatic energy harvesting 54
2.4.4 Comparison of energy harvesting mechanisms 56
2.4.5 Shortcomings in the literature 57
2.5 Contribution of this work 58

DESIGN AND MODELING 59

3.1 Design goals 59
3.2 Design constraints 60
3.3 Detailed design 61
3.3.1 Frequency up-conversion 61
3.3.2 31-mode benders 65
3.3.3 Pre-stressed piezoelectric elements 67
3.3.4 Spring return system 68

3.3.5 Ribbed plunger harvester design 69
3.3.6 Ball screw and cam harvester design 73
3.4 Theoretical behavior 77
3.4.1 Power output 77
3.4.2 Stiffness and force-displacement profile 82

EVALUATION AND EXPERIMENTAL RESULTS 89

4.1 Shoe behavior 89
4.2 Piezoelectric element testing 94
4.3 SBEH prototype testing 98
4.3.1 Ribbed plunger SBEH testing 98
4.3.2 Ball screw and cam SBEH testing 102

DISCUSSION AND CONCLUSION 116

REFERENCES 121

LIST OF TABLES

Tables

2.1 Summary of theoretical total work done by the muscles at major joints or segments in the body during walking. 17

2.2 Comparison of PVDF and PZT-5H material properties. 35

2.3 Comparison of PZT-based shoe-based energy harvester characteristics. 47

3.1 Beam deflection force, average stress, average strain, and maximum strain in a single composite beam PZT layer at various beam deflections. 82

3.2 Theoretical voltage and power output of the developed SBEH. 83

3.3 Maximum torque required to drive BSC design cams of various lobe counts. 87

4.1 Mechanical and energetic parameters of tested shoes and expected values. 93

4.2 Average voltage output and deflection forces at given bender displacements. 97

4.3 Voltage expected from calculations versus measured during bender and ball screw and cam SBEH testing. 110

4.4 Measured versus expected voltage, optimal load resistance, and power output in ball screw and cam SBEH testing. 112

LIST OF FIGURES

Figures

2.1. Exploded view of modern shoe construction. 23

2.2. Force-displacement curve of a cyclically loaded shoe midsole 26

2.3. Force-displacement plots from heel-region testing in shoes 28

2.4 Illustration of the piezoelectric effect at rest (a) and under strain (b). 34

2.5 33-mode and 31-mode piezoelectric transducer configurations. 38

2.7 Dimporh clamshell PZT SBEH developed by Shenck & Paradiso. 42

2.8 Pre-stressed PZT diaphragm SBEH developed by Leinonen et al. 43

2.9 Gear train-based electromagnetic SBEH developed by Xie & Cai. 51

2.10 Magnetic gear-based electromagnetic SBEH developed by Liu et al. 52

3.1 High-level operating principle of the SBEH developed in this work. 63

3.2 Operating principle of the ball screw and cam frequency up-conversion mechanism. 63

3.3 Operating principle of the ribbed plunger frequency up-conversion mechanism 64

3.4 Exploded view of Python series piezoelectric benders sold by Bimitech Inc. 65

3.5 Pre-curved piezoelectric bender elements. 67

3.6. Annotated side (a) and top (b) section views of ribbed plunger harvester design. 70

3.7 Isometric view of ribbed plunger harvester design (a) with one side frame hidden and the top plate transparent (b). 71

3.8. Ribbed plunger geometry..... 72

3.9. Annotated side (a) and top (b) section views of ball screw and cam harvester design. 74

3.10. Isometric view of ball nut and cam harvester design..... 75

3.11. A displacement of 1.4 mm developed in a 40 mm beam results in 0.79 mm displacement in its central 30 mm. 81

4.1. Shoe test setup using the Instron 5969 Universal Testing Machine. 90

4.2. Force-displacement curve of Sketchers GoRun Elevate shoes. 91

4.3. Voltage waveform output of benders deflected 0.4 mm in tension. 95

4.4. Pre-stressed bender test fixture. 96

4.5. Test setup for ribbed plunger SBEH prototype..... 99

4.6. Voltage output waveform from ribbed plunger SBEH testing. 99

4.7. Ribbed plunger SBEH power output versus load resistance. 100

4.8. Force-displacement curve of ribbed plunger SBEH design..... 101

4.9. Assembled ball screw and cam SBEH prototype. 103

4.10. Test setup for ball screw and cam SBEH prototype. 104

4.11.Voltage waveform output of BSC SBEH tested with a single-lobe cam and no pre-stress springs at an input displacement of 4 mm..... 104

4.12. Voltage waveform output of BSC SBEH tested with a three-lobe cam and pre-stress springs at an input displacement of 4 mm. 105

4.13. Force-displacement plot of the ball screw and cam SBEH tested with no pre-stress springs and a single-lobe cam at an input displacement of 4 mm. 105

4.14. Force-displacement plot of the ball screw and cam SBEH tested with pre-stress springs and a three-lobe cam at an input displacement of 4 mm. 106

4.15. Profile of the single-lobe (a) and three-lobe (b) cams used in the ball screw and cam SBEH. 108

4.16. Illustrating unwanted twisting in the system which prevents cam from smoothly deflecting piezoelectric benders according to its profile. 109

ACKNOWLEDGMENTS

The author would like to thank all of those who played a part in and provided support to this project. First and foremost is Dr. Shad Roundy, for his trust in my competence, consistent counsel, technical help, and guidance of all forms, including (and especially) the most basic questions. Thanks go to Dr. Kam Leang and Dr. Steven Mascaro for serving on my committee and offering their insight.

In the manufacturing and testing of the devices developed, the assistance and advice of Tom Slowik the mechanical engineering machine shop and Jared Smith and Thomas Carter of the Center for Medical Innovation's fab lab were indispensable. Kim Watts of the Materials Characterization Lab is thanked for her help in configuring the Instron during all phases of testing.

Christopher Schmittle laid the groundwork for this project and developed the initial design of the ribbed plunger SBEH.

The NSF ASSIST center funded the work on this project and therefore enabled me to pursue this degree; for this support I am immensely grateful.

Lastly, to Dan, Julie, Sophie, and Jacks who support and encouragement me at every turn, and to Roni, who inspires me endlessly.

CHAPTER 1

INTRODUCTION

Distributed sensor networks, the Internet of Things, wearable devices, and all manner of mobile electronics are currently beholden to the limits of battery technology or power distribution hardware networks. In cardiac pacemakers, for example, batteries can occupy half of the device's entire volume [1]. Rather than storing energy generated elsewhere, generating energy from the environment in which a device is deployed can eliminate rechanging, downsize hardware, decrease maintenance, and enable use far from power grids. This is the motivation behind parasitic power harvesting in which energy is scavenged from environmental sources such as vibrations induced by industrial machinery, cars driving on roadways, or the motion of the human body. The aims and applications of a device dictate which environmental sources are good candidates to power it, and the applications for human motion-based devices are significant and far-reaching.

Harvesting energy from walking is the most promising avenue for parasitic power harvesting form human motion: it is high-powered, performed frequently, potentially unintrusive, and lends itself to a surprising array of applications. Devices which harvest power at the foot, for example, can and have been used power blood oxygen level and heartrate sensors [2], improved calorie expenditure measurements [2], RF transmitters [3], geolocation devices [4], and artificial organs [5], among others. The application of interest

in this work is to power a smart insole for real-time gait analysis. By collecting measurements such as plantar center of pressure, step frequency, acceleration, velocity, and rotation, this device could find use in athletics, everyday treatment of conditions such as Parkinson's disease, and clinical studies. In application to gait-affecting conditions, a smart sensing insole could improve diagnoses, aid in preventing falls, and improve interventional treatments by identifying relevant biomarkers and providing a real-time assessment of fall risk. This could increase the mobility, independence, and quality of life of users.

This work presents the development of two novel shoe-based energy harvesters (SBEH) for use in these applications. Many such devices have been developed in the literature, as discussed in Chapter 2, but none so far have placed a rigorous emphasis on decreasing the user burden associated with such a device. To be useful in the context of powering a smart insole and easily translated to other applications, this SBEH targets a power output of >10 mW while remaining *unobtrusive to the user*. This means that the SBEH attempts to minimize effects on user metabolic load, subjective comfort, and gait pattern—the three axes of user burden.

The SBEH developed herein use commercially available piezoelectric elements as their electromechanical transduction mechanism. In the future, these elements can easily be replaced with novel flexoelectric materials developed by collaborators. Flexoelectric materials could enable higher power outputs, higher power densities, and lower costs. By designing with their future use in mind, the SBEH developed in this work can be used to demonstrate the effectiveness of these novel materials and explore their applicability to human-based energy harvesting.

Chapter 2 presents a review of the literature and theory of shoe-based energy harvesting and is structured to act as a general design guide for the development of future SBEH. A clear motivation for harvesting energy from walking is developed by reviewing the various approaches, target motions, and critical parameters relevant to human-based energy harvesting. The theory of harvesting energy using shoe-based devices is then reviewed, considering both device integration and the mechanical and energetic behavior of shoes as design constraints. The concepts and methods necessary to evaluate user burden are then discussed before presenting an exhaustive review of previously-developed SBEH broken into piezoelectric, electromagnetic, and electrostatic transduction mechanisms.

Chapter 3 details the design and analysis of two novel piezoelectric SBEH and illustrates how the successes of previous SBEH, user burden considerations, and application-specific goals coalesced in their development. Design goals, constraints, detailed design, and theoretical behavior of the devices are presented.

In Chapter 4, experimental results obtained from the testing of shoes, piezoelectric elements, and the final SBEH devices are presented and compared to the analysis in Chapters 2 and 3.

Chapter 5 discusses how the results obtained in Chapter 4 affected the design of the harvester devices and the successes and failures of the SBEH developed herein. Future work for these SBEH is briefly discussed and conclusions for future SBEH design are drawn.

CHAPTER 2

THEORY AND REVIEW OF SHOE-BASED ENERGY HARVESTING

Harvesting energy from human motion is an exciting frontier in the transition to a more mobile, sustainable, and connected world. Unobtrusive devices which can harvest power from the body present the opportunity to recharge or eliminate batteries, power biomedical and sensing devices, communicate with the internet of things, and ultimately improve human quality of life. This chapter presents a comprehensive overview and discussion of the theory and literature concerning harvesting energy from human motions, specifically the heel strike during walking.

Section 2.1 motivates why walking is an attractive target for energy harvesting and reviews the physical parameters of walking which must be considered in energy harvester design. Section 2.2 presents principles, advantages, and drawbacks of harvesting energy from shoes. The mechanical and energetic behavior of shoes is discussed in order to match energy harvester behavior to that of normal shoes. Section 2.3 explores how user burden associated with human-powered wearable energy harvesters has been evaluated in the literature, then proposes new means to do so and principles of minimizing user burden in shoe-based energy harvesters. In Section 2.4, mechanisms employed in kinetic energy harvesting and their relative advantages and disadvantages are discussed, focusing especially on the principles of piezoelectric energy harvesting. An exhaustive review of

shoe-based energy harvesters (SBEH) is presented, focusing on those producing over 100 μW of power. Lastly, Section 2.6 characterizes the contribution of this work to the literature. This thesis is intended to both present a novel SBEH and to act as a design guide for those developing SBEH, with emphasis placed on strain-based (piezoelectric and flexoelectric) transduction mechanisms.

2.1 Why harvest energy from walking?

Human locomotion is perhaps the single most attractive target for human-powered systems. In the literature, harvesting energy from body heat, blood pressure, activity-induced inertial forces, relative motion of various joints, and footfall forces have been investigated [6] – [13]. Footfalls and the relative motion of joints during walking are the only methods that have proven capable of providing power greater than 100s of microwatts to energy harvesting devices, and the potential maximum power available is greater than other means by at least one order of magnitude [10], [11], [14].

2.1.1 Approaches to harvesting energy from human sources

Xu & Tam [14] categorized human-based energy harvesters as either direct wearable energy harvesters (DWEH) which attach directly to the human body, indirect wearable energy harvesters (IWEH) which are integrated with or mounted on wearable items like shoes and backpacks, or indirect unwearable energy harvesters (IUEH) which are implemented in the environment, such as energy-harvesting floor tiles. These categories are a useful paradigm in which to view the potential for harvesting energy from human motion. This review focuses on wearable energy harvesters since they are capable of

providing power as mobile as its user. Xu & Tam share the author's view that IWEH are the most promising harvester implementations, as they have the potential to be more convenient, more frequently used, and less burdensome than DWEH.

2.1.2 Target motions for human-based energy harvesting

A central goal of harvesting power from human sources is that the process is unobtrusive [6]; any additional burden placed on the user decreases the utility of the device. In this light, Reimer & Shapiro [10] define the two types of motion relevant to energy harvesting: motion in which energy is lost directly to the surroundings, and motion in which the muscles perform negative work. These motions present the only theoretical opportunities to harvest energy from the human body without increasing user metabolic load. The amount of power potentially available from these motions at the joints and footfall is summarized in Table 2.1. Similar results are found in [12].

Table 2.1. Summary of theoretical total work done by the muscles at major joints or segments in the body during walking [10].

Joint	*Work (J)*	*Power (W)*	*Max torque (Nm)*	*Negative work (%)*	*Negative work (J)*
Heel strike	1-5	2-20		50	1-10
Ankle	33.4	66.8	120	28.3	19
Knee	18.2	36.4	40	92	33.5
Hip	19.0	38	40-80	19	7.2
Center of mass	10	20			
Elbow	1.07	2.1	1-2	37	0.8
Shoulder	1.1	2.2	1-2	61	1.3

These two categories of motion present unique sets of advantages and disadvantages. Harvesting energy from negative work of the musculature operates on a principle similar to regenerative braking in hybrid cars [10], [15]. Inertial energy in a limb in counteracted by muscles performing work to decelerate that limb, so by harvesting that inertial energy through a mechanical device only when the muscles would be performing negative work, it should be possible to harvest energy while *decreasing* the metabolic expenditure of the user. The negative muscular work normally used to decelerate the limb is replaced in part by work provided by the harvesting device's electromechanical transduction mechanism. Harvesting energy from this type of motion opens the door to high-power harvesting targets, such as motion at the knee and ankle joints [10], [16] (see Table 2.1). The amount of negative work in motions can be very high, such as 40% at the ankle and elbow and 90% at the knee [10], [12]. By decreasing the amount of negative work the body performs, a backpack-integrated harvester developed by Rome et al. in [17] was even able to generate more than 1W of electrical power for every 1W increase in metabolic power the device required.

In some cases, however, negative work is performed by connective tissue which elastically stores and then returns energy to the gait cycle [18]. Harvesting energy from negative work would then decrease this returned energy, defeating the goal of extracting no more energy from the user than is normally expended. Harvesting energy from only the portion of a motion in which negative work is performed also runs the risk of affecting how a user executes that motion, as the body continually adapts movement patterns to minimize energy expenditure, as in the case of walking [19]. This could have destabilizing or injury-inducing consequences [6], [17]. The aforementioned backpack harvester, for example,

decreased the user's vertical displacement per step by 18% [17]. In summary, harvesting energy from motions in which the muscles perform negative work offers the potential to harvest large amounts of energy and decrease user metabolic load, but could have cascading effects that change energy expenditure and movement patterns in unforeseen and potentially negative ways.

Human motion in which energy is naturally dissipated to the surroundings presents a more straightforward, unobtrusive avenue for energy harvesting. The high-power representative of this class is the footfall, particularly its heel-strike portion [6], [9], [10], [20], [21]. Energy is directly lost to the environment in the form of heat when the foot pad or shoe midsole is hysteretically compressed and released [20]. So long as the mechanical feedback the user's foot receives from the motion is identical with and without the harvesting device, it should be possible to harvest this energy without affecting the user's motions or metabolic load [10]. Simply put, there are fewer potential ramifications of harvesting energy from this type of motion.

The heel-strike also has the advantage of being a single degree-of-freedom (DOF) motion. Relative motion in the ankle, knee, and elbow also has this advantage over shoulder, hip and center of mass harvesting targets. Single-DOF motions as harvesting targets can significantly simplify an energy harvester's mechanical architecture.

2.1.3 Parameters of walking relevant to energy harvesting

Though this work focuses on shoe-based IWEH, it is useful to establish the overarching parameters relevant to human locomotion before delving into the behavior of shoes when walking. This helps better define the high-level design space.

Walking (35-40%) and running (45-80%) exhibit the highest chemical-to-mechanical conversion efficiency among high-power-output human movement patterns, besting cycling (26%), rowing (20%) and arm cranking (23.4%) [22]. The human body is estimated to be 15-30% efficient overall [15], [23], so harvesting energy from walking affords greater net efficiency in converting chemical energy stored in the body to electrical energy.

A 68 kg (150 lb) man walking at 5.6 km/h (3.5 mph), or 2 steps per second at the average stride length of 152 cm (60 in) [24], uses 280 kcal/h or 324 W of power [25]. 60-65% of this power is dissipated to the atmosphere, mostly as difficult-to-harvest heat [10]. The remaining power used in ambulation is in the amount of 113-130 W. Starner and Paradiso [6] first calculated the often-cited figure of 67 W as the theoretical upper limit of power harvested from the footfall. This is the work—calculated as a force through a displacement—that a 68 kg (150 lb) person could generate walking at 2 steps per second. This assumes a vertical travel in the heel of 5 cm per step, resulting in 67 W of available power

$$68\ kg \cdot 9.8\ \frac{m}{s^2} \cdot 0.05\ m \cdot 2\ Hz = 67\ W \tag{2.1}$$

However, as Starner & Paradiso discuss, harvesting any significant portion of this power would force a person to expend more energy, making them feel as though they were walking in sand or ascending an 5° grade [6]. Additionally, 67 W represents 20% of all energy used while walking or 50% of that needed for ambulation, implying that harvesting energy in this amount would increase a person's energy expenditure during walking by a

similar degree.

This potential energy approach to calculating power available from walking was disputed by Niu et al [12]. The footfall is not truly a free fall, as the potential energy method assumes, and *the actual energy available for power generation comes from the compression of the shoe sole against the ground*, not the vertical displacement of the foot during walking. Thus, the practical limit for power harvested from footfalls in IWEH is far below the figure proposed by Starner and Paradiso and should be viewed as shoe-dependent property. This will be discussed in the following sections where a new benchmark value is proposed.

2 Hz (1 footfall per second per leg) is a safe target step frequency for which energy harvesters should be designed. During normal walking, step frequency was measured as 0.925 Hz in [26], 1.01 Hz in [27], and ranging from 0.8 Hz to 1.2 Hz at walking speeds of 4 to 10 km/h (2.5 to 6.2 mph) [28], [29]. Parameters of the heel-strike are also important to keep in mind, as most energy dissipated and compression experienced during the footfall occurs in this phase [10], [20]. The heel-strike comprises the first 20% of the gait cycle, or 200 ms at a step frequency of 1 Hz.

Reimer & Shapiro [10] list succinctly the five factors which must be considered when harvesting energy from walking: the target motion's positive and negative muscular work phases, how the device is attached to the body, its convenience of use, the metabolic demands on the user, and the device's effects on the body. Each of these factors are explored in this literature review.

2.2 Shoe-based energy harvesting

Shoes provide a convenient platform into which energy harvesters can be integrated. They enable indirect wearability, provide access to the high-energy footfalls, and enable millimeter-scale displacements during which energy is dissipated to the environment. Thus, shoe-based energy harvesters (SBEH) have potential for relatively high power output, high levels of convenience, and low levels of user burden.

2.2.1 Integrating harvesters into shoes

Typical modern shoe construction is illustrated in Figure 2.1. The foot-cradling upper is attached to the midsole, while the outsole makes contact with the ground. A removable insole is typically inserted between the foot and the midsole. Together, all the material between a wearer's foot and the ground is referred to as a shoe's stack, and stack height is a key parameter of shoe design. The insole is a thin layer of foam, cork, gel, or leather meant to improve comfort and fit between the bottom side of the foot and the shoe. The midsole makes up the bulk of a shoe's stack height and is typically a foam polymer: polyvinyl acetate (PVA), polyurethane (PU), or ethylene vinyl acetate (EVA), isoprene, neoprene, or combinations thereof [30]. EVA is the most common midsole material in running shoes. The shoe's outsole is comprised of a harder, more durable rubber, PU, or PVC compound.

In the literature, SBEH have been developed to target one or more of four motions: compression in the heel region, compression across the entirety of the foot's surface area, bending in the sole during the transition from heel-strike to toe-off phases, or vibrations induced throughout the gait cycle.

Figure 2.1. Exploded view of modern shoe construction [31].

Most SBEH have been integrated into a shoe's midsole, replacing material under the heel or throughout. Because the midsole material has a lower Young's modulus than the more abrasion-resistant outsole, the midsole comprises a majority of the sole's compression. Isolated from the foot by the insole and from the ground by the outsole, it is the thickest part of a shoe's stack and therefore lends itself well to integrating energy harvesters.

The physical constraints on SBEH are the most significant restrictions on the design space. Stack heights in modern running, walking, and orthopedic shoes range from 20 mm to 40 mm in the heel region [32] - [35]. The outsole is about 5 mm thick and the insole 1-3 mm thick, with the midsole making up the remainder. This puts an upper limit of 35 mm on the height of a midsole-integrated harvester located beneath the heel [30]. Stack height in the forefoot region is usually considerably lower. The amount of compression in the shoe stack during walking is reported at values from 2 mm to 10 mm [6], [10], [15], [30], [36]. A maximum displacement of no more than 8 mm seems most amenable to user comfort based on comments in the literature and testing summarized in later sections. This

limit applies to soft, large stack height models such as maximalist running shoes; a limit of 5 mm should apply to casual or standard stack height athletic shoes. U.S. Army footwear specifications require limiting shoe stack displacement to 3 mm, a constraint to be mindful of since many SBEH are developed with defense applications in mind. The heel-insole contact area has been represented in the literature as a circle of 40, 45, or 50mm diameter centered at 12% of the foot's overall length relative to the back of the heel [37]–[39], so a strike pad of at least this size should be part of a user-friendly harvester's design.

The mass of any harvester integrated into a shoe is a critical consideration, since it is likely the largest factor in increasing a user's metabolic load versus a standard shoe [39]. The importance of minimizing the harvester's weight is magnified by its location relative to the body: the energetic cost of carrying an added mass on the leg increases the lower the mass is mounted [40], [41]. Mounting a harvester inside of a shoe's sole places the mass as low on the leg as possible, so harvester designs approaching a mass equivalent to the volume of shoe midsole removed are ideal (if difficult to achieve).

2.2.2 Shoe mechanical & energetic behavior

A shoe-based kinetic energy harvester aims to convert the mechanical work of the footfall's force acting through a displacement (in the form of shoe stack compression) into electrical energy,

$$W = \int_0^s F \cdot ds \tag{2.2}$$

where W is the work performed by the foot on the shoe sole, s is linear displacement or compression of the shoes sole, and F is force imparted by the foot. The same force does more work on a compliant shoe sole material with higher displacement than a stiffer material with lesser displacements [20]; therefore, it is important that the harvester takes advantage of the greatest displacement possible when integrated into a shoe.

As discussed in Section 2.2.1, the amount of compression in the heel region of the shoe sole is reported to vary from 2 mm to 10 mm. 8 mm seems to be a safe consensus upper limit; shoes with compression beyond this amount being outliers or special-purpose footwear. Most heel-strike harvesters developed in the literature have displacements between 2 mm and 8 mm (see Section 2.4).

Some publications in the SBEH space have used the ground reaction force (GRF)—the force a shoe's outsole exerts on the ground—to calculate the maximum power available from the heel-strike. The GRF was measured to be greatest during the heel-strike and toe-off phases of the gait cycle at a magnitude of 120% [10], [12] or 130% [6] times the user's body weight, about 1000 N for an average 90 kg (199 lb) US man or 760 N for an average 77 kg (170 lb) US woman [42]. Peak GRF does not seem to be affected significantly by shoe materials [20].

However, direct measurement of the forces in a shoe's heel region tell a different story: [38] recorded maximum forces of 576.8 N at 4.8 km/h (3 mph) and 608.2 N at 6.4 km/h (4 mph), bracketing the 5.6 km/h (3.5 mph) which corresponds to a step frequency of 1 Hz. Stepping as hard as possible on the floor, a peak force of 902.5 N was recorded. These measurements were taken using a 50 mm diameter plate located beneath the heel, an area appropriate to record the full force of the heel-strike. The findings in [43] mirror these

results, with a maximum force amplitude exerted on a heel insert by an 84 kg male subject walking at 5.6 km/h (3.5 mph) found to be 600 N. Therefore, a peak force of about 600 N can be expected in the heel region of a shoe for a user of a typical male's weight walking at a natural pace.

Shoe midsole materials exhibit hysteresis when cyclically loaded, as during walking. Figure 2.2 shows a typical shoe force-displacement curve. The upper line corresponds to loading and the lower to unloading; the area between the two curves is the energy dissipated due to damping effects in the shoe's sole during a single loading-unloading cycle. This energy is dissipated to the environment as heat in a normal shoe [20].

To avoid increasing the energetic cost of wearing a harvester-integrated shoe versus a standard shoe, *the harvester-integrated shoe should dissipate no more energy than the standard shoe in a single loading cycle*. In terms of energetic feedback to the user, electrical energy harvested is equivalent to mechanical energy dissipation in that it is not returned as

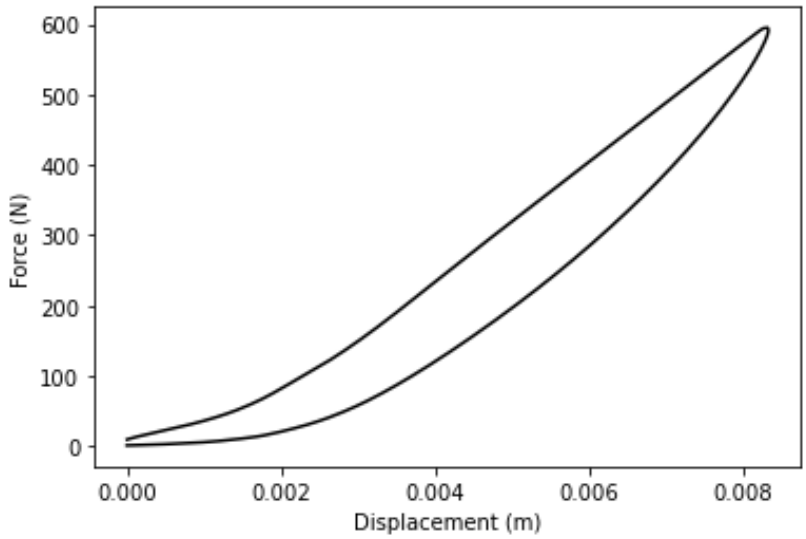

Figure 2.2. Force-displacement curve of a cyclically loaded shoe midsole (Instron 5969 Universal Testing System, Sketchers GoRun Elevate shoe).

mechanical work. This fact establishes the upper bound on the amount of power that can be harvested using a SBEH. Designs that draw more power from the user have been realized in the literature [5], [44], but may impair stability and mobility, increase injury risk, decrease use comfort, and will certainly increase metabolic load [6], [10]. Direct measurements of heel-region shoe force-displacement curves have been published in [30] [36], [45] and are shown in Figure 2.3. Similar results have been obtained by the author and are discussed in Chapters 3, 4 and 5.

The percent of energy returned or dissipated in a shoe during a compression cycle is dependent mainly upon the sole materials. With the force input to the heel, step frequency, and energy return percent of a shoe known, it is possible to calculate the amount of energy dissipated in the shoe's sole per step. The energy return percent (ERP) of shoes has been reported from 50% to 80%: [36] finds that walking shoes return 82.3% of input energy, running shoes 72.3%, and orthopedic shoes 62.9%; [30] finds 71.9-80.6% ERP in running shoes; 50- 69% in [20]; 40-60% in [6]; and 50-80% in [10]. Based on these values and the author's own testing, 70% ERP is a good target for an average casual- or athletic-style shoe and therefore the minimum target value for heel-strike energy harvester design.

With the information reviewed so far, it is possible to calculate a new theoretical limit on the amount of energy that can be harvested using a heel-strike energy harvester without increasing user burden. [6] calculated the 67 W in Equation 2.2, discussed in Section 2.1.2, but acknowledged that this amount of power extraction would burden the user, as it implies an ERP of 0%. [10] and [12] calculated that an 80 kg (176 lb) person exerting 120% of their bodyweight on the ground at heel-strike could generate a maximum

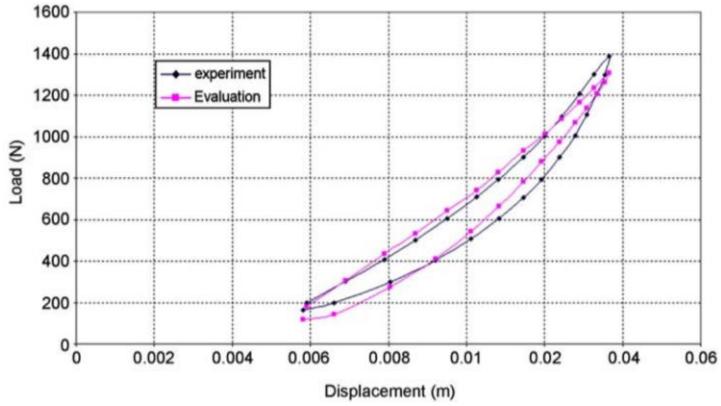

(a)

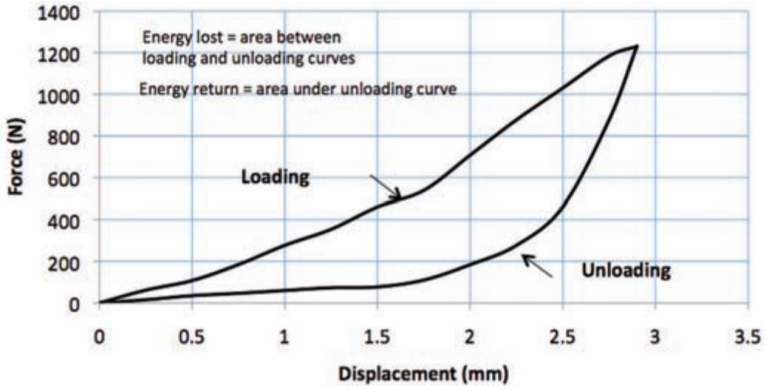

(b)

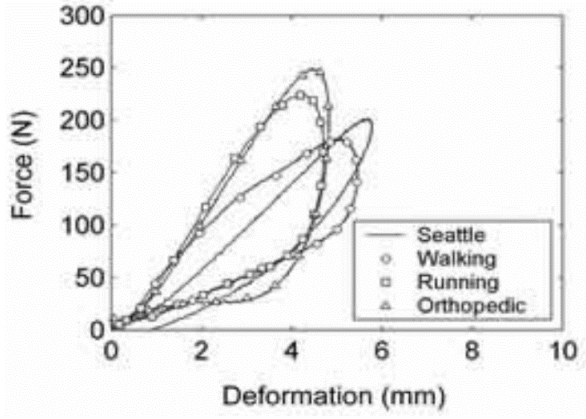

(c)

Figure 2.3. Force-displacement plots from heel-region testing in shoes. (a) compares the nonlinear viscoelastic sole model developed by Ly et al. to measured shoe sole displacement [45]. (b) is a representative force-displacement plot for sunning shoes tested in [30]. (c) compares the force-displacement plot of a prosthetic foot (‘Seattle’) to that same prosthetic foot wearing three different kinds of shoes [36].

of 4W at an ERP of 50%, 5 mm sole displacement, and 1 Hz step frequency. Using the values reviewed in this section, a new maximum power extraction limit of

$$\frac{1}{2} \cdot 600\ N \cdot 8\ mm \cdot 2\ \text{Hz} \cdot (1 - 0.7\ ERP) = 1.44\ W \tag{2.3}$$

is calculated using a heel input force of 600 N, sole compression of 8 mm, 2 steps per second (1 Hz per leg), and 70% ERP. The ½ coefficient on the force term is due to the fact that the reaction force is not a constant 600 N through the entire displacement; instead, it increases in a spring-like manner to a maximum of 600 N, so 300 N is a good estimate of the average reaction force. This 1.44 W figure—or 720 mW per harvester— is the absolute maximum amount of electrical power that could be extracted using a heel-strike harvester in each shoe without increasing the user's metabolic load.

Various models have been developed to describe shoe sole and midsole behavior in the literature. The behavior of a shoe's midsole has been represented as a single linear viscoelastic element [46], a single non-linear viscoelastic element [45], [47], or multiple such elements in parallel [20], with the non-linear representations providing the best match to observed data. The spring coefficients, damping coefficients, and nonlinearity of these models are relevant to designing SBEH which behave like a normal shoe. These will be discussed alongside the author's own results in Chapters 3, 4, and 5.

2.3 Evaluating user burden

Minimizing user burden associated with using an energy harvesting device should be a key consideration during the development process. Even if a SBEH draws less

electrical power than the theoretical maximum of 1.8 W, there may still be significant user burden due to the device's weight, increased mechanical energy input, or changes in mechanical feedback from the shoe. User burden comprises subjective user comfort, gait mechanics, and user metabolic load.

To quantify the metabolic burden of human-based energy harvesters, Donelan et al. [15] propose a dimensionless 'cost of harvesting' (COH) quantity. COH is defined as the additional metabolic power in watts required to generate 1 W of electrical power using a human-based harvester

$$COH = \frac{\Delta\, metabolic\ power}{\Delta\, electrical\ power} \tag{2.4}$$

where Δ indicates the difference between walking while harvesting energy and walking with the device but without harvesting energy. However, this metric fails to account for the additional metabolic load required to carry the harvester, which is a function of its mass and its location on the body [10]. Therefore, it would be beneficial to report an additional 'cost of harvesting and carrying' (COHC) metric

$$COHC = \frac{\Delta\, metabolic\ power}{\Delta\, electrical\ power} \tag{2.5}$$

where Δ is the difference between walking while harvesting energy and walking without the device. Together, these figures give a representation of the efficiency with which the body's chemical energy is converted to electrical energy using an energy harvester. To

measure change in metabolic load caused by wearable energy harvesters, [15] and [17] used respirometry systems during walking which measure O_2 consumption and CO_2 production. From these measures, the power required to walk with and without the harvester can be calculated.

Metabolic load is only one axis of user burden. Thus far, only very limited attempts have been made to quantify subjective user comfort or changes in the gait cycle with wearable energy harvesters. [6] claims that their SBEH was unnoticeable to users and that there was no interference with the gait, but it seems these statements are based on observation rather than determined through study. In [21], electromyography (EMG) experiments were conducted to determine changes in muscle activity in the lower limbs while using their SBEH. These measurements were used as a proxy for changes in user gait and metabolic load. It was concluded that the harvester didn't cause obvious negative influence on the gait, and the ~5% increase in RMS EMG values with the harvester were attributed to the harvester-integrated shoe's mass versus that of a normal shoe. However, it is impossible to truly delineate the metabolic versus gait cycle changes using this method alone. Though not an SBEH, [17] used a cursory kinematic analysis to determine that their backpack-integrated harvester significantly decreased the user's vertical displacement during ambulation. Investigating other gait parameters with this method could prove fruitful in determining the manner and degree to which the gait is affected by using a harvesting device. [48] suggests that shoe-mounted accelerometer measurements will be used to determine whether their SBEH affects gait in future work. Many other works refer quickly to their devices affecting gait or comfort significantly or not, but it seems that no systematic study has been applied to changes in harvester user subjective comfort or gait

pattern so far. This is one area for significant improvement in the wearable energy harvester space and is discussed further in Chapter 5.

2.4 Kinetic energy harvesting mechanisms & review of shoe-based energy harvesters

Kinetic energy harvesters (KEH) convert movement into electrical energy through one of three main transduction mechanisms: piezoelectric, electromagnetic, or electrostatic [6], [9], [11], [14], [49]. Each mechanism couples change in a different mechanical parameter to electrical power output. Piezoelectric transduction utilizes changes in mechanical strain induced by deformation within a system to generate electrical power. Electrostatic transduction converts changes in the relative position of charged conductors separated by a non-conducting medium (i.e. a variable capacitor) to electrical power, and electromagnetic transduction typically couples changes in the relative velocity between magnets and coils to electrical power [49]. Magnetostrictive and triboelectric mechanisms have also been investigated to a lesser degree in the literature [49], [50], but have yet to be developed into KEH capable of power output on the order of the other three mechanisms.

KEH are usually comprised of three components: the transduction mechanism which converts mechanical energy into electrical energy, power conditioning circuitry such as voltage boosters and regulators, and an energy storage element such as a battery or supercapacitor [51]. Each of the three main transduction mechanisms have different power conditioning needs. Though this work focuses mainly on the transduction mechanisms, the efficacy of a mechanism in KEH implementations depends upon its power conditioning needs, so they will be evaluated briefly in turn. Energy storage elements are mostly implementation-dependent and transduction mechanism-agnostic, so they will not be

discussed in this review.

In evaluating the different transduction mechanisms for an energy harvesting application, multiple criteria must be considered: device architecture and size, power output, volumetric and mass power density, power conditioning needs, level of electromechanical coupling, and physical degrees of freedom. Unless otherwise stated, power density refers to *volumetric* power density in the following discussion.

2.4.1 Piezoelectric energy harvesting

The piezoelectric effect is the accumulation of electric charge on the surface of solid materials with a crystal-based structure due to an applied mechanical stress. Piezoelectric materials are non-centrosymmetric, meaning that their crustal structure lacks a center of symmetry. Consequently, these materials have an intrinsic electrical dipole in the unit cell—the positive and negative charge centers of the unit cell are not coincident. When a piezoelectric material is subjected to mechanical strain, its negative and positive change centers move relative to one another, forcing changes to appear at the crystal's surface to maintain electrical neutrality, as shown in Figure 2.4. These strain-induced charges can be extracted by placing electrodes on the charged surfaces and closing an electrical circuit which delivers the charges to an electrical load. If force is removed from the material and it is allowed to return to an unstressed state, this cycle can be repeated, extracting AC electrical power.

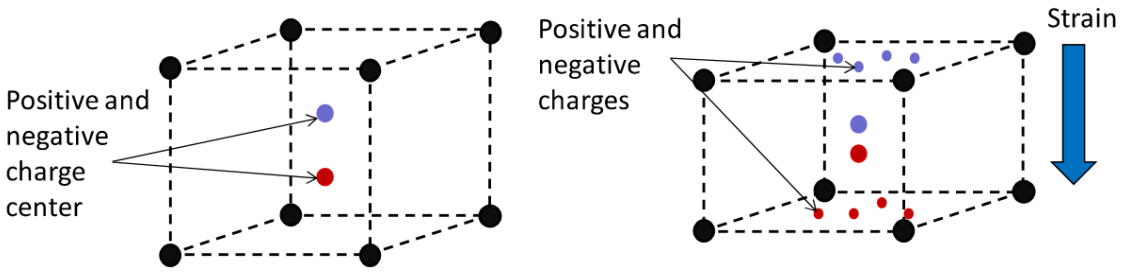

Figure 2.4. Illustration of the piezoelectric effect at rest (a) and under strain (b), adapted from [52].

2.4.1.1 Piezoelectric Materials

Two piezoelectric materials dominate energy harvesting applications in the literature: lead zirconate titanate (PZT), a polycrystalline ceramic, and polyvinylidene fluoride (PVDF), a semi-crystalline thermoplastic polymer. Prominent material and piezoelectric properties of the two materials are compared in Table 2.2, the values being adapted from [53] – [61]. The properties for PZT are listed for PZT-5H, also known as Navy Type VI, which has the largest coupling factor and is most commonly used type. Properties for other PZT types diverge significantly. The subscripts 33 and 31 refer to the direction in which the material is stressed relative to the direction in which it is electrically poled; this is discussed further in Section 2.3.1.2.

The piezoelectric strain coefficient or piezoelectric charge constant d couples the mechanical and electrical behavior of piezoelectric materials according to the piezoelectric constitutive equations

$$\{S\} = [C^E]^{-1}\{T\} + [d]\{E\} \tag{2.6}$$

$$\{D\} = [d]\{T\} + [e^T]\{E\} \tag{2.7}$$

Table 2.2. Comparison of PVDF and PZT-5H material properties.

Property	Symbol	Units	PVDF	PZT-5H
Density	ρ	kg/m^3	1780-1800	7500-7870
Relative permittivity Free dielectric constant	$\varepsilon/\varepsilon_0$ or K^T	Unitless	10-13	K^T_{11}= 3130 K^T_{33}= 3400-3800
Stiffness Young's modulus	C or Y	GPa	2-4	C^E_{11}= 62-64 C^E_{33}= 49-50
Piezoelectric strain coefficient Piezoelectric charge constant	d	pm/V pC/N	d_{31}= -18- -30 d_{33}= 30-33	d_{31}= -265- -320 d_{33}= 585-650
Electromechanical coupling coefficient	k	m/V C/N	k_{31}=0.11-0.12 k_{33}= 0.20	k_{31}= 0.39-0.44 $k_{33=}$ 0.75

where T is mechanical stress (N/m^2), S is strain, C^E is Young's modulus (Pa) measured at constant electric field (also known as short circuit stiffness), E is the induced electric field (V/m), and D is electrical displacement (C/m^2), and e^T is the absolute permittivity measured at constant or zero stress (also called free permittivity). Other commonly referenced piezoelectric coefficients such as g and e can be easily calculated from the properties provided in Table 2.2.

The electromechanical coupling coefficient k represents how much mechanical energy input to the piezoelectric material is converted to electrical energy or vice versa. It is calculated as the square root of the ratio of input mechanical energy to the converted electrical energy. It should be noted that the coupling coefficient is not the same as efficiency: unconverted mechanical energy is often returned as mechanical energy, and no significant energy is necessarily dissipated in the process.

From the values in Table 2.2, advantages and disadvantages of PZT and PVDF in relation to each other emerge. Generally, piezoceramics like PZT exhibit higher values of

d, *k*, and ε than do piezopolymers like PVDF. Piezoceramics are also much stiffer and more brittle than piezopolymers, so they cannot tolerate large strains without being damaged, whereas piezopolymers are highly flexible [50], [62].

PZT exhibits a high energy conversion rate due to its large piezoelectric coefficient, electromechanical coupling coefficient, and a high energy density [50]. PZT's mechanical stress limit is the effective constraint on its implementation: for PZT-5H, the maximum stress is in the range 14-32 MPa while the maximum (surface) strain is a modest 2-5e-4 [6] [59]. As a lead-containing material, PZT also has environmental and health concerns surrounding its widespread use.

Compared to PZT, PVDF is lightweight, flexible, durable, easy to process, relatively low-cost, and safe to produce [6], [63]. However, its electromechanical coupling is almost an order of magnitude lower [19], shaping PVDF reduces its effective coupling due to edge effects, and increasing power transfer through mechanical resonance is difficult to achieve because of its compliance [6].

In view of their implementation in SBEH, PVDF is attractive for parallels in its mechanical behavior to the foam polymers typically used in shoe midsoles. This gives PVDF SBEH advantages in their potential for user comfort and durability. PZT, on the other hand, usually requires a stiffer and more complex mechanism to harvest power effectively because of its low strain tolerance. However, PZT-based SBEH undoubtedly have potential for greater power output within the geometric confines of a shoe sole. Currently, PZT is the material of choice for a piezoelectric SBEH if power output on the order of 10 mW or greater is desired.

Though less common, other piezoelectric materials have been used in wearable energy harvesting applications. The reader is referred to [50] and [64] for comprehensive reviews of piezoelectric materials including new frontiers which present opportunities for improvement in energy harvesting applications. These include new ceramics, polymers, composites, and bio-inspired materials taking the form of different nanostructures and thin films with desirable physical properties such as high piezoelectric coefficient, flexibility, stretch-ability, and durability [50].

2.4.1.2 33-mode versus 31-mode

A piezoelectric material's electromechanical properties are dependent upon the direction in which the material is stressed relative to the direction in which it is electrically poled. The 1, 2, and 3 directions refer to the three axes orthogonal to the faces of a cube. By convention, the direction in which a piezoelectric material is poled is considered the 3 direction. The 1 and 2 directions are both orthogonal to the 3 direction and each other, so the equations defining their relationship to the 3 direction are equivalent. Thus, only the 3 and 1 directions are considered. There are two modes in which a piezoelectric material can act: 33-mode, where stress in applied in the same direction (33-direction) as the material's electrical poling, and 31-mode, in which stress is applied normal (11-direction) to the direction of poling, as shown in Figure 2.5. Most commonly, 33-mode corresponds to direct compression or tension of a piezoelectric material, while 31-mode is achieved by bending. The electric field and therefore voltage developed is in the same direction as applied stress in 33-mode, while in 31-mode the applied stress and induced electric field are normal to each other.

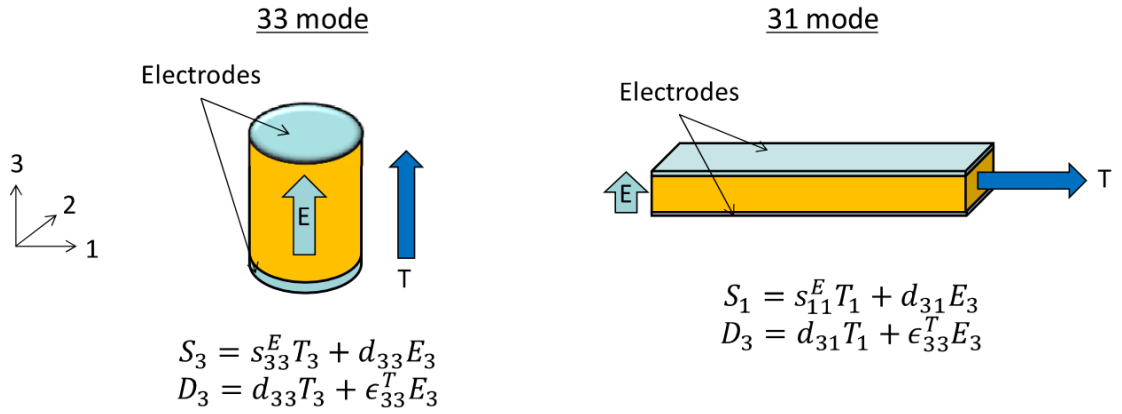

Figure 2.5. 33-mode and 31-mode piezoelectric transducer configurations.

A piezoelectric material's electromechanical material properties depend upon its mode of action, as shown in Table 2.2. Relative permittivity (~9%), piezoelectric strain/charge coefficient (~110%), and electromechanical coupling coefficient (~80%) are all greater in 33-mode, while stiffness is greater in 31-mode (~25%). Therefore, applying a force in 33-mode will produce a larger voltage and convert a greater proportion of the input energy than the same stress applied in 31-mode.

In the literature, conflicting information can be found regarding which mode is more suitable for SBEH implementations. The analysis in [13] finds that 33-mode harvesters have a maximum electromechanical efficiency of 50%, while 31-mode caps out at 11.2%. [14] reports that 33-mode harvesters can deliver 2-3 time more power output than 31-mode. [64] states that 33-mode yields higher voltage output while 31-mode provides higher current output, [65] and [66] find greater power output in 31-mode, and [67] finds just the opposite. Conclusions like these regarding the potential of each mode are often stated in reviews or cited in other works without qualification, potentially confusing the question for readers. By evaluating each conclusion within the context of its

original publication, it can be seen that these conflicting findings boil down to differences in implementation.

Putting each mode into the context of the constraints of forces exerted during walking and the mechanical behavior of shoes clarifies the comparison. Despite its efficiency, 33-mode poses problems for SBEH development. Because of its high stiffness (PZT-5H in 33-mode has about the same stiffness as tin), it takes incredible force to achieve any significant amount of strain in the material. Because work is defined as a force through a distance, the minute levels of displacement achievable under footfall forces imply that the amount of electrical power that can be harvested in 33-mode is very low even at its higher conversion efficiency [6], [12]. This low displacement also implies that it may be difficult to create a 33-mode SBEH that feels comfortable to the user.

Bending a thin piece of piezoelectric material in 31-mode is much easier, achieving higher stress states with the forces and displacements involved in human locomotion and therefore greater power output [12], [39]. As such, 31-mode has been the focus of multiple SBEH in the literature. Xie & Cai [39] even developed and tested two SBEH with very similar architecture and mechanisms, one acting in 31-mode and the other in 33-mode. They found that the 33-mode harvester produced about 2% of the power output by the 31-mode harvester. While the 33-mode design was adapted from the 31-mode design and thus not optimized for 33-mode, it is illustrative of the difference in power output under similar force and displacement conditions. While the SBEH architectures needed to achieve 31-mode actuation of piezoelectric materials are generally more complex than direct compression or tension in 33-mode, they also lend themselves better to mirroring the mechanical behavior of shoe soles due to their greater displacement. A final consideration

is that 31-mode bending elements are often comprised of a piezoelectric material bonded to a substrate which stores and returns mechanical energy, as opposed 33-mode in which all the input energy is applied to the piezoelectric material in many implementations. This results in an effective 31-mode coupling constant 25% lower than the theoretical value [6].

2.4.1.3 Review of piezoelectric shoe-based energy harvesters

The initial draw of piezoelectric transduction mechanisms for electromechanical energy harvesting is their potential for mechanical simplicity: a single material with minimal architecture can convert a mechanical input to electrical energy [9]. However, as discussed in Sections 2.4.1.1 and 2.4.1.2, this picture is complicated by the overbearing advantages of using PZT and 31-mode operation for high-power applications, which necessitates more complex architectures. Still, piezoelectric materials are a natural choice for human-based energy harvesting, especially the heel strike, as they easily convert linear motion to electrical energy in a velocity-independent manner [12].

When used at low frequencies, piezoelectrics are high-impedance devices, so their generated voltages tend to be high (10s to 100s of V) and currents very low (hundreds of μA to 10s of mA) [6], [11], [68]. This means either that these values either need to be transformed into more useful ranges (ex. 3-12 V, currents of mA) through power conditioning circuitry, or harvesting devices and the piezoelectric materials they use be configured specifically to produce usable voltage and current output.

Despite their finding 1W of power available from the heel-strike per foot, [12] concluded that the upper limit of power generation from piezoelectric SBEH is around 100 mW due to high output voltages and low displacements. Even so, they concede that

implementations in the literature which they expect to fall around this target produce less than 10% of this expected power. So far, minus complex and bulky outliers, 10-20 mW is the high end of the range of power generated with piezoelectric SBEH in the literature.

2.4.1.3.1 PZT-based SBEH

Xie & Cai [39] developed what is perhaps the best example of a high-power piezoelectric SBEH to date. This harvester was relatively light and compact at 105 g and 46 cm^3 and generated 18.6 mW at a 2.6 mm displacement of 1 Hz for an impressive power density of 0.404 mW/cm^3. This was achieved by placing 20 PZT-5H bimorph benders in parallel mechanically which were bent about their center point for 31-mode operation as shown in Figure 2.6. Because of its relative mechanical simplicity and good power output results, the harvester developed in the current work was inspired in part by Xie & Cai's success.

Shenck & Paradiso along with colleagues at MIT's media Lab developed one of the earliest and most frequently cited piezoelectric SBEH in [3], which still stands as an

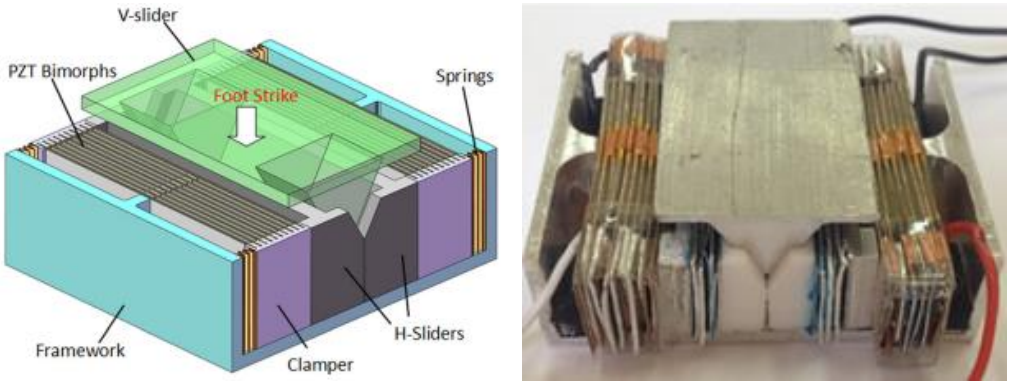

Figure 2.6. Simply supported 31-mode bender SBEH developed by Xie & Cai [39].

excellent high-power implementation over 20 years later. They placed two large pre-curved PZT unimorphs (commercially available Thunder TH-6R actuators developed by Face International Corp.) on either side of a midplate, creating a clamshell-like ‘dimorph’ architecture shown in Figure 2.7. Perhaps the most mechanically simple SBEH in the literature, its weight was unreported but had reasonable volume of about 73 cm^3 (estimated) and produced 8.4 mW with a 1 Hz input of 8.5 mm deflection (estimated), yielding a power density of 0.115 mW/ cm^3. The authors describe the device as rigid but claim that integrated in a work boot’s stiff heel, it was barely perceivable to users and did not affect gait. This may imply that the device is not compliant enough for casual or athletic shoes which they explicitly decided against using.

Leinonen et al. [69] developed a very compact SBEH with good power output which may be the most practical PZT-based SBEH in the literature. Shown in Figure 2.8, it used four layers of pre-stressed circular PZT bimorph diaphragms compressed in 31-mode. The device was very compact and lightweight at 31 cm^3 and 44 g, and at 1 Hz and 1.9 mm deflection produced 3.65 mW at when integrated in a shoe and 11.3 mW when

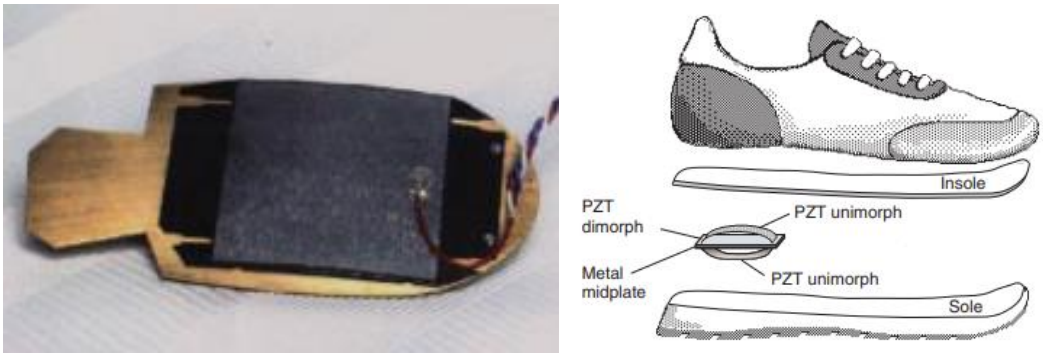

Figure 2.7 Dimporh clamshell PZT SBEH developed by Shenck & Paradiso [3].

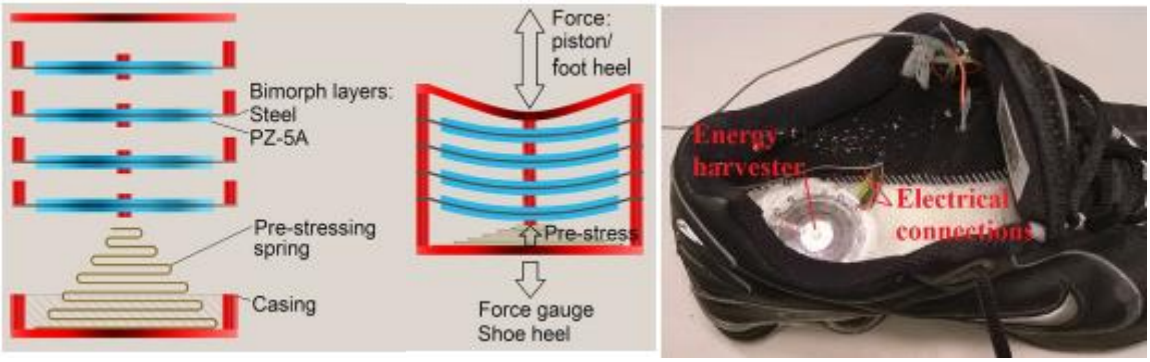

Figure 2.8. Pre-stressed PZT diaphragm SBEH developed by Leinonen et al. [69].

actuated with a testing machine. These correspond to power densities of 0.118 mW/cm^3 and 0.365 mW/cm^3 respectively, and the authors state that the power could easily be doubled with only a 25% increase in harvester height. The only downsides to this harvester are its limited displacement (the piezoelectric elements fractured at 2.0mm displacement) and imperfect transfer of energy from the foot to the harvester because of its small size, which contributes to the loss in power observed in the shoe-integrated tests versus the testing machine condition.

Haghbin [38] designed a different diaphragm-type PZT-based SBEH which uses an air pump to deflect the diaphragm. Because the air pump imparted force on the PZT rather than the footfall directly, it was suggested that this design had improved durability and robustness. However, its power output of 1.14 mW at a volume of 60.0 cm^3 results in a low power density of 0.019 mW/cm^3.

Antaki et al. [5] developed the first high-powered SBEH, and its power output remains unmatched in the literature. It consists of hydraulic pistons and oscillators which pulse two long (200 mm) PZT stacks in 33-mode at 5 Hz. Information surrounding the device is not complete, however, and only a 1/17th scale prototype was ever assembled.

Based on testing of this prototype, 6.2 W of power was estimated from a full-scale device, a huge amount—likely undesirably high. Additionally, the PZT stacks alone weighed 640 g, 10 mm sole displacement was required, and the device appears impractically bulky (~720 cm^3 based on estimates from diagrams) though its size was not reported. This results in a ballpark power density of 8.66 mW/cm^3. While its hydraulic up-conversion mechanism could be investigated further in a lower-profile design, this SBEH appears to be an outlier in many ways and can't be evaluated properly until a full-scale model is tested.

Howells [70] developed a SBEH which replaces a boot's heel and provides 12V DC regulated output. At 465 g and 307 cm^3, this harvester was very heavy and bulky, but produced 90.3 mW at an unstated frequency and input displacement for a power density of 0.294 mW/cm^3. Its mechanism of a lead screw connected to a gear train which causes four PZT-5A bimorph stacks to deflect sinusoidally is novel and, though very complex, could have potential for even greater power output with further work.

Qian et al. [71] employed 8 300-layer stacks of PZT compressed in 33-mode using two-stage force amplification frames to achieve ~5x force amplification in their SBEH. The resulting device had a volume of 167 cm^3 and 11.0 mW power output at 1 Hz for a power density of 0.066 mw/cm^3. There was vanishingly little displacement in the harvester, meaning it is not a good candidate to replace shoe sole material without increasing user burden, and though unreported, the device was likely quite heavy. The same authors created an earlier SBEH using a single-stage force amplification mechanism which achieved a 9.3 mW power output in a similar volume. [72] developed a similar single-stage force-amplification mechanism which calculations show could generate 0.8 mW of power

in a very small package. However, a prototype was never constructed, and device dimensions were not supplied, so it is difficult to evaluate this device fully.

Kuang et al. [73] developed the highest-power example of a cymbal-type piezoelectric SBEH, a common architecture for 31-mode piezoelectric energy harvesters. Their design delivered 2.5 mW of power when embedded in a shoe's forefoot region. With its compact 23.4 cm^3 volume, the power density is a respectable 0.107 mW/cm^3. Though not reported directly, the input displacement is estimated at 3 mm. In [74], a rigorous design optimization study found that the maximum power output of similar cymbal-type human-based energy harvesters was 6.5 mW with a safety factor of 2.0.

Yin et al. [75] developed a SBEH which uses a ratcheting mechanism and one-way bearings to achieve mechanical frequency up-conversion in plucking a cantilevered piezoelectric beam 8 times per step. The device was very light at 55 g but possibly not robust, as its components were all 3D printed. With a volume of 75 cm^3 and a power output of 0.23 mW at 1 Hz, it achieved a very low power density of 0.003 mW/ cm^3. Thus, its power output disqualifies it from high-power applications, but the novel mechanism presents an interesting avenue for increasing power through mechanical frequency up-conversion. The high volume of the device's complex architecture versus the low volume of piezoelectric material limits its power output and density.

Vibration-type SBEH in the form of cantilevered piezoelectric beams are another common architecture. Moro & Benascuiutti [76] developed such a device which was easily integrated in the sole and generated 0.378 mW at 1 Hz. The size of the overall device placed in the sole was never reported, and seems to be oversized relative to the cantilevered beam

structure, so it is unlikely that this specific implementation had a high power density. However, Li et al. demonstrated that such devices can certainly exhibit high power density on their own, with their SBEH generating 0.049 mW at a volume of 0.242 cm^3 for a power density of 0.242 mW/cm^3. Though not sufficient for high-power applications, the device's small size could allow multiple to be integrated into the sole rather than simply strapped to the outside of the shoe as presented in their work. von Buren et al. estimated that a cantilevered vibration-type SBEH could produce 0.2 mW with a 1 g proof mass [77] or 1.5 mW with a 2 g proof mass [78] given 5 mm tip displacement. Though many more vibration-type piezoelectric energy harvesters have been developed and even applied to shoes in the literature, none have managed to significantly exceed this benchmark. Thus, this architecture is not a good candidate for high-power applications.

Fan et al. [79] created a piezoelectric SBEH consisting of a cantilevered PZT beam magnetically coupled with a ferromagnetic ball and a crossbeam. This harvester is unique in that it harvests energy from multi-DOF motions, including swinging of the foot, impact vibrations, and compressive force. At a 1 Hz displacement of 8 mm, this harvester produced 0.28 mW. Given a volume of 32.4 cm^3, the power density was low at 0.009 mW/cm^3, but this device proves the feasibility of multi-DOF SBEH.

Of these 12 SBEH, those developed by Xie & Cai, Shenck & Paradiso, and Leoinen et al. (corresponding to the three figures in this section) seem to show the most promise for practical, high-power implementations. Each has power output potential > 8 mW, a power density > 0.1 mW/cm^3, a volume < 100 cm^3, and is easily integrated with a shoe's heel. Table 2.3 summarizes the characteristics of all harvesters reviewed in this section.

Table 2.3. Comparison of PZT-based shoe-based energy harvester characteristics.

Authors	*Year*	*Avg. power @1Hz (mW)*	*Pwr. density (mW/cm^3)*	*L x W x H (mm)*	*Volume (cm^3)*	*Mass (g)*	*Deflection (mm)*	*Mode*	*Mechanism*
Xie & Cai	2014	18.6	0.404	50 x 50 x 23	46	105	2.6	3-1	*20 simply-supported benders in parallel*
Shenck & Paradiso	2001	8.4	0.115	128* x 60* x 9.5*	73*	Low*	8.4*	3-1	*Clamshell dimorph flattened*
Leoinen et al.	2016	3.65	0.118	45.5 x 45.5 x 15	31	44	1.9	3-1	*4 layered pre-stressed diaphragms*
Haghbin	2011	1.14	0.019	50 x 50 x 24	60	?	4.5	3-1	*Air pimp deflects diaphragm*
Antaki et al.	1995	6200	8.66*	300* x 50* x 48*	720*	>>640	10	3-3	*Hydraulic pulser hammers PZT stacks*
Howells	2008	90.3[a]	0.294	89 x 79x x 43	307	465	?	3-1	*Lead screw drives gear train and cam*
Qian et al.	2019	11.0	0.066	68 x 98 x 25	167	High*	~ 0*	3-3	*8 two-stage force amplification frames*
Kuang et al.	2017	2.5	0.107	52 x 30 x 15	23.4	?	~ 3.5	3-1	*Rectangular cymbal-type*
Yin et al.	2021	0.23	0.003	70 x 43 x 25	75	55	?	3-1	*Ratchet plucks cantilevered beam*
Moro & Benasciutti	2010	0.38	?	?	?	?	NA[b]	3-1	*Cantilevered beam, large clamping mech.*
Li et al.	2009	0.05	0.202	?	0.24	Low*	NA[b]	3-1	*Cantilevered beam, L-shaped tip mass*
Fan et al.	2017	0.28	0.01	45 x 30 x 24	32	22	8	3-1	*Multi-DOF cantilevered beam*

? value unreported. * value estimated. a. frequency unreported. b no harvester compression necessary in vibration-type harvesters**.**

2.4.1.3.2 PVDF-based SBEH

Han & Kaajakari [80] developed a very promising PVDF-based SBEH which has the potential to be the most practical SBEH thus far if developed further. By rolling a PVDF thin film into a 120-layer structure, a simple harvester was created which provides 4 mW raw or 2.6 mW regulated power in a 24 cm^3 package for a power density of 0.108 mW/cm^3 after regulation. However, the true upsides of this harvester go beyond its power and volume metrics: it has a Young's modulus of 3-6 MPa which matches normal shoe sole materials, it is the same weight as the removed volume of shoe midsole material at 6.5 g, and it cost less than $0.50 to manufacture which bests PZT-based harvesters by multiple orders of magnitude. Han & Kaajakari believe that the device's power output could be increased 80% and that three devices could be integrated in a shoe for a total regulated power output of 21 mW. If realized, this could be the best SBEH implementation for applications in this power range.

Thus far, no other PVDF-based SBEH has a power density greater than 0.06 mW/cm^3 or a power output greater than 1.5 mW, nor do they have the ability to scale that Han & Kaajakari's design possesses. Kymissis et al. [81] developed a PVDF stave that harvests power from the flexion of a shoe's forefoot which produced 1.3 mW with a power density of 0.054 mW/cm^3. Zhao & You [82] and Han et al. [83] developed insole-replacement SBEH which compress layers of PVDF between two ribbed surfaces for a large-area but low-profile design. These devices produced 1.1 mW and 0.129 mW of power respectively for power densities of 0.020 mW/cm^3 and 0.001 mW/cm^3. Lastly, Fourie [84] developed a rather bulky heel-shaped harvester with layered stacks of PVDF placed in parallel which produced 0.06 mW for a power density of 0.001 mW/cm^3. None of these

implementations seem to show promise for significant power or power density increases that would warrant further development for high-power applications. While other PVDF-based SBEH have been presented in the literature such as [85] [86], they lack enough information to evaluate against these better-documented examples.

2.4.2 Electromagnetic energy harvesting

Electromagnetic transduction in KEH is based on the relative motion of an electric coil and a magnetic field. Mechanical forces cause this motion, which is captured in the electric circuit as a voltage induced across a coil due to changing magnetic flux density through that coil according to Faraday's Law of Induction. The generated power depends on the strength of the magnetic field, the number of coil turns, and the rate of magnetic flux density change due to relative motion.

Opposite of piezoelectric KEH, small-scale electromagnetic generators tend to produce very low AC voltages and moderate currents due to their high impedance [11], [14], [68]. Electromagnetic transducers can have higher potential power output than piezoelectrics but tend to take the form of more burdensome packages due to their large size and the imposed dynamics of an inertial mass [9], [14]. The most common configuration for electromagnetic energy harvesters is a fixed coil and a moving magnet, though the inverse is also used. Linear displacement generators similar to the commercial shake-driven flashlight are one of the most common KEH architectures [11]. However, electromagnetic generators are generally most efficient (and higher-powered) at higher speeds, often accomplished through rotary motion [12]; the linear input of a heel-strike or foot swing is thus not an ideal candidate input motion. Electromagnetic KEH have the

advantages of proven designs translated from other applications, relatively low cost, and good efficiency, but are dragged down by their high weight and volume [12].

2.4.2.1 Review of electromagnetic shoe-based energy harvesters

Kymissis et al. [81] and Hayadhida et al. [87], both in the MIT Media Laboratory, developed two early rotary electromagnetic SBEH. Both devices were reportedly extremely bulky, fragile due to the high torques imposed on small geartrains, and interfered with the wearer's gait. They required uncomfortably large displacements (~30 mm) and caused the wearer to feel significant resistance while stepping down. However, they produced 250 mW and 58 mW respectively, demonstrating that this architecture has high power output potential.

Xie & Cai [21] followed up in this lane, creating a low-profile sole-embedded rotary electromagnetic generator with ~950 mW power output in a package of 82.7 cm^3 shown in Figure 2.9. This resulted in an excellent power density of 11.5 mW/cm^3. At a weight of 137 g and displacement of 5 mm, this harvester stacks up well with the best examples of piezoelectric energy harvesters in the literature and far exceeds their power output. Its complex gear train may decrease durability, but this design proves that rotary generators can be successfully integrated in the sole. Though user comfort was not addressed, this appears to be the highest-power SBEH which satisfies known geometric and displacement constraints.

Purwadi et al. [88] designed a rotary electromagnetic SBEH with a very similar form factor, mechanism, and geartrain which achieved even better results: 1100 mW (at an unreported frequency and displacement), a volume of 45.7 cm^3, and power density of 24.1

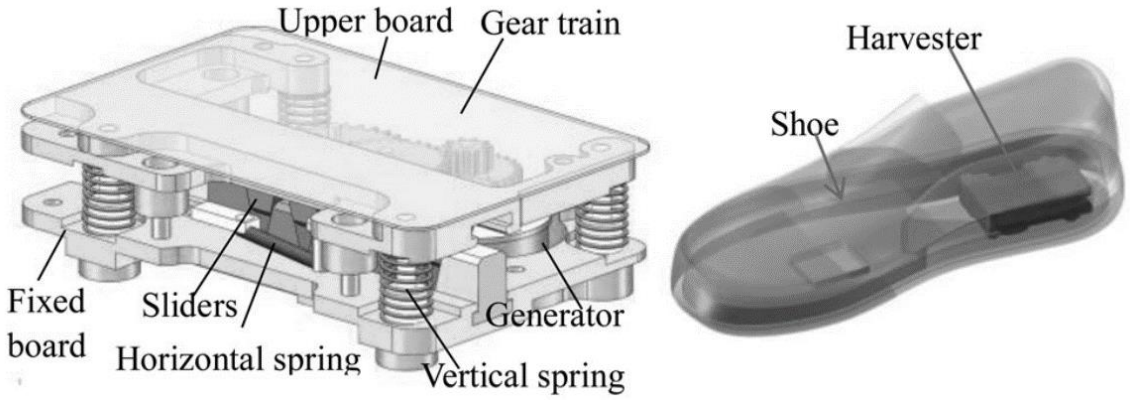

Figure 2.9. Gear train-based electromagnetic SBEH developed by Xie & Cai [21].

mW/cm^3. However, the harvester requires significantly increased effort from the user and is uncomfortable, disqualifying it from many applications. Given its similarities to the SBEH developed by Xie & Cai, that design may suffer the same disadvantages.

Liu et al. [89] created a generator with a novel mechanism for converting the linear heel-strike into rotary motion. They employed a magnetic gear which is analogous to the mechanical lead screw, and the rotation induced by this device generated power through an axial-flux permanent magnet generator as shown in Figure 2.10. The device's volume of 108 cm^3 and theoretical power output of 1400 mW result in power density of 12.96 mW/cm^3 at a 1 Hz displacement of ~4 mm. Though a physical prototype has yet to be developed, this design offers advantages over other electromagnetic generators such as overload protection, elimination of high mechanical torques, much lower friction, and quiet performance. This is a very promising implementation which merits further investigation since it is both high-powered and has the potential to offer low user burden.

Niu & Chapman [90] developed an early high-powered, high-volume SBEH, but rather than being integrated within the shoe, it was strapped to the outside. A linear

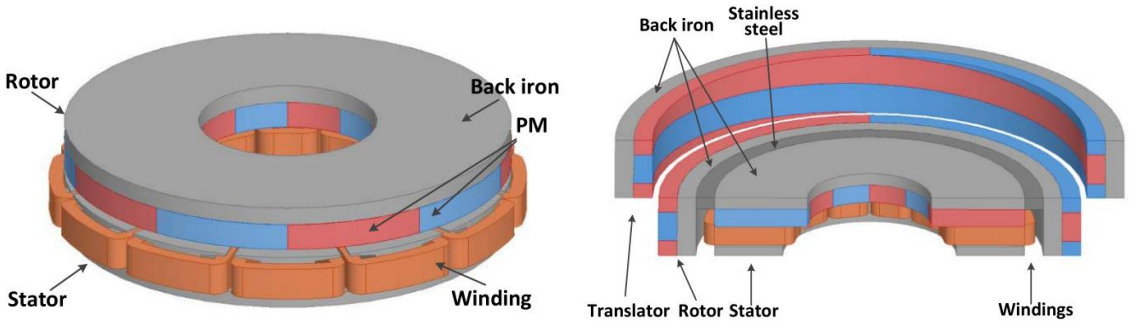

(c)

Figure 2.10. Magnetic gear-based electromagnetic SBEH developed by Liu et al. [89].

displacement generator with moving coils, it generated 80 mW at 280 cm^3 for a power density of 0.286 mW, but its excessive volume and awkward attachment mechanism means it serves strictly as a proof-of-concept device.

Caroll & Duffy [48], on the other hand, developed a compact linear displacement electromagnetic SBEH, in which two coil tubes with moving magnets are embedded in the shoe sole pictured in Figure 2.11. This device produced 28 mW within a volume of 45 cm^3, achieving a power density of 0.622 mW/cm^3. This design is certainly worth exploring further, with user burden considerations at the forefront.

Figure 2.11. Linear displacement electromagnetic SBEH developed by Caroll & Duffy [11], [48].

Ylli et al. developed two electromagnetic SBEH in [91]: a linear displacement swing harvester mounted outside the shoe producing 0.84 mW for a power density of 0.040 mW/cm^3, and a unique oscillating heel-strike harvester producing 4.13 mW at 48 cm^3 and 3mm displacement for a power density of 0.086 mW/cm^3. While soundly designed, the architecture of the latter was quite complex and does not seem to be the most elegant solution in this space.

Wu et al. [92] developed a 3-DOF electromagnetic vibration-based SBEH comprised of a permanent magnet suspended by two elastic strings in a box with coils on its faces. This device produced 0.014 mW and was attached outside of the shoe, making this less attractive than other implementations.

Akay et al. [4] developed an air-pump-and-turbine SBEH utilizing a DC generator. Their system placed three air bladders in the shoe sole which drove a miniature 3D-printed turbine connected to the DC generator that was mounted outside of the shoe, weighing 130 g in total. It produced an average power of 86.4 mW at a 1 Hz displacement of 10 mm and a volume of 370 cm^3 for a power density of 0.223 mW/cm^3. Other attempts at air-bladder based systems have been made [93], but thus far do not seem to justify their large volumes, displacements, and complex mechanisms.

Lastly, Rahman et al. developed four generations of multi-channel microfluidic electromagnetic SBEH culminating in [94]. Though this device was designed within the context of a sole insole replacement, the most impressive power output numbers of 456 mW and 8.13 mW/cm^3 were achieved at an input frequency of 3 Hz and an input displacement of 20 mm, much greater than normal walking conditions. At 10 mm input displacement and 1 Hz input, the device produced about 10 mW for a power density of

0.187 mW/cm^3. This architecture shows promise for low-profile, high-power output, but reports on its integration are not detailed enough to make a full assessment of its practicality.

Of these 12 SBEH, the gear-train based rotary generator of Xie & Cai, the magnetic gear-based rotary generator of Liu et al., and the linear displacement generator of Caroll & Duffy seem the most promising and worthy of further investigation. These three designs were pictured in this section. Because many of the publications on electromagnetic SBEH do not provide as much characteristic information as those of piezoelectric SBEH, a comparison table was not compiled.

2.4.3 Electrostatic energy harvesting

Electrostatic transduction of kinetic energy is based on the charging of capacitor plates. Mechanical forces separate the plates of a pre-changed capacitor, changing its capacitance and thus the voltage across the capacitor according to the relationship

$$Q = CV \tag{2.8}$$

where Q is the charge on the capacitor electrodes, C is capacitance, and V is voltage. Thus, the mechanical energy input to change the capacitor plate distance is converted into electrical energy [11]. Electroactive polymers (EAP), and specifically dielectric elastomers, are by far the most promising means of electrostatic transduction for SBEH.

These compliant dielectric materials, coupled with compliant electrodes on opposing faces, enable the use of polymers with similar mechanical behavior and weight to normal shoe soles. Because of their high compliance, large displacements, large

voltages, and high power output can be achieved with the material. EAPs offer good power-to-weight ratios, can display efficient transduction [10], and are able to withstand higher strains than piezoceramics [12]. They also easily achieve the 2-5 mm displacements that occur in shoe soles and afford more elegant designs and easier handling than piezoceramic and electromagnetic-based mechanisms.

However, electrostatic transduction has one significant barrier not found in electromagnetic and piezoelectric SBEH: cold-start issues. Devices require an initial charge to be placed on the capacitor before energy harvesting can begin, which must be supplied by some other energy source such as a battery or piezoelectric device. High voltages (kilovolt-range) and low currents (low microamps range) characterize EAP performance, necessitating power conditioning circuits to regulate their output into useful ranges which intrinsically come with a loss in performance [12]. Power conditioning and cold-start remedies can increase the cost and volume of EAP-based SBEH.

EAP are also relatively new materials, meaning that there is much potential for improvement and a current dearth of SBEH implementations in the literature.

2.4.3.1 Review of electrostatic shoe-based energy harvesters

The only prominent electrostatic SBEH in the literature is that developed in 2002 by Kornbluh et al. [95], which is surprising given its success, though details on the device remain scarce. Replacing the heel portion of a boot, their SBEH produced ~800 mW within 3 mm of compression, an has an estimated volume of 108 cm^3 for a power density of 7.41 mW/cm^3 [96], but it is purported that the device felt difficult to walk in, implying that it demanded too much energy input or provided too little energy return to the user. This

device used a gel or fluid to push layers of EAP into a perforated grate, straining it and changing the thickness of its layers.

The only other EAP SBEH in the literature was developed by McKay and collaborators at the University of Auckland's biomimetics laboratory, though details of this shoe's performance have never been formally published; [97] is the best source of information on the device. They used multiple cylindrical stacks of layered EAP in parallel under the heel of a shoe which were integrated seamlessly and seemed to mimic closely the behavior of the normal shoe sole. Details of the stack structures outside of the context of the shoe have been published in [98], and show energy densities of 3.8 mW/cm^3 for a device of ~1.4 cm^3, or 5.4 mW power out. Multiple such stacks are placed in mechanical parallel in the shoe, so the SBEH power output is likely on the order of 10s of mW.

While EAP SBEH show promise for user-friendly implementations and high power output, further attention is needed to mature this technology.

2.4.4 Comparison of energy harvesting mechanisms

In summary, each transduction mechanism offers its own blend of advantages and disadvantages. In each design, power output, user burden, mechanical robustness, size, and cost must be considered. Piezoelectric SBEH can have mechanically simple implementations but are limited in power to 10s of mW and vary in their user friendliness. Electromagnetic SBEH can have far higher power outputs on the order of 1 W, but tend to increase user burden, and are quite mechanically complex and thus less robust. Electrostatic SBEH using EAP show promise of high power output and user comfort at the cost of cold-start issues but have not been explored thoroughly enough to make conclusive

statements. Piezoelectric and electrostatic SBEH benefit from micromanufacturing technologies which enable more elegant, compact device design, whereas electromagnetic generators tend to be larger and more complex, though they have established topologies which can be adapted from other applications. Piezoelectric and electrostatic devices tend to have high voltage output and low currents, while electromagnetic harvesters show the inverse [11], [68]. For all three types of harvesters, efficiency tends to decrease with size [11], increasing the challenge of high-powered designs that don't increase user burden. Relatively high coupling coefficients of 0.6-0.8 can be achieved with each mechanism, so the design and integration of SBEH implied by its transduction mechanism are of greater importance than the transduction mechanism alone [68].

2.4.5 Shortcomings in the literature

Too often, critical parameters of SBEH are left unreported in the literature. For each design, the device's average power output at 1 Hz, dimensions, volume, mass, input displacement, energy return percent, input force-displacement curves, and cost should be reported. From these values, the device's volumetric and mass power densities, power output per unit displacement, and energy consumption percent can be calculated. With these figures, devices could be more accurately evaluated against one another, and fruitful research directions better identified. For EAP and piezoelectric devices, the volume of EAP or piezoelectric material should be reported so power per material volume can be derived, another useful metric for comparison.

Perhaps the greatest deficit in the literature is a lack of user burden evaluation. As discussed in Section 2.3, quantifying the three aspects of user burden (subjective user comfort, gait mechanics, and user metabolic load) would afford much better insight into which devices and directions have potential for practical implementations, and which serve only as proof-of-concept. Approaching SBEH design from a perspective in which user burden is of equal importance to power output can increase the quality and applicability of future SBEH.

2.5 Contribution of this work

This work aims to present a piezoelectric SBEH designed from the joint perspective of maximizing power output and minimizing user burden. In Sections 2.1 and 2.2, a more comprehensive overview of the SBEH design space, constraints, and guidelines is given than elsewhere in the literature, and, though not all-encompassing, Section 2.4 represents the most comprehensive review of SBEH (> 0.1 mW power output) to date. By leveraging this information, a PZT-based SBEH with a novel mechanism combining previously successful elements is designed which targets > 10 mW power output, > 0.1 mW/cm^3 power density, ≥ 70% energy return percent (ERP), and < 100 g weight. A regime for evaluating the three axes of user burden is also proposed which can be applied to the development of future SBEH.

CHAPTER 3

DESIGN AND MODELING

3.1 Design goals

In developing this shoe-based energy harvester (SBEH), the central goals are to 1) minimize user burden and maintain comfort by developing the harvester within a solution space bounded by the behavior of normal shoes, 2) achieve high power density relative to harvester and piezoelectric material volume, and 3) produce a robust final product that can be implemented in varied applications. In approaching its design, piezoelectric transduction was selected for its amenability to designs with low user burden and because piezoelectric SBEH can be adapted for use with flexoelectric materials (as discussed in Chapter 1). Flexoelectric materials have numerous advantages over piezoelectrics for the aims of this SBEH. A greater range of materials can be made highly flexoelectric, and some of these materials are more readily micromachined than piezoelectric materials such as PZT. This allows for economical and practical creation of flexoelectric structures with electromechanical coupling larger than existing piezoelectrics, meaning that more of the mechanical energy input to the material is converted to electrical energy. Therefore, the power density and resultant power output of a flexoelectric SBEH could be much greater than current piezoelectric implementations. The piezoelectric transduction mechanism in this SBEH therefore has advantages beyond its performance alone.

3.2 Design constraints

To minimize user burden associated with SBEH use, the device should mirror the geometric, mechanical, and energetic parameters and dynamic behavior found in normal shoes. The three axes of user burden which must be considered during SBEH design are user metabolic load, gait cycle disruption, and subjective comfort (see Section 2.3).

The geometric constraints on the developed SBEH were derived from shoe measurements and previous SBEH implementations, as discussed in Section 2.2.1. A maximum length of 70 mm, width of 50 mm, and height of 35 mm bound the overall volume. Based on the displacements found in normal shoe soles, an input displacement of 4-6 mm was selected, affording 1-2 mm displacement to occur in the remaining outsole material beneath the harvester. A heel-strike pad 45 mm in diameter ensures ample and comfortable force transfer from the heel to the transduction mechanism. A device weight limit of 100 g is targeted to minimize the user burden associated with the harvester.

In order to match the mechanical behavior of the harvester to normal shoes, three design parameters must be aligned: energy dissipation per step, energy return percent (ERP), and equivalent stiffness or Young's modulus. Based on the testing of multiple pairs of shoes in Section 4.1 and results in the literature discussed in Section 2.2.2, 70% ERP, 720 mJ of energy dissipation (mechanical loss plus electrical energy harvested) per loading cycle, and a Young's modulus of ~1.5 MPa are good design targets. This Young's modulus corresponds to an equivalent spring constant of 72 N/mm under the 45 mm diameter heel pad. The above metrics align the behavior of the harvester with a pair of Sketchers GoRun Elevate shoes, a good representative of standard running shoes as shown in Section 4.1.

To enable use in high-powered applications and compare favorably to other PZT-

based SBEH, this design targets a power output of >10 mW and a volumetric power density >0.1 mW/cm^3. .

3.3 Detailed design

The two SBEHs produced in this work were based on a combination of elements previously employed in the literature: mechanical frequency up-conversion, 31-mode benders placed parallel, a spring-return system, and mechanically pre-stressed piezoelectric elements.

3.3.1 Frequency up-conversion

The power output of a piezoelectric material under sinusoidal excitation is a function of input frequency ω, coupling coefficient k, material stiffness c^E, material volume (volume = Ah), and average strain S

$$P_{rms} = \frac{1}{4}\omega k^2 c^E (Ah) S^2 \tag{3.1}$$

These parameters are the five design levers which can be manipulated to increase power output of a piezoelectric energy harvester. Based on the discussions in Sections 2.4.1.1 and 2.4.1.2, PZT-5H piezoelectric benders acting in 31-mode were selected as the basis for SBEH design. In 31-mode actuation, according to [6], the maximum surface strain is about 5e-4 [6], a level easily achieved using a simply supported or cantilevered bender. Many

31-mode SBEH in the literature seem to approach or even exceed this limit (implying decreased durability). Thus, increasing bender displacement alone is not a good avenue for improving power output. The coupling coefficient of PZT-5H and its stiffness are intrinsic properties which cannot be significantly changed. PZT is an inherently expensive and heavy (7500 kg/m^3) material, so maximizing power output from a small volume of material is a more practical strategy than increasing power output through material volume increases alone. This leaves increasing input frequency as a promising an under-investigated avenue for getting more power out of SBEH.

The frequency of footfalls during normal walking is a relatively fixed parameter at about 1 Hz, so converting this low frequency into a higher frequency imparted on the piezoelectric material is the central challenge. This has been accomplished previously through vibration-type cantilevered beam SBEH excited by the impulse of a footfall, which exhibit low (< 0.5 mW) power output, or higher-powered mechanical frequency up-conversion mechanisms such as the hydraulic oscillator implemented by Antaki et al. [5], Howells' [70] lead screw-coupled geartrain, or Yin et al.'s [75] plucking of a cantilevered beam with a ratcheting gear mechanism. In the SBEH developed here, two novel mechanical frequency up-conversion mechanisms are implemented: a ribbed 'plunger,' and a ball screw-driven multi-lobed cam.

A high-level diagram of the key aspects of these SBEH designs is shown in Figure 3.1. Multiple 31-mode piezoelectric benders are mechanically coupled to a frequency up-conversion mechanism, which increases the frequency of the force input to the benders above the 1 Hz of walking. Figures 3.2 and 3.3 show how this general principle is

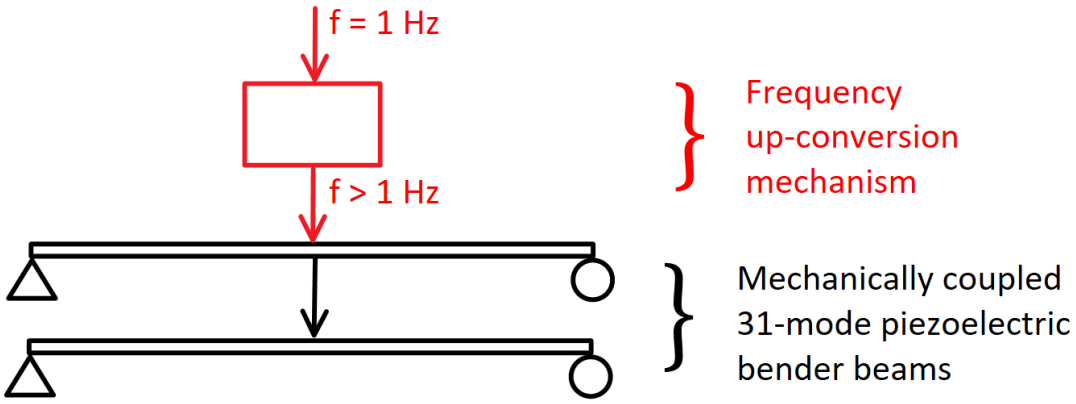

Figure 3.1. High-level operating principle of the SBEH developed in this work.

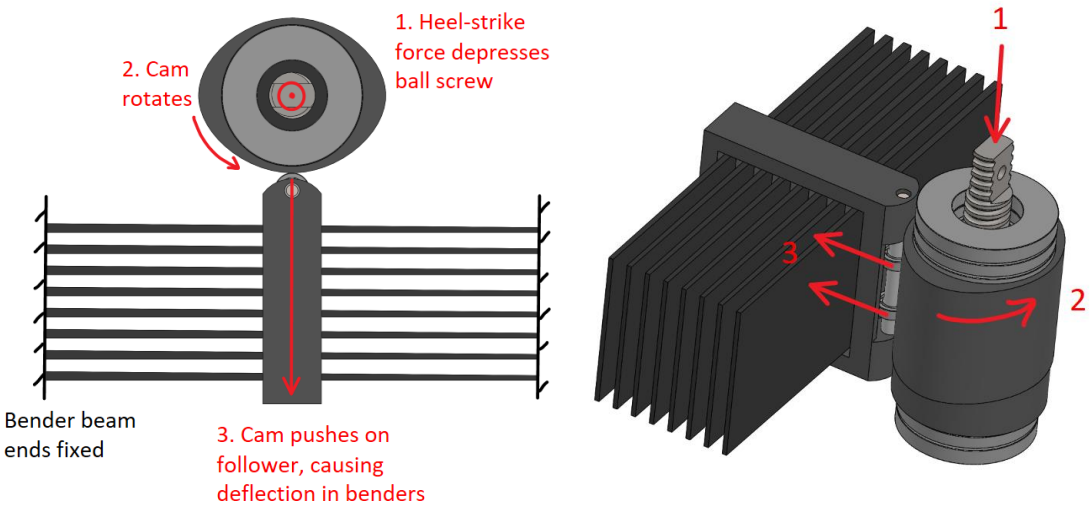

Figure 3.2. Operating principle of the ball screw and cam frequency up-conversion mechanism.

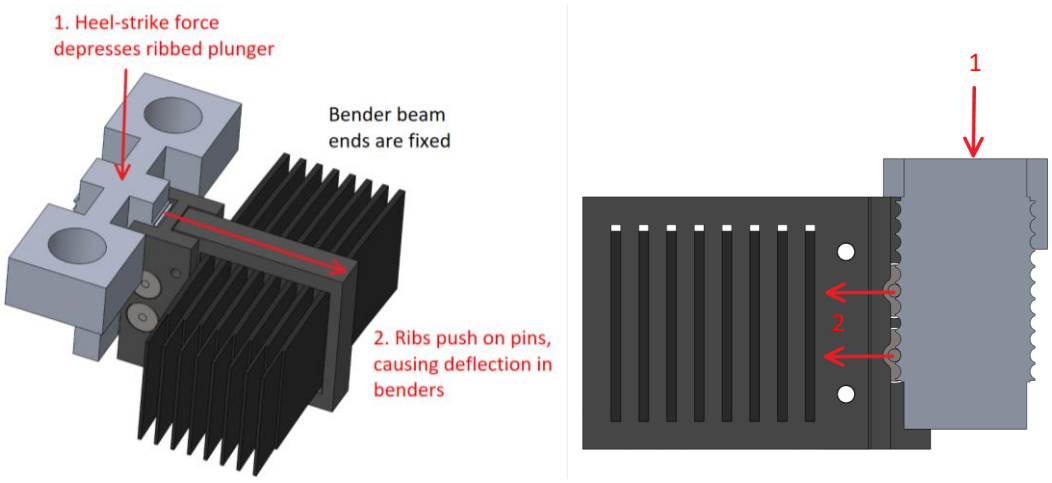

Figure 3.3. Operating principle of the ribbed plunger frequency up-conversion mechanism.

implemented in the ball screw-driven cam (BSC) and ribbed plunger (RP) frequency up-conversion mechanisms, respectively.

In order to develop the SBEH designs in which these frequency up-conversion mechanisms are realized, other aspects of the design must first be considered. Section 3.3.2 discusses how 31-mode piezoelectric bender elements can be implemented in an SBEH design. Section 3.3.3 then discusses the advantages of and mechanisms necessary to pre-stress these piezoelectric elements. Section 3.3.4 reviews how spring return mechanisms can be combined with the other elements to increase power output and match SBEH behavior to shoes. Then, in Sections 3.3.5 and 3.3.6, the RP and BSC frequency up-conversion mechanism are reviewed in-depth. Section 3.4 analyzes the two SBEH designs based on these up-conversion mechanisms, which requires incorporating the interactions of all the aforementioned elements.

3.3.2 31-mode benders

A central consideration in the design of this SBEH was reproducibility. Using commercially available PZT benders allows this design to be easily reproduced, modified, and reconfigured. Based on the space efficiency and power output of Xie & Cai's 2014 SBEH [39] design, a similar configuration placing a two rows of benders mechanically and electrically in parallel was adopted. These benders are deflected horizontally (normal to the vertical force imparted by the heel strike) through the two aforementioned frequency up-conversion mechanisms, rather than Xie & Cai's direct transfer using a wedged plunger. The benders selected were Python PUA 3014-5H200 manufactured by Bimitech Inc. These benders are comprised of a layer of PZT-5H bonded to a carbon fiber substrate sandwiched between epoxy and silicone rubber layers, as shown in Figure 3.4.

This single piezoelectric layer bonded to a non-piezoelectric substrate is referred to as a unimorph or asymmetric heterogenous bimorph in the literature. Publications in the

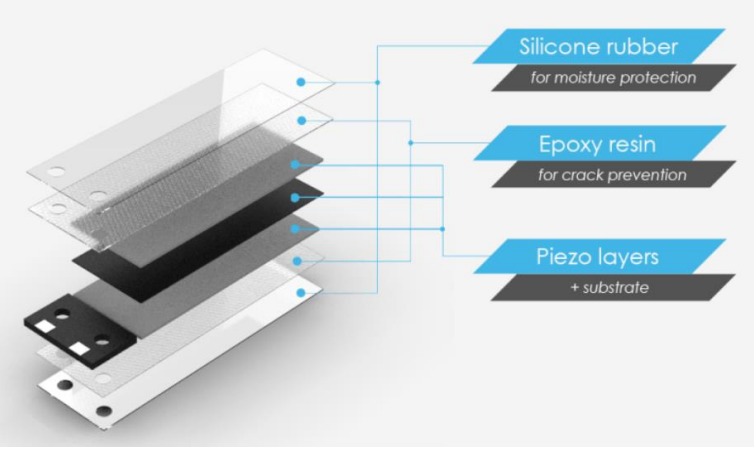

Figure 3.4. Exploded view of Python series piezoelectric benders sold by Bimitech Inc. [99].

last 15 years tend to use bimorph to refer to a non-piezoelectric substrate with a piezoelectric film bonded to both sides, so the term unimorph will be used here to differentiate.

PZT, like other ceramics, has a significantly higher stress limit in compression than in tension. When deflected, bimorph benders place one piezoelectric layer in tension and the other in compression. Thus, the maximum deflection is always limited by the stress state of the side in tension. A unimorph, on the other hand, can be deflected such that it puts its single piezoelectric layer in tension or compression, deflected in either direction a distance appropriate to near its maximum stress state. Thus, unimorphs can be configured to get more power output per volume of piezoelectric material.

These benders were selected for their small package, relatively high deflection, and durability-focused design choices such as thermally isolated solder pads, moisture resistance, and anti-cracking layers. The bender's overall length is 40 mm (modified), width 14 mm, and thickness 0.55 mm, while the PZT-5H patch itself measures 30x14x0.2 mm. Total failure of a piezoceramic element can occur when micro-cracks grow under cyclic stress or a crack suddenly splits the piezoelectric film due to high deflection. This is a chief performance tradeoff for any piezoceramic-based 31-mode SBEH: too little deflection and power output per volume of piezoelectric material decreases, too much deflection and the device can fail due to chronic or acute over-stressing.

3.3.3 Pre-stressed piezoelectric elements

The bender elements selected for this SBEH have a pre-curved design: with no applied stress, they have a dome height of 0.45 mm, as shown in Figure 3.5. Flattening the bender (maximum deflection of +0.42 mm) puts the PZT layer in tension, while further curving the bender (maximum deflection ~ -1.0 mm) puts the PZT in compression. Greater displacements can be achieved in the latter direction due to PZT's higher stress limit in compression. In the same piezoelectric bender without pre-curve, 0.4 mm and 1.0 mm deflection corresponds to strains of 0.018% and 0.044% versus PZT's strain limit of 0.050% reported in [6]. Private correspondence with the bender's manufacturer indicates that these displacements actually near the stress limit in each direction due to the pre-curved state.

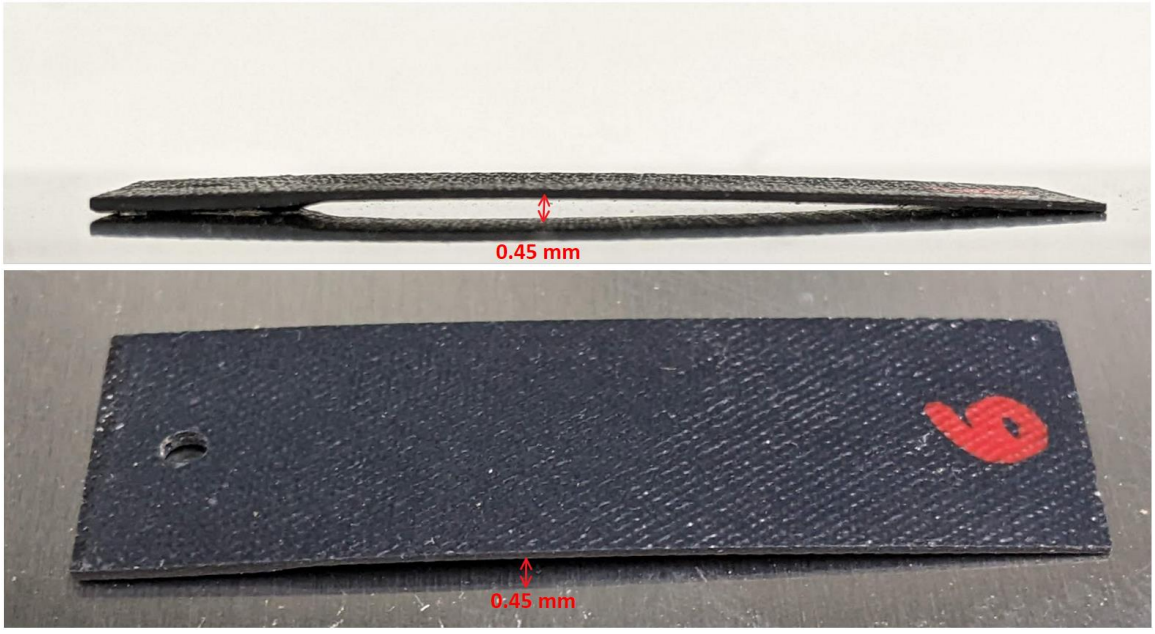

Figure 3.5. Pre-curved piezoelectric bender elements. 0.45 mm dome height is indicated by the red arrow.

In [100], it was found that pre-stressing a piezoelectric element (in this case achieved with a domed RAINBOW bender) can increase its effective d_{31} coefficient, with [101] finding an energy harvesting efficiency increase of 141% with an optimal level of pre-stress. Leinonen at al. [69] applied the findings in [101] by using springs to mechanically pre-stress PZT diaphragms in their SBEH. In the ball screw-driven SBEH presented in this work, springs are similarly used to pre-stress each row of PZT benders. Specifically, the benders are deflected +0.4 mm to placed them close to their stress limit in tension, and then can be deflected -1.4 mm to approach their stress limit in compression.

3.3.4 Spring return system

Any SBEH which experiences a vertical displacement due to the heel-strike must have mechanical elements to restore its original position. In most PZT-based implementations thus far, this has been achieved through the restoring force of the bender beams themselves, supplied mainly by the substrate material to which the PZT film is bonded. However, this is only possible if there is a single bender deflection per step; any mechanical frequency up-conversion mechanism will result in bender forces restoring harvester position only to the position of its last deflection cycle. Thus, the frequency up-conversion-based SBEH developed Yin et al. and Howells et al. both used rotational springs to return the harvester's heel-strike pad to its original position. Though such a system adds mechanical complexity, it also has some distinct advantages.

Spring systems generally have 95% ERP compared to the ~70% ERP of foam polymers that comprise shoe soles [6]. Thus, a spring return system in an SBEH can

provide the same restoring force or ERP found in shoe soles, leaving the energy normally dissipated as heat in foam polymers to be harvested through the electromechanical transduction mechanism. Spring systems in non-harvesting shoes have even been shown to increase running economy by 2-3% [6], suggesting that these systems need not increase the metabolic cost dimension of user burden. Spring return systems are also a convenient avenue to easily adjust overall harvester stiffness to match the behavior of specific shoes. Additionally, the mechanism enables energy generation from the restorative energy output in addition to the input forces, such as in Xie & Cai's 2015 electromagnetic SBEH [21]. This effectively doubles the time during which energy can be generated during the gait cycle from the heel-strike's 0.2 compression to 0.4 s, or $2/5^{th}$ of the overall gait cycle time of 1.0 s (see in Section 2.1.3).

3.3.5 Ribbed plunger harvester design

The first SBEH developed in this work served as a proof-of-concept for frequency up-conversion using 31-mode benders and a spring return mechanism and utilizes a ribbed plunger frequency up-conversion mechanism (RP). Annotated section views of the device are shown in Figure 3.6.

A force imparted on the heel-strike pad (1) depresses the ribbed plunger (2) which is limited to vertical Y-direction displacement by post-mounted (3) linear bearings (4). The ribbed plunger, in turn, compresses two springs (5) which are concentric with the linear bearings. When displaced vertically, each rib pushes bearing-mounted roller pins (6) horizontally in the Z-direction, which displaces the grate (7) that clamps the centerline of

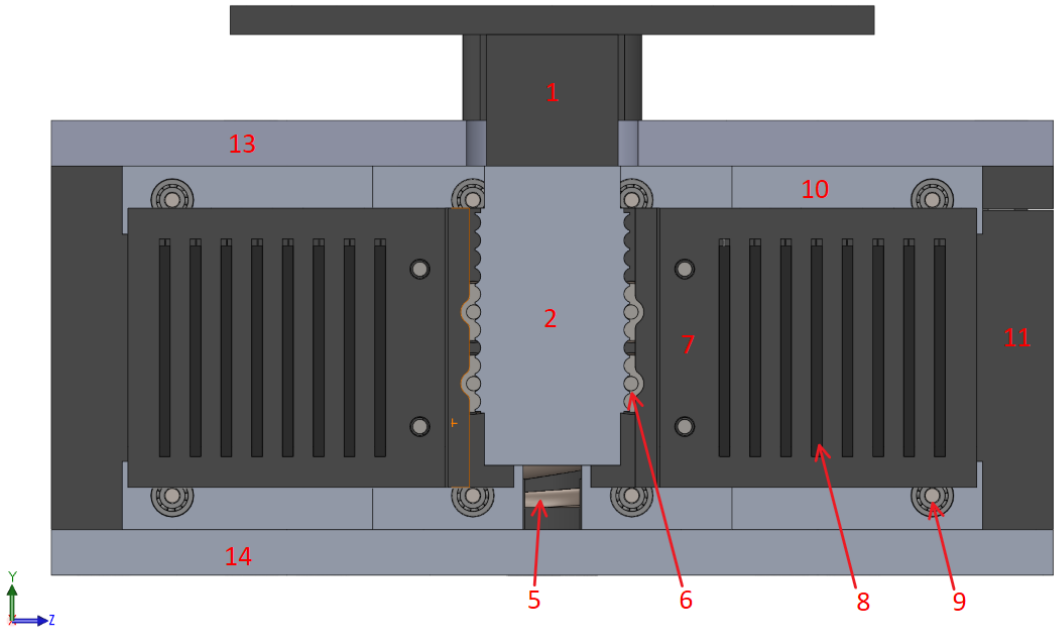

(a)

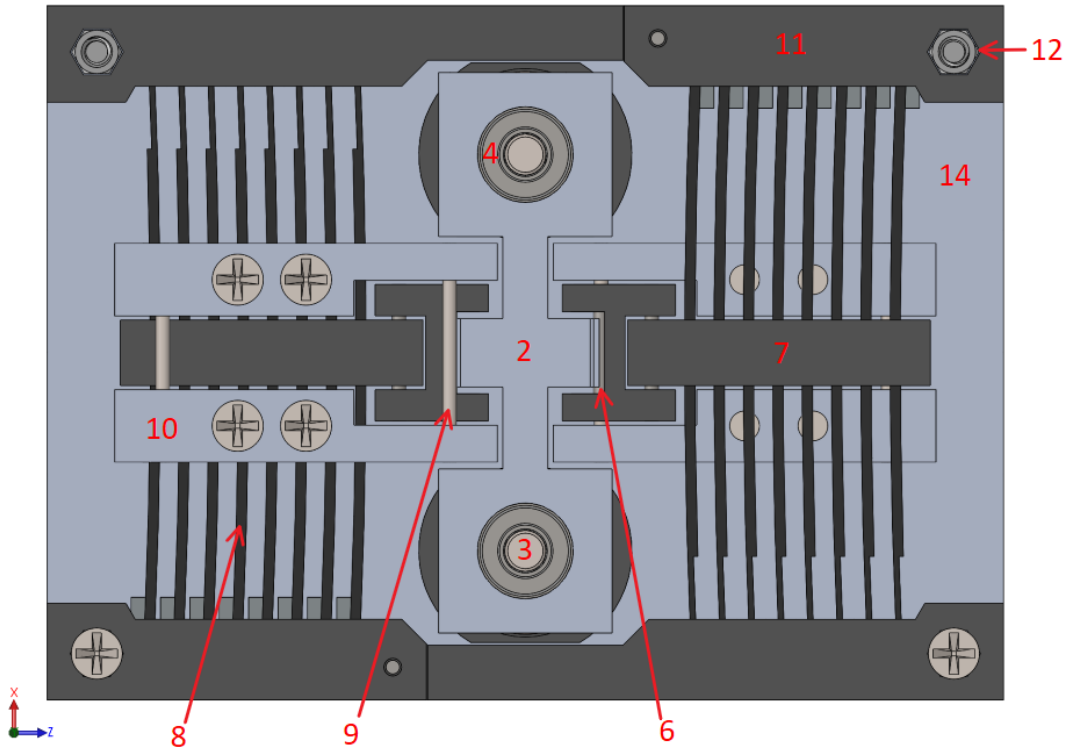

(b)

Figure 3.6. Annotated side (a) and top (b) section views of ribbed plunger harvester design.

the 8 PZT benders (8) placed in parallel on either side of the harvester. Each grate is constrained to Z-direction-only displacement by four more bearing-mounted roller pins (9) that prevent Y-direction displacement, and the machined aluminum bearing blocks (10) that prevent X-direction displacement. The ends of the benders are held stationary in slots within the harvester's 3D printed side frames (11). Steel female-to-female threaded hex standoffs (12) run through the frame at each corner and connect the 2 mm-thick water-jetted aluminum top (13) and bottom plates (14), creating a robust structural skeleton that protects internal components from overloading. Once the force on the heel pad is removed, the compressed springs force the ribbed plunger upwards into its original position, deflecting the beams again as each rib passes over the grate's roller pins. Isometric views of the design are shown in Figure 3.7.

The benders, 16 in total, are oriented such that the rib-induced deflection displaces

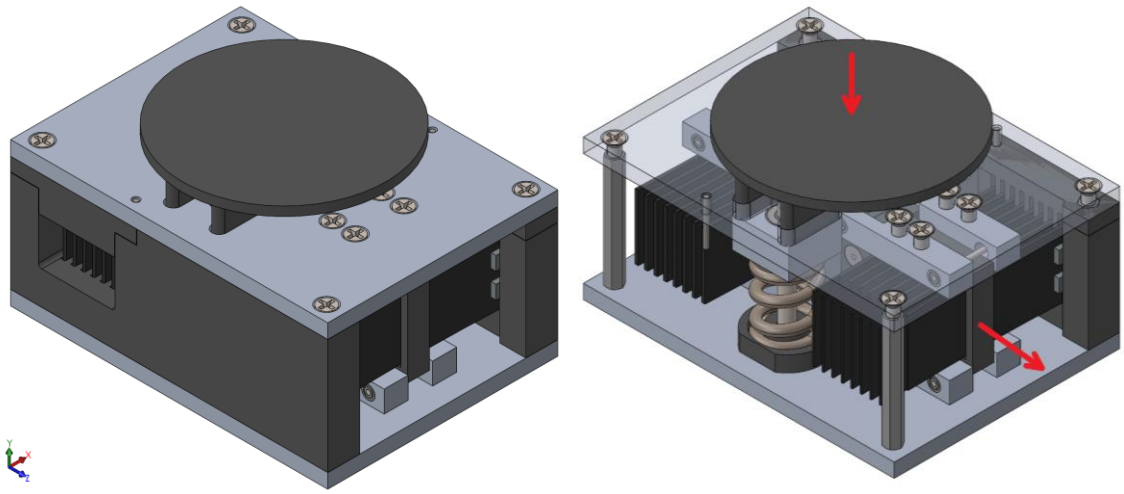

(a) (b)

Figure 3.7. Isometric view of ribbed plunger harvester design (a) with one side frame hidden and the top plate transparent (b). Red arrows indicate element displacements.

them +0.4 mm in tension, flattening their pre-curved state. The restoring force which keeps the grate roller pins (6) pressed against the ribbed plunger (2) is supplied by the stress developed in the benders. The number of ribs on the ribbed plunger, shown in Figure 3.8, was constrained by the diameter of the grate roller pins, which were in turn limited by the shaft diameter of the bearings in which they were mounted. The smallest readily available bearings have a shaft diameter of 1 mm, and any smaller diameter for the roller pins could compromise their robustness. Based on testing many different ribbed plunger geometries, it was determined that a rounded, roughly sinusoidal pattern of period 1.25 mm and a peak-to-valley amplitude of 0.4 mm were ideal. Besides being the maximum allowable deflection in tension, a rib amplitude of 0.5 mm or greater resulted in the roller pins not fully entering the valley of the ribbed curve under 1 Hz dynamic loading. The same

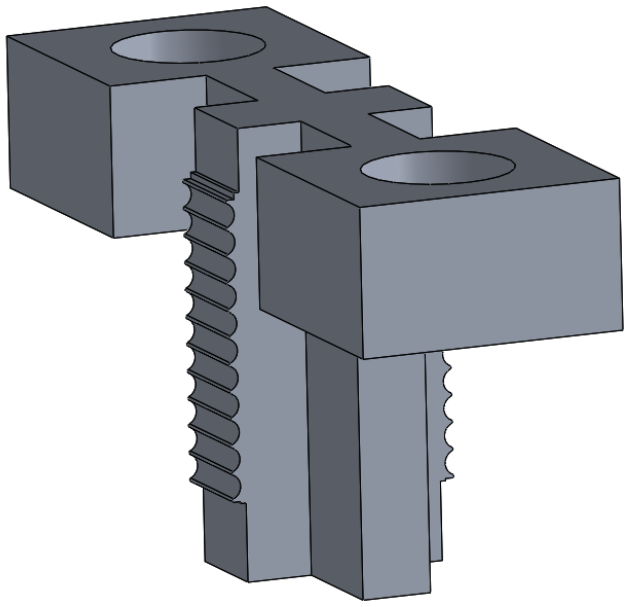

Figure 3.8. Ribbed plunger geometry. The rib pattern has an amplitude of 0.4 mm and a period of 1.25 mm. Linear bearings are press-fit in the top surface's two holes.

occurred at rib periods less than 1.25 mm. This results in reduced bender displacement and increased rib wear. Thus, an input displacement of 3.75 mm results in 3 bender displacements on the downstroke and 3 on the spring-powered upstroke for a total 6x up-conversion, while a 5 mm input displacement results in 8x up-conversion. This design can accommodate a maximum displacement of 7.5 mm for 12x up-conversion.

Because the RP SBEH design served as proof-of-concept rather than an end product, it was designed for maximum configurability and ease of testing rather than minimum size. The result, at 70 mm long, 51 mm wide, and 38 mm high, was impractically large but demonstrated the feasibility of design choices. Because of its size, this harvester was not intended to be integrated in a shoe, though many of the improvements implemented in the next SBEH design could easily be applied to this prototype.

The power output performance of this prototype is discussed in Section 4.3.1, while the upsides and downside of its performance are summarized in Chapter 5.

3.3.6 Ball screw and cam harvester design

The second SBEH design shares many parts with the RP design in a more compact form factor. The main differences are its ball screw and cam (BSC) frequency up-conversion mechanism, increased bender displacement, and a bender pre-stress mechanism. Annotated section views of the device are shown in Figure 3.9; isometric views of the device are pictured in Figure 3.10.

When a force is applied to the heel-strike pad (1), the ball screw shaft (2) imparts force on the ball bearing ‘threads’ of the ball nut (3), back driving the nut. The ball nut is

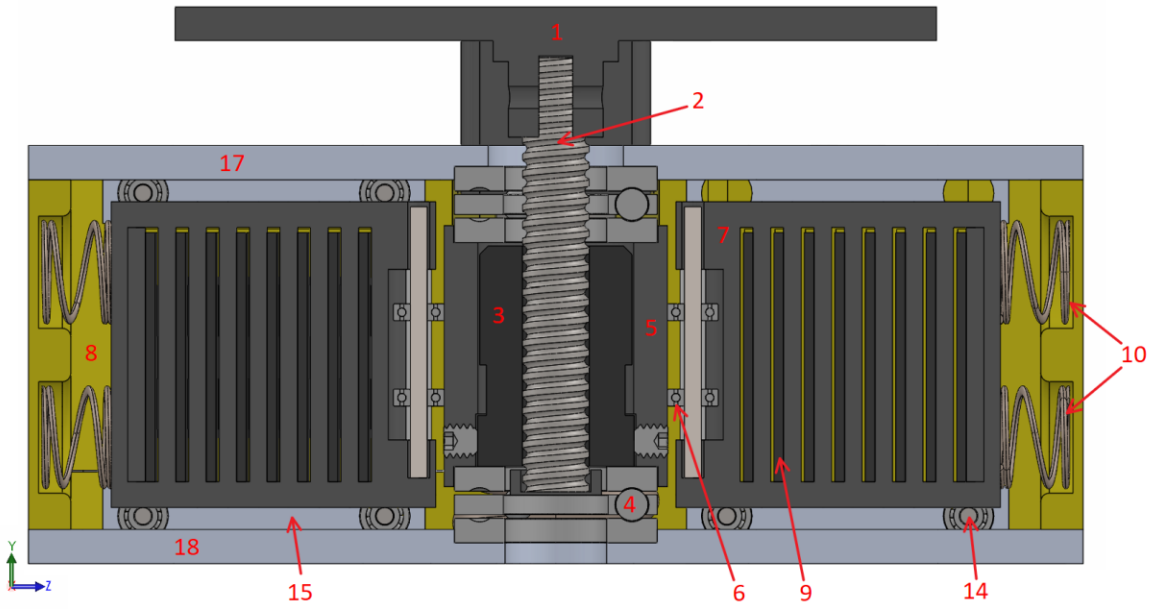

(a)

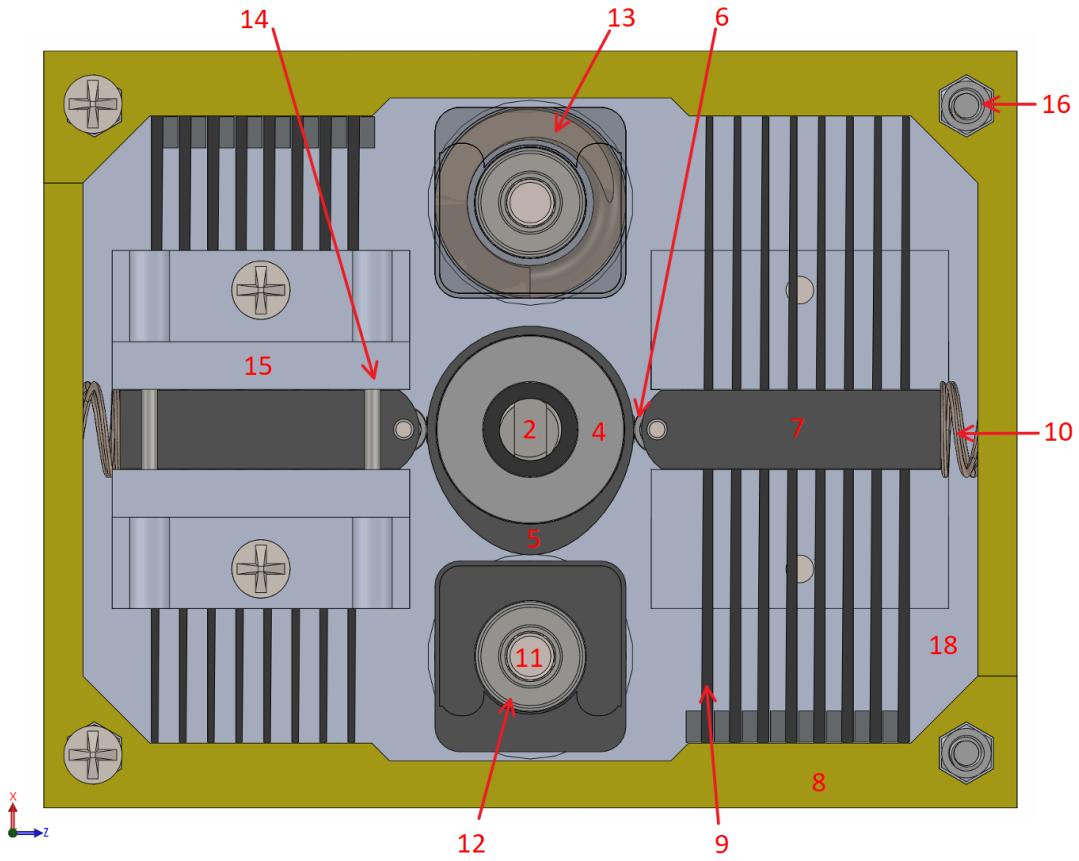

(b)

Figure 3.9. Annotated side (a) and top (b) section views of ball screw and cam harvester design. The frame is shown in yellow for clarity.

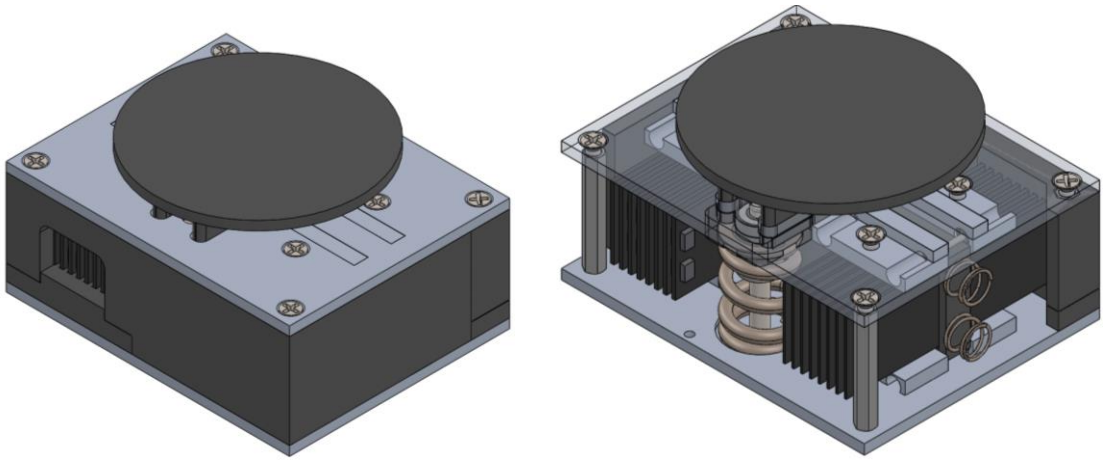

(a) (b)

Figure 3.10. Isometric view of ball nut and cam harvester design (a) with half of the frame hidden and the top plate transparent (b).

held in place by two thrust bearings (4) to which it is coupled to through a 3D printed cam sleeve (5). As the nut rotates due to back driving, the cam presses on the bearing roller follower (6) at the front of the grate (7). Again, this grate clamps the bender elements at their center point while their ends are held stationary by the side frames (8), shown in yellow for clarity. Thus, the cam displaces the grate, deflecting each bender (9). Rather than the restoring force against the cam being supplied by the benders alone, two pre-stress springs (10) are embedded in the side frame per grate. These springs deflect the beams +0.4 mm in tension when the system is at rest and are compressed -1.4 mm by the cam lobes as the cam rotates, achieving a final deflection in the bender of -1.0 mm relative to its unstressed state.

The heel-strike pad's motion, guided again by post-mounted (11) linear bearings (12), compresses two springs (13) which supply the restorative force to drive the cam in the opposite direction when the input force is removed. The same combination of bearing-

mounted horizontal roller pins (14) and bearing blocks (15) constrains the motion of the grates, and the same system of hex standoffs (16) and aluminum top (17) and bottom (18) plates gives the device structural rigidity. Though these views show the harvester with a single-lobe cam, cams with up to five lobes were tested in the device.

The miniature ball screw used in this design is model SR0401K Ct7 manufactured by KSS Co. It has a single start and 1 mm lead, meaning displacing it 1 mm relative to the ball nut will result in one complete revolution of the nut. Thus, with a single-lobed cam, an input displacement of 4 mm will result in 8x frequency up-conversion, or 8 1.4mm PZT bender deflections per step. A five-lobed cam at this design's maximum input displacement of 6 mm yields 60x frequency up-conversion.

In contrast to the ribbed plunger design, this SBEH was designed with minimal volume in mind. Its overall dimensions are 62.3 mm long, 48.4 mm wide, and 30.9 mm or 32.9 mm tall in its 4 mm and 6 mm displacement configurations, respectively. This equates to overall volumes of 93.2 cm^3 and 99.2 cm^3, just barely below the maximum target volume of 100 cm^3. However, the overall height of the device could easily be decreased by 5 mm if the flange on the ball nut was completely machined off; this was not done because of the risk of damaging the ball nut and affecting the project's timeline. This would decrease the volume to 78.1 cm^3 or 84.1 cm^3 for the 4 mm and 6 mm displacement configurations. The device weighs 104 g in its final assembled state, barely exceeding the target of 100 g.

3.4 Theoretical behavior

3.4.1 Power output

Both SBEH designs developed in this work operate on the principle of deflecting simply supported PZT benders in 31-mode through loading at their center points. To evaluate theoretical performance during the design phase and validate prototype performance against expected benchmarks, a MATLAB model was built to calculate SBEH power output at a given frequency, input force, input deflection, and beam deflection.

The benders are represented as simply supported composite beams comprised of one layer of PZT and one layer of carbon fiber substrate. It is assumed that the epoxy and silicone layers make no significant contribution to the bender's overall stiffness. The PZT layer is 0.2 mm thick with a Young's modulus of 63 GPa, while the carbon fiber layer is 0.15 mm thick with a Young's modulus of 180 GPa (manufacturer supplied). The beam's supported dimensions are 40 mm long and 14 mm wide, though the PZT material only covers 30 mm of this span. Assuming that the PZT covers the entire length of the beam simplifies calculations and was adopted. Additionally, the mechanics of the bender's pre-curved state were ignored and the following calculations assume a bender which is flat under zero stress.

Using the transformed section method, the neutral axis of this beam was found as

$$z_{neutral} = \frac{t_{PZT}}{2} \frac{1 + 2\left(\frac{t_S}{t_{PZT}}\right) + \left(\frac{Y_s}{Y_{PZT}}\right)\left(\frac{t_S}{t_{PZT}}\right)^2}{1 + \left(\frac{Y_s}{Y_{PZT}}\right)\left(\frac{t_S}{t_{PZT}}\right)^2} \tag{3.2}$$

[66] where $z_{neutral}$ is the location of the neutral axis through the beam's thickness starting from the substrate size, t_{PZT} is the thickness of the PZT layer, t_S is the thickness of the substrate layer, Y_{PZT} is the 11-direction Young's modulus of PZT, and Y_s is the Young's modulus of the substrate layer. From the figure, the moment of inertia about the beam's neutral axis ($I_{transformed}$) can be calculated using the parallel axis theorem.

This work's SBEH designs are based on a prescribed maximum beam deflection rather than a force imparted on the beam. Thus, the force necessary to deflect the PZT benders was calculated as

$$F_{beam} = 48 * Y_{PZT}^{11} * I_{transformed} * \frac{\delta_{max}}{L^3} \tag{3.3}$$

where F is the force imparted on the beam, Y_{PZT} is the 11-direction Young's modulus of PZT, $I_{transformed}$ is the moment of inertia of the transformed beam (transformed into PZT rather than carbon fiber), δ_{max} is the maximum centerline displacement achieved in the beam, and L is the beam's length.

The maximum bending moment developed in the beam occurs at its centerline and is calculated as

$$M_{max} = \frac{F_{beam}L}{4} \tag{3.4}$$

The average bending moment in the PZT layer is necessary to calculate the average strain developed and therefore the voltage output. The moment in the beam reaches a maximum value at its centerline and decreases linearly to zero at each end, so the average moment in the beam is half the value of the maximum moment. The average stress in the PZT is then

$$T_{PZT,avg} = \frac{M_{avg} * c_{avg}}{I_{transformed}} \tag{3.5}$$

where c_{avg} is the distance from the composite beam's neutral axis to axis of average stress in the PZT layer, which can be found by linearly interpolating the maximum (surface) and minimum (bond line) stresses in the PZT layer. The average strain in the PZT layer can then be calculated according to Hooke's law

$$S_{PZT,avg} = \frac{T_{PZT,avg}}{Y_{PZT}^{11}} \tag{3.6}$$

The preceding steps can be represented by the equation

$$S_{PZT,avg} = \frac{3\delta_{max} t_{PZT}}{L^2} \frac{t_s}{t_{PZT}} \frac{1 + \frac{t_s}{t_{PZT}}}{1 + \frac{t_s}{t_{PZT}} / \frac{Y_s}{Y_{PZT}}} \tag{3.7}$$

as derived in [66], where t_s and Y_s are the thickness and Young's modulus of the substrate material. The peak voltage can then be calculated as

$$|V_p| = \frac{d_{31} Y_{PZT} A S_{PZT,avg} \omega R}{\sqrt{1 + \omega^2 C^2 R^2}} \tag{3.8}$$

[66], [12] where *A* is the area of the beam, ω is the input angular frequency, *R* is the load resistance, and *C* is the capacitance of the piezoelectric material— 45 nF per bender, in this case. Normally, the generated power would be consumed by a low-power device or stored in a supercapacitor or battery, but for the purposes of power generation testing it is sufficient to measure the power through a load resistance which stands in for a useful electronic load. The peak power output can then be expressed as

$$P = \frac{1}{2} \frac{|V_p|^2}{R} = \frac{\left(d_{31} Y_{PZT} A S_{PZT,avg} \omega\right)^2 R}{2(1 + \omega^2 C^2 R^2)} \tag{3.9}$$

The optimal load resistance for a piezoelectric material at a given excitation frequency and capacitance is

$$R_{opt} = \frac{1}{\omega C} \tag{3.10}$$

and, substituting Equation 3.10 into Equation 3.9, the maximum peak power is

$$P_{max} = \frac{d_{31}^2 Y_{PZT}^2 S_{PZT,avg}^2 A^2 \omega}{4C} \tag{3.11}$$

In order to get accurate estimates for the input force needed to deflect the PZT benders, it was necessary to assume that the piezoelectric material covered the entire 40 mm length of the beam instead of its 30 mm actual length. However, to accurately estimate the strain developed in the PZT layer and thus voltage and power output, it is useful to rerun these calculations assuming the entire beam is 30 mm long and that the input deflections are equivalent to the deflection experienced by the central 30 mm of the 40 mm long beam. For example, an input deflection of 1.4 mm imparted on the 40 mm simply supported beam results in 0.79 mm deflection in the 30 mm central section of the beam covered by the PZT material, as shown in Figure 3.11.

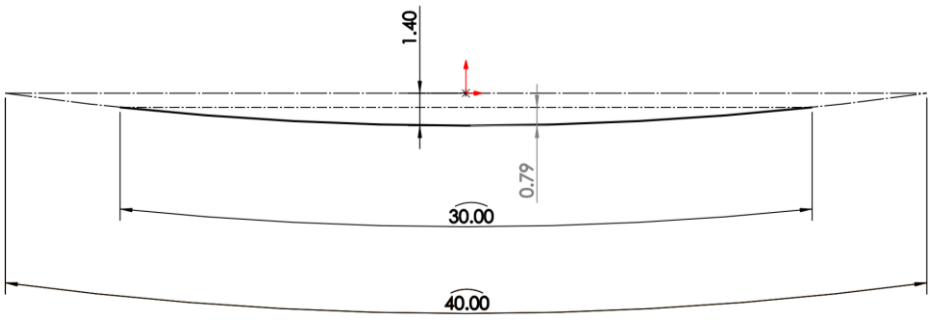

Figure 3.11. A displacement of 1.4 mm developed in a 40 mm beam results in 0.79 mm displacement in its central 30 mm.

Based on these figures, Table 3.1 presents the requisite input force, PZT layer average stress, average stain, maximum strain, peak voltage, and RMS voltage. Note that it was determined experimentally that RMS voltage is equal to about 0.175 times the peak voltage at a simulated walking input frequency of 1 Hz.

Table 3.2 presents theoretical values for the peak voltage, RMS voltage, and RMS power output of the SBEH developed in this work as a function of their vertical input displacement *x*, maximum bender deflection $\delta_{\max}$, and frequency up-conversion.

3.4.2 Stiffness and force-displacement profile

Matching the stiffness of an SBEH to the sole in which it is integrated is key to minimizing user burden. Part of designing a SBEH from a user burden-first perspective, then, is to develop the design with its stiffness in mind.

The stiffness of the RP design is determined by the sum of the spring return system force and the force necessary for a rib to deflect a row of benders. The spring forces are simply calculated as

Table 3.1. Beam deflection force, average stress, average strain, and maximum strain in a single composite beam PZT layer at various beam deflections.

δ_{max} (mm)	F *(N)*	$T_{PZT,avg}$ *(MPa)*	$S_{PZT,avg}$ *(%)*	$S_{PZT,max}$ *(%)*	V_{pp} *(V)*	V_{rms} *(V)*
0.4	1.49	11.3	0.018	0.066	22.5	3.93
1.0	3.74	28.2	0.045	0.164	54.7	9.57
1.4	5.23	39.5	0.063	0.230	77.1	13.50

Table 3.2. Theoretical voltage and power output of the developed SBEH.

Design	*x (mm)*	δ_{max} (mm)	*No. benders*	δ_{max} (mm)	*Frequency (Hz)*	V_p *(V)*	V_{rms} *(V)*	P_{rms} *(mW)*
Ribbed plunger	3.75	0.4	16	0.4	6	22.5	3.94	0.40
Ball screw (minimum)	4	1.4	16	1.4	8	77.1	13.5	3.18
Ball screw (maximum)	6	1.4	16	1.4	60	77.1	13.5	47.4

$$F = kx \tag{3.12}$$

where *k* is the spring constant and *x* is the compression of the springs, equivalent to the vertical displacement of the heel-strike pad. The vertical input force necessary for the ribs to deflect a row of benders horizontally can be calculated using energy methods as

$$F = \frac{F_{beam} * \delta_{max} * N_{beams}}{T_{rib}} \tag{3.13}$$

where F_{beams} is the force necessary to deflect the bender beams a distance δ_{max}, which is calculated using Equation 3.3, N_{beams} is the number of beams placed in parallel and T_{rib} is the rib's period. At a bender displacement of 0.4 mm, F_{beams} is 1.49 N (as shown in Table 3.1). Assuming that the ribs on either side of the ribbed plunger are in phase, the plunger deflects two sets of 8 benders placed in parallel simultaneously for N_{beams} of 16, and a rib period of 1.25 mm was found to be optimal (see Section 3.3.5). This results in a

peak vertical reaction force of 7.63 N each time the beams are deflected; the magnitude of this force varies sinusoidally between its maximum value and zero according to the roughly sinusoidal rib geometry. It is possible to half this maximum vertical reaction force if the ribs on either side of the plunger are 180° out of phase, but this configuration was found to introduce lateral play in the system, decreasing the overall deflection experienced by the benders.

Since this force varies sinusoidally, it does not contribute to the equivalent stiffness of the system but does contribute to the system's force-displacement behavior. Thus, the compression springs must supply the full measure of the shoe sole's equivalent stiffness and should be selected to match the stiffness of the shoe's sole; in this case, about 72 N/mm. The force-displacement profile therefore should look like a sinusoidal force component of magnitude 7.63 N superimposed upon an otherwise smooth hysteresis curve. The energy dissipated in this system should be quite low and is due almost entirely to frictional losses at the interface between the grate roller pins and the ribbed plunger surface as well as friction in bearings and minimal losses in the springs.

A similar case is found with the BSC mechanism, though the sinusoidal contribution to the force-displacement profile is much greater; perhaps excessively so. The torque developed by the ball screw when a linear force is applied can be calculated as

$$T = \frac{l\,\eta_B F}{2\pi} \tag{3.14}$$

[102], [103] where l is the ball screw's lead, η_B is its back driving or reverse efficiency, and F is the applied force. Back driving is the condition in which a linear displacement is

being translated into a torque rather than positive or forward driving operation in which a torque is converted to a linear displacement. The back driving efficiency is calculated as

$$\eta_B = \frac{1 - \frac{\mu}{\tan(\beta)}}{1 - \mu \tan(\beta)} \tag{3.15}$$

[103] where μ is the coefficient of friction between the ball nut and screw, and β is the ball screw's lead angle

$$\tan(\beta) = \frac{l}{2\pi d_r} \tag{3.16}$$

calculated using the screw's lead and root diameter d_r.

The miniature ball screw used in the BSC design has a lead of 1.0 mm, a major diameter of 3.95 mm, and a root diameter of 3.4 mm. Though not supplied by the manufacturer, the coefficient of friction μ was conservatively estimated at 0.01 through the guidance in [102], though 0.05 may be more realistic. These figures yield a lead angle of 5.35°, a back driving efficiency of 89.2%, and a developed torque of 0.89 Nm.

In this design, the force imparted on the cams by the cam followers is significantly higher than the force imparted on the ribs by the grate roller pins in the RP design. This is because of the increased deflection the BSC design imparts on the benders (1.4 mm versus 0.4 mm in RP design), and because the cams must also compress the springs used to pre-stress the benders in tension. The total force of the cam follower on the cam lobe as a function of beam deflection is represented by

$$F_{follower} = F_{beam}\delta N_{beams} + 2k_{pre-stress}\delta \tag{3.17}$$

where F_{beam} is bender beam reaction force calculated using Equation 3.3, δ is the bender deflection caused by the cam lobe, and $k_{pre-stress}$ is the spring coefficient of the pre-stress springs, of which there are two per row of 8 bender beams. In this BSC design, the pre-stress springs have been selected and configured to result in zero follower force on the cam at zero bender displacement.

With the cam follower force known, it is possible to calculate the torque necessary to drive a cam of a given geometry. That torque is given by

$$T_{cam} = F_{follower}d_{SC}\tan(\alpha) \tag{3.18}$$

where d_{SC} is the distance from the shaft center (in this case, the center of the ball screw) to the point of contact between the cam and cam follower, and α is the pressure angle between the cam and follower.

The maximum torques required to drive cams of various lobe counts developed for this design are summarized in Table 3.3. Generally, as the number of lobes increases, larger pressure angles occur which increases the required driving torque. It should be noted that cams with an odd number of lobes have lower maximum required torques than a cam with a lesser, even number of lobes; this is because even-lobed cams deflect both rows of benders simultaneously, doubling the follower force in the cam, while odd-lobed cams avoid this issue. An odd-numbered cam also benefits from that fact that the resisting

Table 3.3. Maximum torque required to drive BSC design cams of various lobe counts.

No. lobes	*1*	*2*	*3*	*4*	*5*	*6*
$T_{cam,max}$ *(Nm)*	0.060	0.120	0.077	0.217	0.126	0.333
$F_{reaction,max}$ *(N)*	340	681	437	1231	715	1889

torques [104] developed by the follower forces from bender rows on either side of the cam oppose each other and therefore decrease the net torque imposed on the cam. For example, in the 5-lobed cam, the follower being lifted imparts a +0.136 Nm torque on the cam, while the follower being lowered imparts a -0.010 Nm torque on the cam, decreasing the net torque imposed to +0.126 Nm.

Compared to the ball screw's driving torque of 0.089 Nm, the 1- and 3-lobed cams can be driven without issue, while the 4- and 5-lobed cams seem to be a stretch. It can be seen that a 6-lobed cam requires expected driving torques too great to use as designed.

The maximum vertical reaction forces imposed on the user's foot through the heel-strike pad due to the resisting torque of the follower on the cam in this design are calculated as

$$F_{reaction,max} = \frac{2\pi\eta_F T_{cam,max}}{l} \tag{3.19}$$

where η_F is the ball screw's forward-driving efficiency. This force is equivalent to the minimum force needed to deflect the beams using a given cam profile. Its magnitude is on the same order as the heel-strike input force itself, which could be expected to cause significant discomfort to the user. Having a sinusoidal component of the force-

displacement curve is a necessary condition of mechanical frequency up-conversion mechanisms. Thus, it is important to investigate the effects of this behavior on user burden later, as experimental evaluation alone can determine the true extent of these effects.

CHAPTER 4

EVALUATION AND EXPERIMENTAL RESULTS

4.1 Shoe behavior

To validate the analysis of shoe mechanical and energetic behavior developed in Section 2.2 and acquire more specific targets for harvester behavior, multiple pairs of shoes were tested using an Instron 5969 Universal Testing System to evaluate their force-displacement behavior. The guidelines of ASTM standard F1976-13 "Standard Test Method for Impact Attenuation of Athletic Shoe Cushioning Systems and Materials" were followed as closely as possible. Since the SBEH developed in this work was to be embedded in the sole's heel region, a 'tup' or indenter in a rough shape of the heel was machined per the specifications of ASTM F1975-13: a flat, circular surface 45 mm in diameter with a 1 mm edge fillet radius. When fixed in the testing machine, the tup was placed over the point in the center of the shoe's width and at 12% of its length from the heel. The test setup is shown in Figure 4.1

The test procedure for the shoes was matched to the input conditions of walking within the limits of the testing machine's capabilities. The shoe's sole was compressed between the tup and a flat platen by a triangle wave displacement input having a peak force of 600 N and an input frequency of 1 Hz. Thus, the loading rate (in N/mm and mm/s) depends upon the displacement achieved in the shoe sole with a 600 N force input and was

Figure 4.1. Shoe test setup using the Instron 5969 Universal Testing Machine.

adjusted to the shoe being tested. Before starting the test, the shoes' insoles were removed and a pre-load of 10 N was applied and established as the zero point of displacement to eliminate the effects of geometric variations in the shoes' sole surfaces. The notable deviations of this test from the conditions found in walking are 1) that a normal heel strike's compression occurs in the first 0.2 s of the 1 Hz gait cycle rather than the 0.5 s as in this test, and 2) that the heel strike input force is more accurately represented as a sinusoidal impulse than a triangle wave. However, the capabilities of the testing machine limited the tests to the aforementioned conditions.

The force-displacement curves collected from this test procedure enable calculation of the sole's Young's modulus, equivalent spring constant, total energy input, energy return

percent (ERP), and total energy dissipated. An ideal SBEH would match each of these values to eliminate user burden, these shoe tests directly yield target values for SBEH design. Figure 4.2 shows the force-displacement curve of a pair of Sketchers GoRun Elevate shoes, which is typical of the shoes tested. The maximum compression or displacement achieved at 600 N is 8.32 mm. The area underneath the top curve represents energy input; 2.15 J in this case. The area underneath the bottom curve is the energy returned to the shoe's wearer, or in this case the tup, and is in the amount of 1.52 J. The difference of these values—or the area enclosed by the two curves—is 0.63 J, the total energy dissipation in a single step and therefore the amount of energy available for harvesting. This equates to an ERP of 71%.

As discussed in Section 2.2.2, a shoe sole's force-displacement behavior is best represented as a nonlinear viscoelastic system, but in this case linear-equivalent figures are calculated for simplicity. Assuming a linear stress-strain relationship, Young's modulus values are calculated as

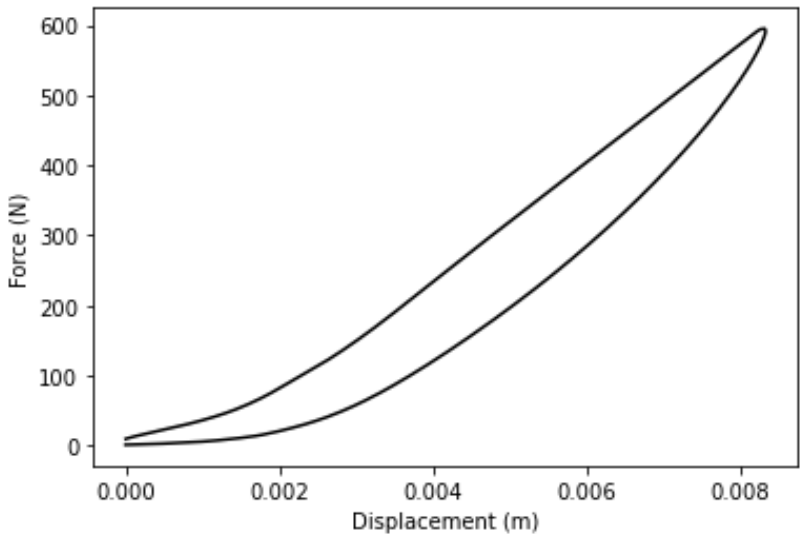

Figure 4.2. Force-displacement curve of Sketchers GoRun Elevate shoes.

$$E = \frac{FL_0}{A\Delta L} \tag{4.1}$$

where E is Young's modulus, F is the applied force, L_0 is initial length or the stack height of the shoe, A is the area of the tup used to compress the sole (analogous to the area of the heel), and ΔL is the amount of compression developed. The equivalent spring constant can then be calculated as

$$k = \frac{EA}{L_0} \tag{4.2}$$

where k is the equivalent spring constant.

Three pairs of shoes were tested for three trials each: a pair of casual shoes (Athletic Works), a pair of general-purpose athletic shoes (Adidas RunFalcon 2.0), and a pair of cushioned running shoes (Sketchers GoRun Elevate). The average results of the test trials conducted on these shoes (in which very low variances were observed) are summarized in Table 4.1, alongside assumed values from the literature and the expected values calculated using the methods of Equation 2.3.

All three shoes behave similarly to the expected conditions, with the Sketchers and Athletic Works especially so. Using the measured ERP and displacement at a known maximum input force of 600 N, Equation 2.3 predicts that the Sketchers would dissipate 0.73 J rather than the 0.63 J observed (14% lower); 0.96 J is expected in the Athletic Works versus the 0.92 J observed (4% lower). Thus, it seems that modeling the sole's behavior as

Table 4.1. Mechanical and energetic parameters of tested shoes and expected values.

Shoe	*Athletic Works (Casual)*	*Adidas (Athletic)*	*Sketchers (Running)*	*Expected (Eq. 2.3)*
Max. displacement (mm)	8.68	5.29	8.32	8.00*
Energy input (J)	2.50	1.64	2.15	2.4
Energy returned (J)	1.58	1.13	1.52	1.68
Energy dissipated (J)	0.92	0.51	0.63	0.72
ERP (%)	63.2	68.9	70.7	70*
Stack height (mm)	26.0	27.8	33.0	NA
Young's modulus (MPa)	1.13	1.98	1.50	NA
Equiv. spring const. (N/mm)	69.1	113.3	72.3	75

*Assumed value

a simple linear spring slightly overestimates the energy dissipation and power available at a given input force and resultant displacement. However, the model is certainly accurate enough to obtain useful estimates. Additionally, the 7% variation in ERP observed between these shoes is well within the range found in the literature, and may suggest that a lower ERP and thus higher energy dissipation can be found in more casual shoes.

In conclusion, the results of shoe testing align well with results in the literature and analysis developed in Section 2.2.2. To match eth behavior of normal shoes and therefore decrease user burden, SBEH should dissipate or harvest a maximum of 0.70 J per step and

exhibit an ERP of 70%.

4.2 Piezoelectric element testing

The piezoelectric bending elements around which the SBEH developed in this work are based were also tested using the Instron 5969. The goals of this testing were first to compare their mechanical and electrical behavior to that expected based on the analysis in Section 3.4.1, and then to establish a baseline against which the SBEH prototypes' performance can be evaluated.

To test the beams in tension—that is, flattening their pre-curved state—a simple 3D printed fixture and a small tup were used. The bender beams were deflected 0.4 mm in tension using a triangle wave input of frequency 1.0 Hz. This bender displacement matches that achieved in the ribbed plunger (RP) SBEH design. The voltage output of the beams varied widely due to previous handling and damage: among functional beams, an average beam peak-to-peak voltage (V_{pp}) output of 16.4 V and standard deviation of 6.0 V were observed. However, the benders clearly fell into three categories: normally functioning, damaged, and defunct. Examining only the normally functioning beams, an average peak-to-peak voltage of 19.5 V and standard deviation of 1.2 V were observed. This compares well with the 22.5 V peak-to-peak voltage expected from Equation 3.8 given that equation's many simplifying assumptions. Based on private correspondence with the bender's manufacturer, the lower 19.5 V achieved aligns with their expected output. Figure 4.2 shows a typical voltage output waveform for these tests, collected using a Tektronix MDO3014 Oscilloscope.

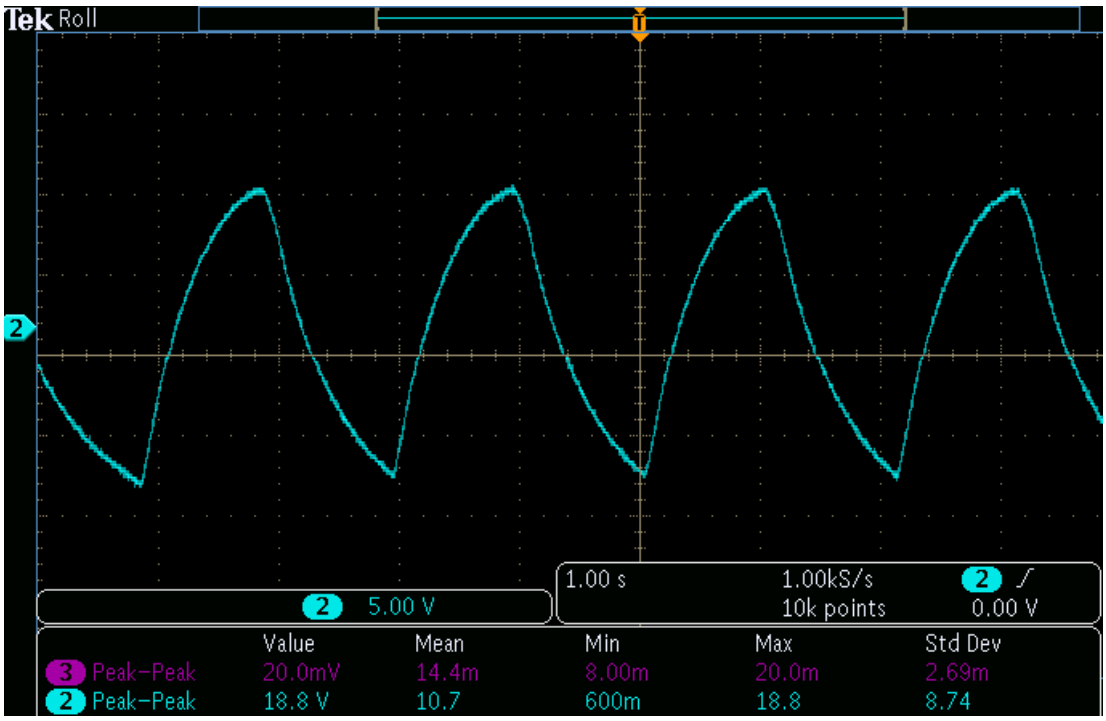

Figure 4.3. Voltage waveform output of benders deflected 0.4 mm in tension.

Using the Instron 5969, an average force to deflect a bender beam 0.4 mm in tension was found to be 1.42 N with very low variance, just under the 1.49 N predicted by Equation 3.3. This may indicate that the assumptions used in developing that equation—including ignoring the effects of the epoxy and silicone rubber layers, assuming that the PZT layer runs the full length of the bender, and ignoring the effects of the beam's pre-curved state—are in fact acceptable. To test the beams in a condition matching the design of the ball screw and cam (BSC) SBEH design, a spring-loaded 3D printed test fixture shown in Figure 4.4 was used to pre-stress the beams 0.4 mm in tension (flattening them), then allow a total deflection of 1.4 mm from this starting point. This achieves 0.4 mm of deflection in tension and 1.0 mm deflection in compression relative to the beam's resting state.

The average peak-to-peak voltage output of benders in this test setup was found to be 49.5 V with a standard deviation of 2.7 V, which is close to the manufacturer's expected

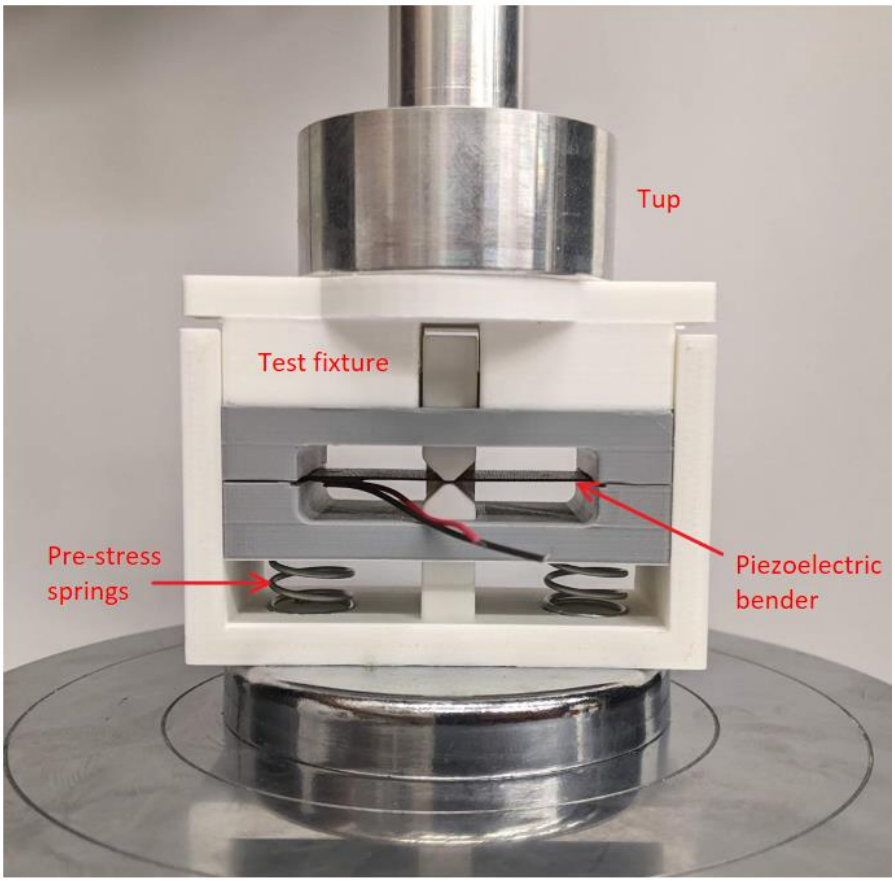

Figure 4.4. Pre-stressed bender test fixture. Red arrow indicates direction of force imparted on the strike pad by testing machine.

50-60 V but significantly below the 77.1 V predicted by Equation 3.8. The force necessary to deflect the beams in this manner (calculated as the difference between the force required to displace the fixture 1.4 mm with without a beam inserted) was found to be 3.37 N compared to the 5.23 N expected from Equation 3.3. This large difference could be due to the equation's assumptions versus the complex test condition: the equation assumes a normally flat beam is being deflected in one direction, while in reality a normally curved beam is being pre-stressed and then deflected through states of tension, neutrality, and compression.

The complete results of bender testing are summarized in Table 4.2. From this data, the necessary spring rate of the springs used to pre-stress the benders in the BSC design

Table 4.2. Average voltage output and deflection forces at given bender displacements. All figures are for normally functioning benders.

Displacement	*0.4 mm*	*1.4 mm*
Displacement in tension (mm)	0.4	0.4
Displacement in compression (mm)	0	1.0
Average V_{pp} *(V)*	19.5	49.5
Expected V_{pp} *(Equation 3.8)*	22.5	77.1
Standard deviation (V)	1.2	2.7
Force to deflect (N)	1.42	3.37
Expected force (Equation 3.3)	1.49	5.23

can be calculated simply as the number of benders to be pre-stressed multiplied by the force needed to deflect them the 0.4 mm in which they are pre-stressed: 1.42 N in this case. Thus, with eight benders per side, the springs must supply 11.36 N to fully pre-stress the benders.

These piezoelectric element tests reveal that voltages lower than those predicted by Equation 3.8 are to be expected in properly-functioning SBEH prototypes. The amount of force to deflect a bender 0.4 mm in tension is predicted well by Equation 3.3, so the magnitude of the periodic force peaks to be expected in the RP SBEH force-displacement curve should be close to the 7.63 N calculated from Equation 3.13. On the other hand, the magnitude of the force periodic peaks to be expected in the BSC SBEH should be significantly lower than those reported in Table 3.3 since the force needed to deflect a bender 1.4 mm from its pre-stressed state was measured at 3.37 N versus the calculated 5.23 N.

4.3 SBEH prototype testing

The protocol used in testing the SBEH prototypes is identical to that used in the testing of shoes: a triangle wave input force up to a peak of 600 N at a frequency of 1.0 Hz on the Instron 5969. The prototypes were set on a test platen while the tup imparted compression on the system through the SBEH's heel strike pad. The heel strike pad and tup are of equal diameter, simulating the interface between the heel and the harvester.

4.3.1 Ribbed plunger SBEH testing

The test setup for the RP SBEH is pictured in Figure 4.5. The bender leads are connected to a bread board so that discrepancies in the performance of individual beams outside of and within the harvester can be measured. To evaluate total power output performance, the benders are wired in parallel and connected to a load resistance.

Figure 4.6 shows a voltage output waveform from these tests. On average, it was found that the peak-to-peak voltage output of individual benders decreased by 13% when integrated inside of the harvester versus tested individually. This resulted in an average voltage output of 17.0 with a standard deviation of 1.2 V. This could be due to the beams being clamped more tightly at the ends, additional 33-mode effects from compression due to the beam-holding grate, or may simply demonstrate that the ribs of the plunger did not result in a full 0.4 mm deflection. This difference decreases the expected harvester power output by 20%. The voltage waveform also illustrates that the design achieves precisely 6.0x frequency up-conversion as expected, demonstrating the feasibility of the ribbed plunger mechanisms for this purpose.

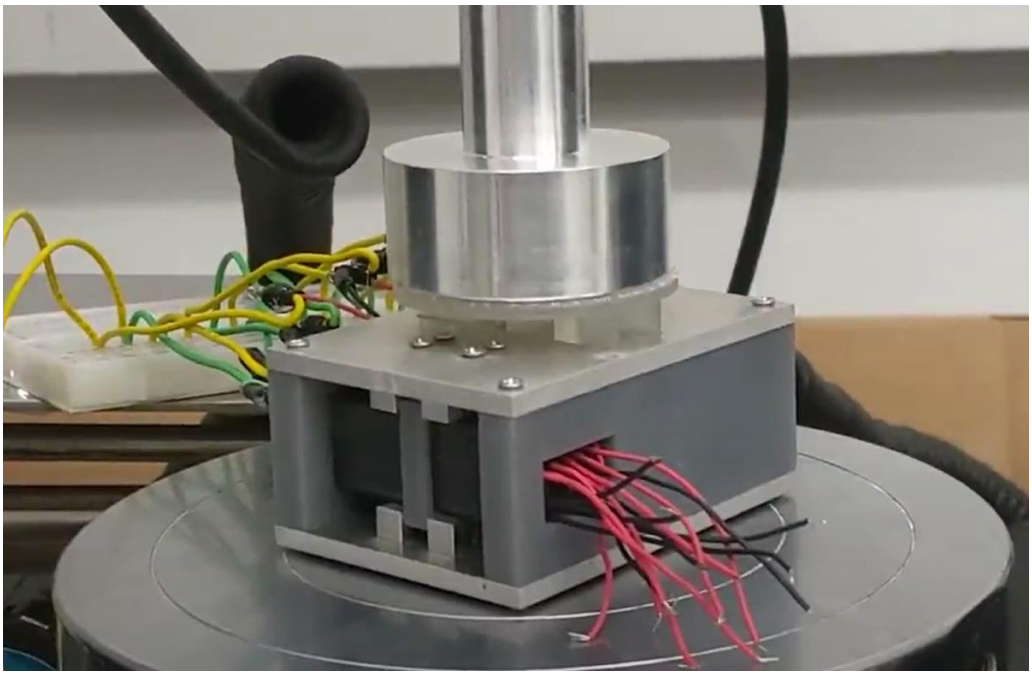

Figure 4.5. Test setup for ribbed plunger SBEH prototype.

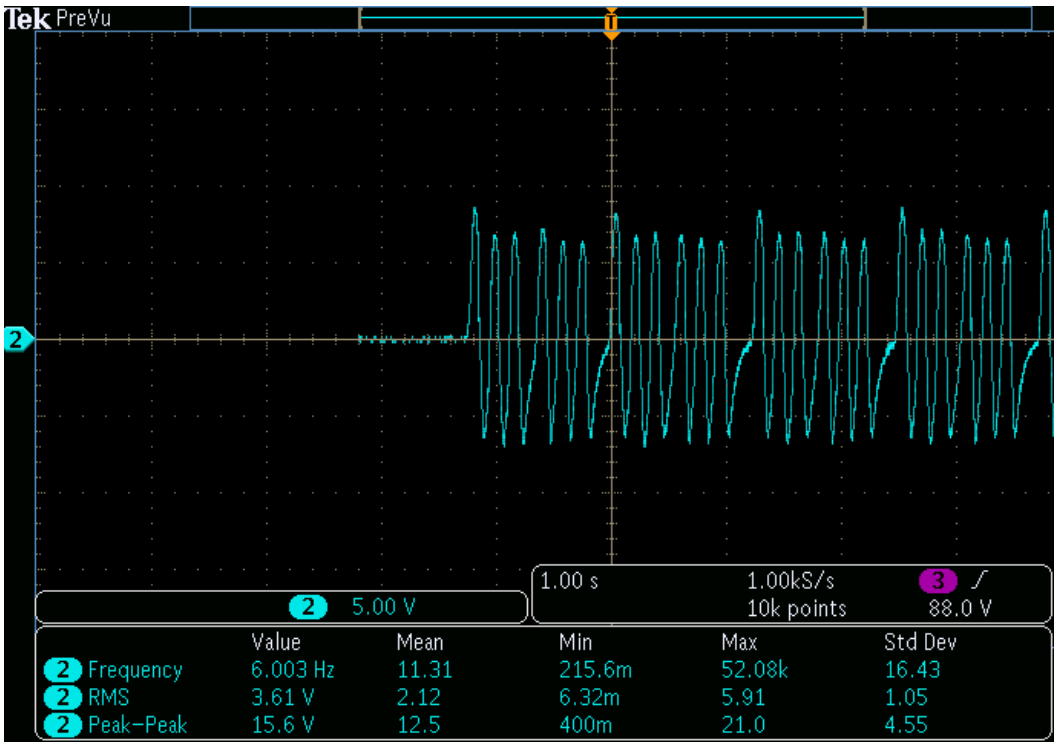

Figure 4.6. Voltage output waveform from ribbed plunger SBEH testing.

To test power output, the benders were wired in parallel and connected to a load resistance across which a voltage was measured. RMS power is the quantity of interest, which is calculated as

$$P_{rms} = \frac{V_{rms}^2}{R} \tag{4.1}$$

where V_{rms} is the RMS voltage across the load resistance R. The power-maximizing optimal load resistance (calculated according to Equation 3.10) at a 345 nF net capacitance across 8 benders and an input frequency of 6 Hz was calculated to be 7.7 kΩ. In practice, it was found that a load resistance of 8.0 kΩ yielded the greatest power output: 0.11 mW per row of benders, or 0.22 mW total. This is 55% of the 0.40 mW predicted by Equation 3.11; a

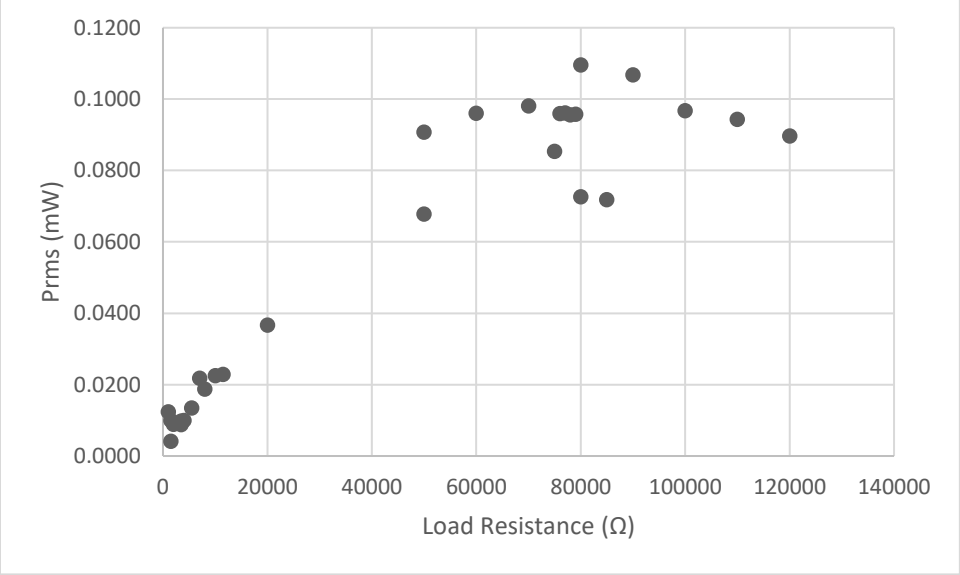

Figure 4.7. Ribbed plunger SBEH power output versus load resistance.

25% drop is accounted for in the difference between the voltage calculated using Equation 3.10 and that measured from individual beams, with the remaining 20% decrease due to the drop observed when the beams are integrated within the harvester versus tested individually. Figure 4.7 plots the power output versus load resistance for one row of eight benders. The obvious inconsistencies in this plot are due to the fact that the 3D printed plunger's ribs wear down very quickly during testing: the best power outputs are always recorded within the first 10 trials before the plunger must be replaced. A machined aluminum plunger was also tested and while it did not display the same rapid decay, it lacked the geometric precision to produce regular voltage waveforms. This is an obvious downfall of the RP design.

Figure 4.8 shows a force-displacement curve from RP SBEH testing in which the total spring rate of the return springs was 113.6 N/mm. The fluctuations in this curve are due to the periodic increase in force needed to overcome a rib in the plunger. The magnitude of this force and therefore of the fluctuation in the curve was estimated to be

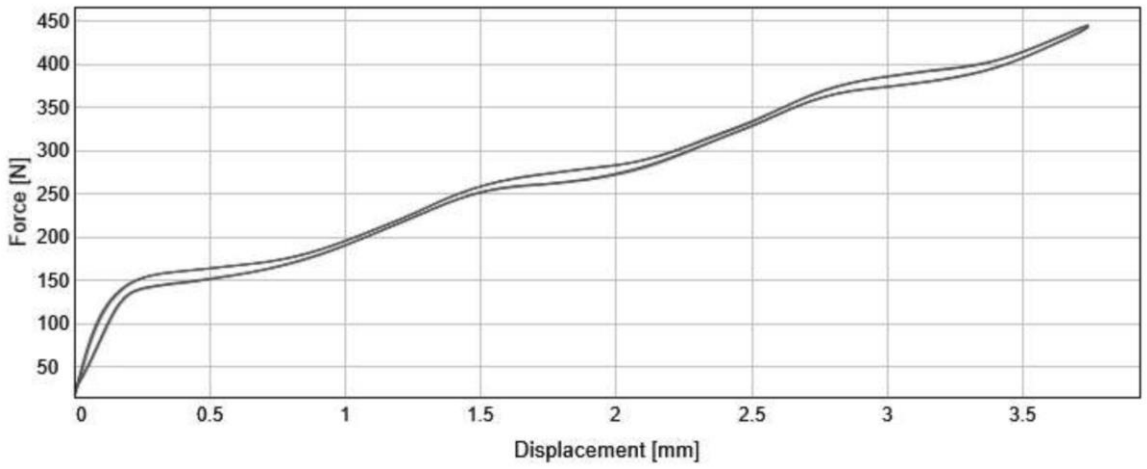

Figure 4.8. Force-displacement curve of ribbed plunger SBEH design.

7.6 N using Equation 3.13, which is significantly lower than the measured magnitude of 16.7 N. This could be due to frictional effects and a lack of complete rigidity in the system which were not accounted for in the energy balance used in Equation 3.13. However, the forces are on the same order of magnitude and therefore not a major concern.

The area enclosed by the hysteresis curve in Figure 4.8 represents the energy dissipated by the SBEH: 0.022 J, in this case. 1 Hz step frequency, this is equivalent to 22 mW power dissipation. Compared to the 0.22 mW electrical energy harvested, the RP SBEH is 1% efficient in converting mechanical energy dissipation to electrical energy. The prototype's energy input, returned, and ERP are 1.03 J, 1.01 J, and 97.8%, respectively. The energy input is within 7% of the Sketchers shoes' value when scaled by the ratio of displacements achieved in the shoe and the RP SBEH. This demonstrates that the overall stiffness of the two systems is closely matched. The very high ERP may indicate that the device would alter the user's gait, but could also imply that any increase in user metabolism because of the device's weight may be offset to some degree by the increase in energy retuned to the user with each step. Additionally, the non-harvester parts of the shoe will have a lower ERP, so the net ERP of the system will be below this 97.8%.

4.3.2 Ball screw and cam SBEH testing

The BSC SBEH represents the culmination of the goal of maximizing power output within a user burden first design perspective. The assembled device is shown in Figure 4.9. The test setup for the BSC SBEH is identical to that of the RP SBEH and is shown in Figure 4.10. The prototype was tested in three configurations: 1) a single-lobed cam without pre-

stress springs resulting in piezoelectric bender displacement of 1.0 mm, 2) a single lobed cam with pre-stress springs resulting in bender displacement of 1.4 mm, and 3) a three-lobed cam with pre-stress springs also achieving 1.4 mm bender displacement. All three conditions had an input displacement of 4 mm imparted on the heel strike pad. Further conditions were not tested due to part failures. Figures 4.11 and 4.12 show the voltage output waveforms across a load resistance of eight benders wired in parallel for tests conditions 1) and 3), respectively, while Figures 4.13 and 4.14 show the force-displacement profiles of these tests.

The implications of these results on mechanical behavior will be discussed first, focusing on underlying causes and potential changes, and the power output and energetic behavior results presented afterwards.

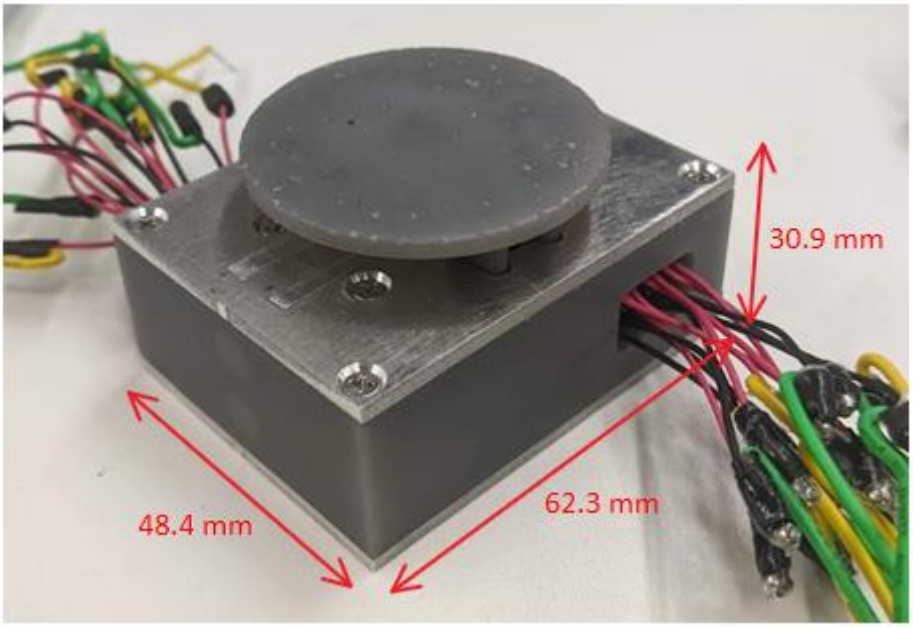

Figure 4.9. Assembled ball screw and cam SBEH prototype. In practical implementations, the piezoelectric elements would be wired in parallel such that only four total leads are necessary.

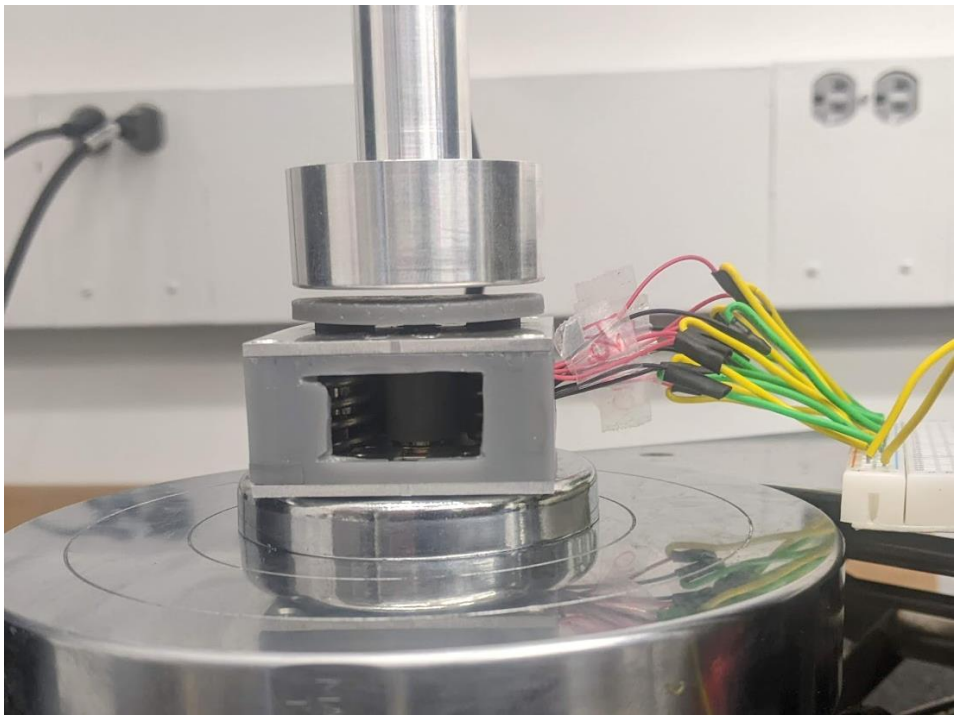

Figure 4.10. Test setup for ball screw and cam SBEH prototype.

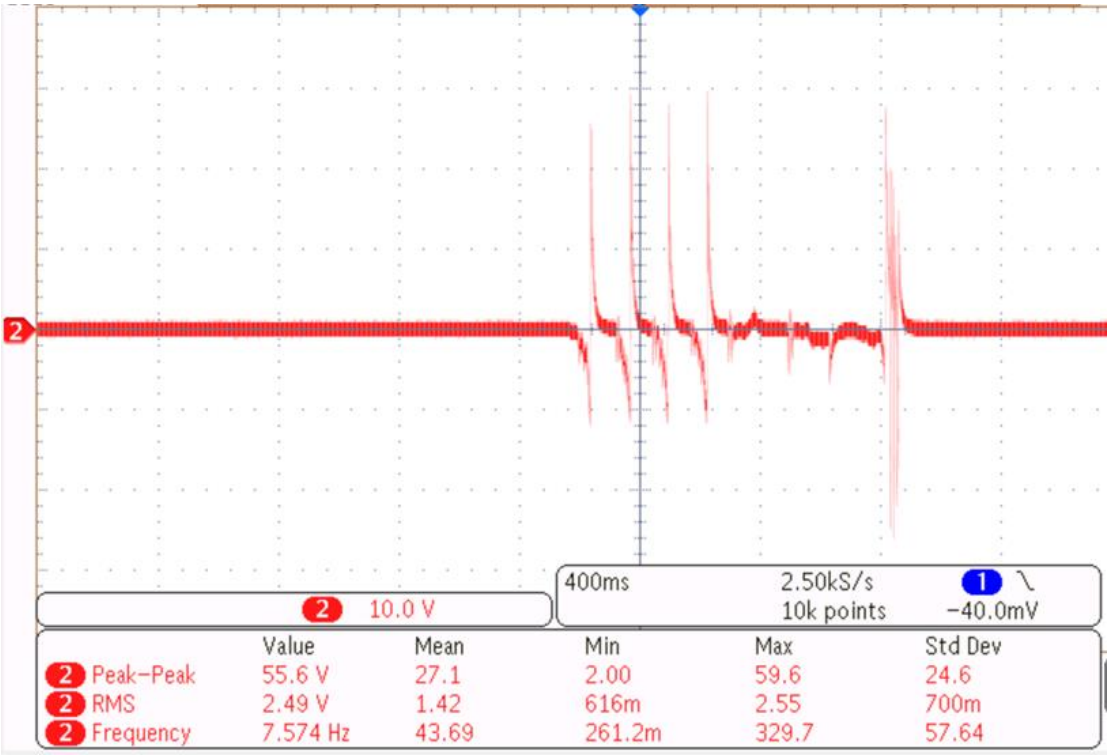

Figure 4.11.Voltage waveform output of BSC SBEH tested with a single-lobe cam and no pre-stress springs at an input displacement of 4 mm. The time scale is 400 ms/div.

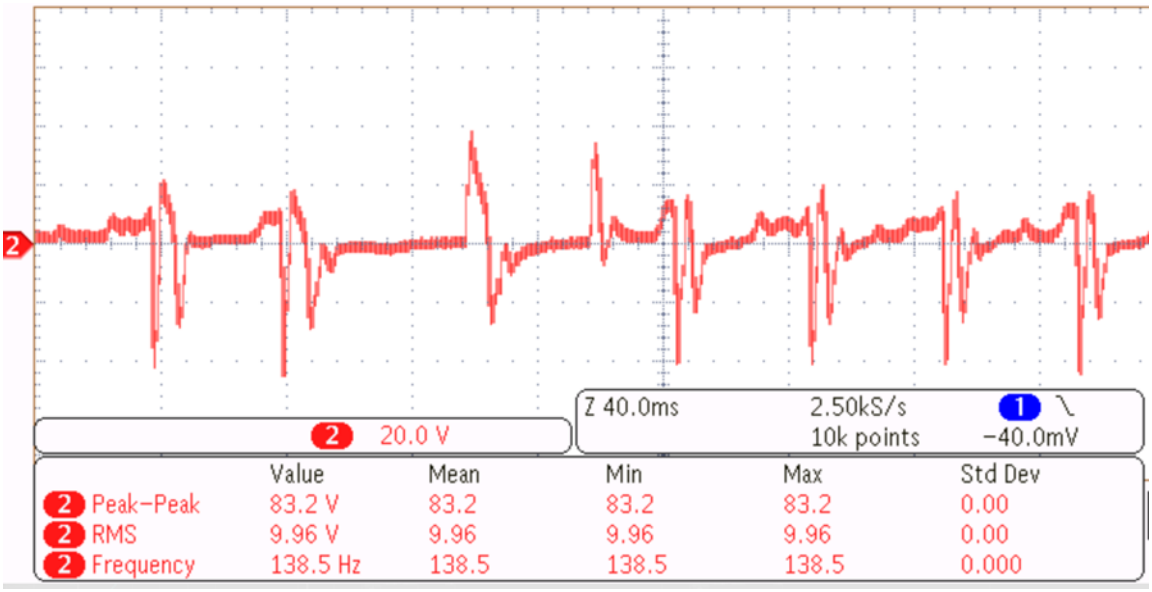

Figure 4.12. Voltage waveform output of BSC SBEH tested with a three-lobe cam and pre-stress springs at an input displacement of 4 mm. The time scale is 40 ms/div.

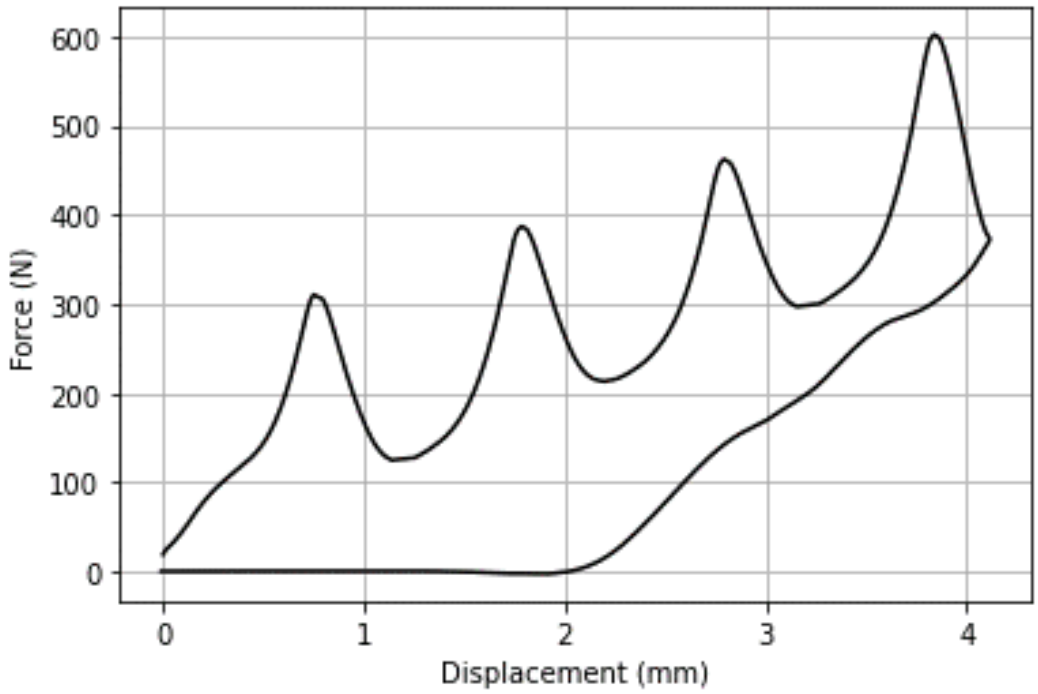

Figure 4.13. Force-displacement plot of the ball screw and cam SBEH tested with no pre-stress springs and a single-lobe cam at an input displacement of 4 mm.

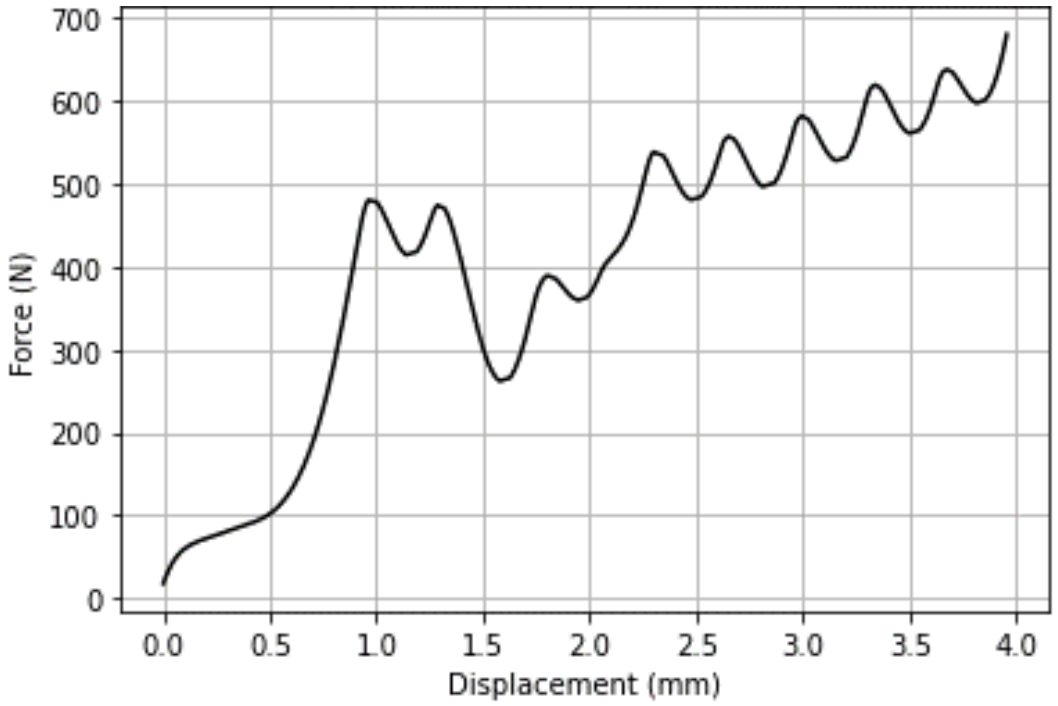

Figure 4.14. Force-displacement plot of the ball screw and cam SBEH tested with pre-stress springs and a three-lobe cam at an input displacement of 4 mm.

4.3.2.1 BSC SBEH mechanical behavior

In Figure 4.11, four clear voltage peaks corresponding to the four beam deflections expected during positive displacement (or compression) of the SBEH are observed. These peaks are followed by a pause before the return springs force the ball screw upwards rapidly in negative displacement, resulting in four voltage peaks grouped nearly imperceptibly close. The latter peaks, occurring at much higher frequency, have a peak-to-peak voltage magnitude 20% greater than the positive displacement peaks since the mechanical time constant on the return path is higher, and thus further above the RC time constant of the electrical load circuit.

The pause between the two sets of peaks is due to the fact that the system becomes stuck in its fully compressed state during testing and the cam must be physically nudged beyond this sticking point before the return springs can induce negative displacement, returning the ball screw and cam to their initial positions. This is why there are no periodic force peaks observed in the negative displacement portion of the force-displacement curves in Figures 4.13 and 4.14: the heel strike pad is stuck in a compressed state, so the Instron's tup moves back to its initial position mostly without a reaction force to measure. Figure 4.14 shows no return path line because the test was stopped due to part failure at this point.

This sticking behavior is unexpected given that the return springs are supplying a net force of 364 N at this point while the expected maximum input force necessary to drive the cam and deflect the beams is 174 N according to Equation 3.17. With a light nudge to start the process, however, the return springs face no issue in deflecting the beams the remaining four times as seen by the closeness of their voltage peaks. Since this occurs at lower levels of return spring compression, it is clear that the mechanism has ability to easily deflect the beams. It is hypothesized, then, that this sticking behavior is due to static frictional forces not accounted for in Equation 3.19, such as the clamping of the bender-holding grate between its roller pins, the cam-follower interface, and the ball bearings integrated in both of those locations. When the SBEH is actuated manually such that the duration of the compression phase is closer to 0.2 s (as it would during a heel-strike) than 0.5 s (as occurs in Instron testing) and is quickly released, the cam does not encounter this sticking behavior, likely because it remains in motion and thus static frictional forces do not come into play. With further testing the source of this sticking-inducing static friction

could likely be identified and the return spring mechanism restored to its as-designed behavior.

The shape of the voltage peaks in Figure 4.11 also suggests mechanical behavior that deviates from the expected. The deflection profile of the single-lobed cam is symmetric and smooth due to its geometry, shown in Figure 4.15. Thus, a voltage waveform output of a similar shape (though slightly narrower due to the optimal load resistance) is expected. What is observed instead is an asymmetrical voltage peak in which the voltage rises nearly vertically before declining from this peak in a smoother manner. This implies that the beams suddenly transition from a low to high deflection state. The cause of this can be observed during testing: instead of rotating at a constant angular velocity, the cam slows down to a near-pause as it attempts to deflect the beams which likely indicates that the ball screw is slightly twisting within its socket in the 3D printed heel strike pad, as illustrated in Figure 4.16. As seen in Figure 4.13, the force-displacement curve of the test is relatively smooth throughout, suggesting that the linear displacement imparted on the ball screw is being translated to rotational displacement somewhere in the design, just not at the ball nut

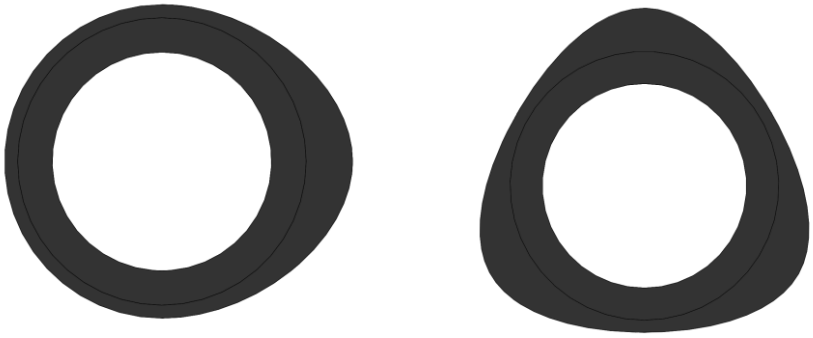

(a) (b)

Figure 4.15. Profile of the single-lobe (a) and three-lobe (b) cam used in the ball screw and cams SBEH.

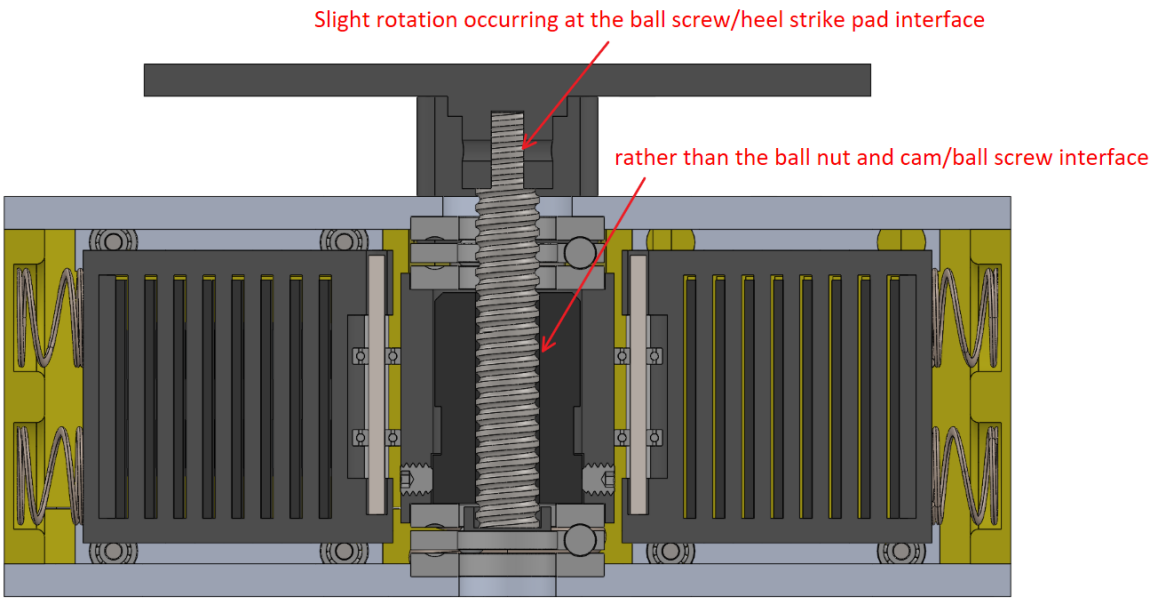

Figure 4.16. Illustrating unwanted twisting in the system which prevents cam from smoothly deflecting piezoelectric benders according to its profile.

and cam/ball screw interface. This hypothesis is given additional merit by the fact that this interface is the failure point of the SBEH under high-torque conditions. Once the torque necessary to deflect the beams and overcome this stuck position is reached, the cam experiences high angular acceleration and rapidly deflects then releases the cam follower, with the ball screw likely restored to its original position within the heel strike pad socket. This unexpected behavior could likely be eliminated by making the ball screw/heel strike pad interface more rigid with a machined insert or similar, which could also eliminate this interface as the device's failure point.

A potential third source of deviant mechanical behavior can be inferred from the voltages achieved during BSC SBEH testing. Figures 4.11 and 4.12 show peak-to-peak voltage outputs close to those expected from Equation 3.8 and far larger than those measured during piezoelectric bender element testing, as shown in Table 4.3 This difference could be due to one of two factors. The piezoelectric bender elements were

tested at 1 Hz in the text fixture, whereas these benders are being deflected at 8 Hz in the 1.0 mm displacement configuration (single-lobe cam), and 24 Hz in the 1.4 mm displacement configuration (three-lobed cam). In these conditions, the RC time constant of the system relative to its mechanical time constant may have changed significantly enough to produce the differences observed; in the expected and SBEH testing conditions, the optimal load resistance was used, while in the individual beam tests a load 2.8x the optimal was used. This hypothesis is given credence by the fact that greater voltages are observed in the three-lobe (higher frequency) tests than the single-lobe tests at the same displacement (1.4 mm) when the same voltages would be expected in the two conditions.

Alternatively, it could be that the cam lobe moves away from the follower so quickly after it deflects the benders that the follower is not always in contact with the cam. Once the restorative force of the benders causes this air gap to close, the follower would impact the cam and send an excitation with 33-mode and 31-mode components into each of the beams through their clamping grate. This could be the reason a higher voltage is observed in the SBEH than in individually tested beams. While there is no extra voltage

Table 4.3. Voltage expected from calculations versus measured during bender and ball screw and cam SBEH testing.

Displacement	Cam lobes	*Voltage expected Equation 3.8 (V)*	*Voltage measured in bender tests (V)*	*Voltage measured in SBEH (V)*
1.0 mm	*1*	54.7	39.3	55.6
1.4 mm	*1*	77.1	49.5	67.6
1.4 mm	*3*	77.1	49.5	83.2

peak in the single-lobe came waveform to indicate the presence of such behavior (though the peak may be in phase with existing peaks or valleys), the three-lobe cam's waveform shows two voltage peaks per bender deflection. This second peak could be evidence of this impacting behavior. However, the second voltage peak has a lower magnitude than the first. Thus, it likely contributes to increasing the RMS voltage but would not explain the increase in peak-to-peak voltage observed.

The force-displacement and voltage waveform plots of the three-lobe cam pose additional questions. The negative-displacement portion of the curve is missing due to part failure at that point. However, it can be seen that 9 distinct voltage and force peaks are observed instead of the 12 expected during the positive displacement phase. Without further testing, it is difficult to ascertain why nine peaks are observed rather than 12, though it is clear that the 'missing' peaks occur during the first 2 mm of displacement while the last 2 mm exhibit the expected up-conversion behavior.

A second interesting observation from Figure 4.14 is that the magnitude of the periodic force peaks caused by the cam deflecting the benders are far lower than expected. This decrease in force occurs without a decrease in voltage output (at an increase, in fact) is promising for the user burden aspects of this SBEH. Based on the results in Table 3.3, the force peaks in the single-lobe configuration are expected to be 240 N in magnitude, which aligns closely with the observed ~255 N on average. With the three-lobed cam, however, the expected 309 N magnitude is far greater than the ~80 N average force peak observed in testing. To the user, this means the force feedback form the harvester will feel far less irregular than the expected conditions would imply. It may also suggest that the magnitude of these peaks for an even higher-powered configuration such as a 5-lobe cam

could also be far lower than expected without sacrificing power output. In order to understand the mechanism underlying this fact, further testing and complete force-displacement curves would need to be examined.

4.3.2.2 BSC SBEH power output

The measured versus expected power output behavior of the BSC SBEH is summarized in Table 4.4. A clear conclusion which can be drawn from this data is that the relationship between peak-to-peak and RMS voltage (V_{rms} = 0.175 V_{pp}) determined experimentally from the voltage waveforms observed in RP SBEH and individual bender

Table 4.4. Measured versus expected voltage, optimal load resistance, and power output in ball screw and cam SBEH testing. The optimal load resistance is for one row of 8 benders in parallel.

Bender disp. (mm)	*1.0*	*1.0*	*1.4*	*1.4*	*1.4*	*1.4*
Measured or expected?	Measured	Expected	Measured	Expected	Measured	Expected
Cam lobes (#)	1	1	1	1	3	3
Input disp. (mm)	4	4	4	4	4	4
Frequency (Hz)	8	8	8	8	18	24
V_{pp} *(V)*	55.6	54.7	67.6	77.1	83.2	77.1
V_{rms} *(V)*	7.02	9.57	9.48	13.50	9.96	13.50
$R_{L,\,opt}$ *(kΩ)*	59	58	59	58	20	19
P_{rms} *(mW)*	1.67	3.31	3.05	6.59	9.92	19.77

testing does not hold in the BSC SBEH. Instead, the average ratio seen across the three experimental conditions is V_{rms} = 0.129 V_{pp}. Comparing the voltage output waveforms of the BSC SBEH (Figures 4.11 and 4.12, RP SBEH (Figure 4.6), and individually tested beams (Figure 4.3) illustrates why: the voltage waveform output of the RP SBEH is of higher frequency but roughly the same shape as the individually tested beams, while the BSC SBEH's waveform is of significantly different shape than the other two conditions. As discussed in the previous section, this is likely due to the differences between the as-designed and observed mechanical behavior in the BSC SBEH; remedying these issues may make the BSC SBEH's waveform closer to the expected condition and thus increase its RMS voltage. If changes are made which enable the follower to remain in contact with the cam and the angular velocity of the cam to remain constant, the voltage waveform output of the BSC SBEH would likely be smoother and its RMS voltage to peak-to-peak voltage ratio greater.

Across the three test conditions, the power output measured is 49.0% of the expected power output, aligning with the fact that measured RMS voltage values are 72% of that expected and the optimal load resistances are 3% greater than expected. With further testing, the causes of these discrepancies can be precisely identified, starting the investigation from the hypothesis already proposed.

In the highest-powered test condition (9.9 mW with three-lobe cam at 1.4 mm bender displacement), this BSC SBEH achieved a device power density of 0.106 mW/cm^3 given its volume of 93.2 cm^3. Per volume of piezoelectric material, it achieved a power density of 73.7 mW/cm^3.

4.3.2.3 BSC SBEH energetic behavior

Examining the energetic behavior of the BSC SBEH has two goals: to determine how closely it matches that of a normal shoe, and to determine how efficiently it converts observed mechanical energy dissipated to electrical energy. Unfortunately, only limited conclusions can be drawn on these two questions because of the limitations of the data gathered.

Figures 4.13 and 4.14 show the force-displacement curves of single-lobe and three-lobe cam conditions. However, as discussed in Section 4.3.2.1, the negative displacement portion of the data is missing due to the BSC SBEH becoming stuck in a compressed state. Thus, while the energy input can be calculated, the energy returned, dissipated, and ERP cannot.

The energy input in the one-lobe cam, 1.0 mm piezoelectric bender displacement condition is 1.02 J; for the three-lobe cam, 1.4 mm displacement condition it is 1.60 J. Scaling by their relative input displacements (4 mm in BSC SBEH, 8.32 mm in the Sketchers shoe), the energy input to the BSC SBEH is matched well to the shoe—1.3% lower and 55% higher, in these cases. The increased value of the latter is due in large part to the large force spike before the first two bender displacement peaks, which may be caused by the same sources of static friction that result in BSC SBEH becoming stuck in a compressed state. This bodes well for the SBEH's ability to draw no more power from the user than is expender during normal walking. However, to complete this picture, the amount of energy returned to the user would need to be known. These values could be obtained easily through further testing once the SBEH's sticking behavior is remedied.

With only the positive displacement portion of the force-displacement profiles known, the equivalent spring constant is the other energetic metric of the SBEH which can be calculated. An average value for the superimposed force peaks was added to the linearly increasing force-displacement profile of the return springs to estimate the spring constants: 125 N/mm in the single-lobe condition, and 163 N/mm in the three-lobe condition. Both of these values are significantly higher than the target 72 N/mm the Sketchers shoes exhibit, so to better match this parameter return springs of a lower spring rate can be substituted which should pose no new issues if the previously discussed static friction sticking problem can be resolved.

In summary, the preliminary data shows that the BSC SBEH meets the target power output of 10 mW, exceeds the target power density of 0.10 mW/cm^3, slightly overshoots the target weight of 100 g, and has the potential to match the behavior of normal shoes well. One of the most promising and surprising results which needs to be clarified is the far lower magnitude of force peaks observed in the three-lobe cam condition, seemingly without a corresponding drop in voltage and therefore power output. With further testing and the few design changes proposed, the author believes that both the power output and user comfort dimensions of the BSC SBEH can be significantly improved.

CHAPTER 5

DISCUSSION AND CONCLUSION

The results obtained in testing shoes, piezoelectric elements, and SBEH prototypes in Chapter 4 indicate that the SBEH developed in this work is promising for high-powered, low user burden implementations.

Testing multiple pairs of shoes illustrated that the 720 mJ of total energy available for harvesting per footstep and ERP of 70% arrived at in Section 2.2.2 are characteristic of shoe behavior and therefore good benchmarks for SBEH performance. The pair of Sketchers running shoes tested aligns especially well with these expectations.

The piezoelectric bender element tests indicate that the expected voltage output calculations of Section 3.4.1 are sound, though they overestimate the voltage output by 20%. The actual values measured are in line with the expectations of the bender's manufacturer. The experimental agreement with the analysis of Section 3.4.2 is more varied: at 0.4 mm displacement solely in tension, the maximum force to deflect the bender is calculated to within 5% of the measured value, whereas at 1.4 mm compression in which the pre-curved bender is pre-stressed and displaced through states of tension, neutrality, and compression, the measured force to deflect the beam is only 64% of the calculated figure. It is hypothesized that the difference is due to the latter condition's complex mechanics not being represented well with the assumptions of Equation 3.2.

The RP SBEH design achieved a power output of 0.22 mW at 1.0 Hz, or 55% of the expected 0.40 mW. This could be because of effects introduced by clamping the beam ends in the SBEH frame, 33-mode effects imparted by the bender-holding grate, or simply that the 3D printed ribbed plunger does not result in full deflection of the beams due to system dynamics or the geometry of the plunger's ribs. The RP SBEH was found to be 1% efficient in converting mechanical energy dissipated to electrical energy output. An obvious downfall of this design is that the ribs on the plunger being to wear down in less than 10 cycles, decreasing its power output. Therefore, it is not a feasible design for practical, long-term implementations.

The BSC SBEH design, on the other hand, is very promising for high-power, low-user burden applications. With a three-lobed cam imparting 1.4 mm deflection on the pre-stressed piezoelectric benders, 9.9 mW of power was measured across an optimal load resistance with a force input of 1.0 Hz. This results in a device power density of 0.106 mW/cm^3. Multiple mechanical issues were identified in its operation—including sticking-inducing static frictional behavior, unwanted motion between parts due low rigidity—which decrease the RMS voltage output and increase the energy input required. If remedied, the device's power output could be increased and its energetic input requirements decreased.

Because of the mentioned mechanical issues, a full force-displacement profile for this device could not be obtained, and so a full evaluation of its electromechanical conversion efficiency and comparison to the energetic behavior of shoes is impossible. However, the initial indications from energy input required (5% - 54% different from target shoe values) and equivalent spring rate (74% - 126% greater than target shoes values) of

the device indicate that the SBEH's behavior is in the same neighborhood as the shoe values. Simple changes such as replacing the return springs could easily bring these values more in line with the expected behavior. With further testing, energy returned, energy dissipation, and ERP metrics could be established to better understand the extent to which the BSC SBEH achieved its power output and user burden goals.

One noteworthy deviation from expected performance is that while the force peaks in the single-lobe cam's force-displacement profile are 6% greater than expected, the force peaks of the three-lobed cam are 74% *lower* than expected, seemingly without a decrease in power output. This difference would likely drastically improve the subjective user comfort of the SBEH and decrease the extent to which the device alters the user's gait. Additionally, it could imply that cams with 5+ lobes are in fact viable options, not limited by the large calculated reaction forces that would impart as initially thought. Perhaps such a cam would even decrease the force peaks further through an as-yet unknown mechanism such as the inertia stored in the ball screw-cam system.

Clearly, further testing is needed to fully characterize the BSC SBEH design. However, extrapolating the results obtained to other possible configurations yields tantalizing results. Given that the three-lobe cam deflecting pre-stressed benders 1.4 mm through a vertical input displacement of 4 mm produced 50% of the expected power output, configuring the SBEH with a five-lobe cam and an input displacement of 6 mm could yield 24.8 mW (0.250 mW/cm^3). If addressing the mechanical issues discussed increases the RMS voltage output, this configuration could move even closer to the 49.4 mW (0.500 mW/cm^3) theoretical maximum power output calculated.

The first steps in any future work on this SBEH would be to address the mechanical issues identified and quantify its energetic behavior though complete force-displacement testing. Beyond that, human trials should be conducted to evaluate the user burden associated with the device. Using an instrumented treadmill, peak ground reaction force (GRF), step frequency, and GRF force profiles could be compared between normal and SBEH-integrated shoe conditions. A well-designed subjective user comfort questionnaire could be used to quantify that dimension of user burden, while respirometry could be employed to quantify increases in user metabolic load. This would give a complete picture of the three aspects of user burden laid out in Section 2.3. Additionally, long-term cyclic testing within shoes and in a test fixture would need to be conducted to determine the robustness of this design.

This SBEH is a prototype designed for configurability; redesigning to minimize volume could help the device be better suited for practical applications. For example, machining the flange off of the ball nut could decrease device height by 5 mm and device volume by 16%.

In Chapter 2, the theoretical framework and benchmarks for designing a SBEH from a user burden-first perspective were developed. The BSC SBEH design has demonstrated that a SBEH developed in this manner can produce a result which aligns well with shoe behavior *and* achieves high power output. At 0.106 mW/cm^3 in its current configuration, the BSC SBEH achieves a power density only reached by 4 other practical PZT-based SBEH in the literature, with clear avenues for significant improvement. Additionally, this design is highly adaptable and can be configured to achieve a range of

vertical input displacements and equivalent stiffnesses to match the behavior of a wide range of shoes.

Going forward, the author hopes that the user burden first design perspective and benchmarks developed in the work can help others develop SBEH which will eventually become practical and unobtrusive enough to find widespread use.

REFERENCES

[1] V. S. Mallela, V. Ilankumaran and N. S. Rao, "Trends in cardiac pacemaker batteries," *Indian Pacing and Electrophysiology Journal*, vol. 4, no. 4, pp. 201-212, 2004.

[2] Inviza LLC, "Inviza Health," [Online]. Available: invizahealth.com/inviza®-health. [Accessed 8 4 2022].

[3] N. S. Shenck and J. A. Paradiso, "Energy scavenging with shoe-mounted piezoelectrics," *IEEE Micro*, vol. 21, no. 3, pp. 30-42, 2001.

[4] H. Akay, R. Xu, D. C. X. Han, T. H. Teo and S.-G. Kim, "Energy Harvesting Combat Boot for Satellite Positioning," *Micromachines*, vol. 9, no. 244, 2018.

[5] J. F. Antaki, G. E. Bertocci, E. C. Green, A. Nadeem, T. Rintoul, R. L. Kormos and B. P. Griffity, "A Gair-Powered Autologous Bettery Charging System for Artificial Organs," *American Society for Artificial Internal Organs*, vol. 41, no. 3, pp. 588-595, 1995.

[6] T. Starner and J. Paradiso, "Human Generated Power for Mobile Electronics," in *Low-Power Electronics Design*, Boca Raton, Florida: CRC Press, 2004, pp. 45(1-33).

[7] C. Sun, G. Shang and H. Wang, "On Piezoelectric Energy Harvesting from Human Motion," *Journal of Power and Energy Engineering*, vol. 7, pp. 155-164, 2019.

[8] J. L. González, A. Rubio and F. Moll, "Human Powered Piezoelectric Batteries to Supply Power to Wearable," *International Journal of the Society of Materials Engineering for Resources*, vol. 10, no. 1, pp. 34-40, 2002.

[9] E. M. Nia, N. A. W. A. Zawawi and B. S. M. Singh, "A review of walking energy harvesting using piezoelectric materials," *IOP Conference Series: Materials Science and Engineering*, vol. 291, 2017.

[10] R. Reimer and A. Shapiro, "Biomechanical energy harvesting from human motion: theory, state of the art, design guidelines, and future directions," *Journal of NeuroEngineering and Rehabilitation*, vol. 8, no. 22, 2011.

[11] E. Romero, R. O. Warrington and M. R. Neuman, "Energy scavenging sources for biomedical sensors," *Physiological Measurement*, vol. 30, no. 9, 2009.

[12] P. Niu, P. Chapman, R. Riemer and X. Zhang, "Evaluation of Motions and Actuation Methods for Biomechanical Energy Harvesting," in *2004 35th Annual IEEE Power Electronics Specialists Conference*, Aachen, Germany, 2004.

[13] J. L. González, A. Rubio and F. Moll, "Human Powered Piezoelectric Batteries to Supply Power to Wearable Electronic Devices," *International Journal of the Society of Materials Engineering for Resources*, vol. 10, no. 1, 2002.

[14] Q. Xu and L. M. Tam, Mechanical Design of Piezoelectric Energy Harvesters : Generating Electricity from Human Walking, Elsevier Science & Technology, 2021.

[15] J. Donelan, Q. Li, V. Naing, J. Hoffer, D. Weber and A. Kuo, "Biomechanical Energy Harvesting: Generating Electricity During Walking with Minimal User Effort," *Science,* vol. 318, no. 5864, pp. 807-810, 2008.

[16] T. von Büren, P. D. Mitcheson, T. C. Green, E. M. Yeatman, A. S. Holmes and G. Tröster, "Optimization of Inertial Micropower Generators," *IEEE SENSORS,* vol. 6, no. 1, pp. 28-38, 2006.

[17] L. Rome, L. Flynn, E. Goldman and T. Yoo, "Generating Electricity While Walking with Loads," *Science,* vol. 309, no. 5741, pp. 1725-1728, 2005.

[18] R. Alexander, "The Spring in Your Step," *New Scientist,* no. 30, pp. 42-44, 1987.

[19] E. Gonzalez and P. Corcoran, "Energy expenditure during ambulation," in *The Physiological Basis of Rehabilitation Medicine*, Boston, Massachussetts: Butterworth-Heinemann, 1994, pp. 413-446.

[20] M. R. Shorten, "The Energetics of Running and Running Shoes," *Journal of Biomechanics,* vol. 26, no. Suppl. 1, pp. 41-51, 1993.

[21] L. Xie and M. Cai, "An In-Shoe Harvester With Motion Magnification for Scavenging Energy," *IEEE/ASME Transactions on Mechatronics,* vol. 20, no. 6, pp. 3264-3268, 2015.

[22] J. Partridge and R. Bucknall, "An analysis of the energy flow and energy potential from human energy harvesting with a focus on walking," *Cogent Engineering,* vol. 3, no. 1, 2016.

[23] D. Winter, Biomechanics and Motor Control of Human Movement, vol. 3, Hoboken, New Jersey: John Wiley and Sons, 2005.

[24] D. W. Grieve and R. J. Gear, "The Relationships between Length of Stride, Step Frequency, Time of Swing and Speed of Walking for Children and Adults," *Ergonomics,* vol. 9, pp. 379-399, 2007.

[25] D. Morton, Human Locomotion and Body Form, Baltimore, Maryland: The William & Wilkins Co., 1952.

[26] D. Winter, A. Patla and S. Walt, "Biomechanical walking pattern changes in the fit and healthy elderly," *Physical Therapy,* vol. 70, no. 6, pp. 340-347, 1990.

[27] Y. Barak, R. C. Wagenaar and K. G. Holt, "Gait Characteristics of Elderly People With a History of Falls: A Dynamic Approach," *Physical Therapy,* vol. 86, no. 11, pp. 1501-1510, 2006.

[28] N. Elvin and A. Elvin, "Vibrational energy harvesting from human gait," *IEEE/ASME Transactions on Mechatronics,* vol. 18, no. 2, pp. 637-644, 2013.

[29] K. Ylli, D. Hoffman, A. Willman, P. F. B. Becker and Y. Manoli, "Energy harvesting from human motion: Exploiting swing and shock excitations," *Smart Materials and Structures,* vol. 24, no. 2, 2015.

[30] S. Boedicker, S. Hunter, P. Klesmith, T. Nearn and P. Spreen, "Mechanical Properties Testing of Running Shoes," *Journal of Undergraduate Materials Research,* vol. 4, 2010.

[31] Lift Your Game, "12 Best Tennis Shoes (2022) | For Men, Women, Nurses, And Flat Feet," [Online]. Available: https://liftyourgame.net/best-tennis-shoes/. [Accessed 10 March 2022].

[32] S. Robbins, E. Waked, P. Allard, J. McClaran and N. Krouglicof, "Foot Position Awareness in Younger and Older Men: The Influence of Footwear Sole Properties," *Journal of the American Geriatrics Society,* vol. 45, no. 1, pp. 61-66, 2015.

[33] A. Ramanathan, E. Parish, G. Arnold, T. Drew, W. Wang and R. Abboud, "The influence of shoe sole's varying thickness on lower limb muscle activity," *Foot and Ankle Surgery,* vol. 14, no. 4, pp. 218-223, 2011.

[34] J. Hannigan and C. D. Pollard, "Differences in running biomechanics between a maximal, traditional, and minimal running shoe," *Journal of Science and Medicine in Sport,* vol. 23, no. 1, pp. 15-19, 2020.

[35] B. Borja Muniz-Pardos, S. S. K. Angeloudis, F. M. Guppy, A. Bosch and Y. Pitsiladis, "Recent Improvements in Marathon Run Times Are Likely Technological, Not Physiological," *Sports Medicine,* vol. 51, pp. 371-378, 2021.

[36] G. K. Klute, J. S. Berge and A. D. Segal, "Heel-region properties of prosthetic feet and shoes," *Journal of Rehabilitation Research Development,* vol. 41, no. 4, pp. 535-546, 2004.

[37] *ASTM Standard Test Method for Impact Attenuation of Athletic Shoe Cushioning Systems and Materials,* ASTM F1976-13.

[38] N. Haghbin, "Shoe embedded air pump type piezoelectric power harvester," M.S. thesis, Dept. of Mech. Eng., Ryerson Univ., Toronto, 2011.

[39] L. Xie and M. Cai, "Increased piezoelectric energy harvesting from human footstep motion by using an amplification mechanism," *Applied Physics Letters,* vol. 105, no. 143901 , 2014.

[40] R. Browning, J. Modica, R. Kram and A. Goswami, "The effects of adding mass to the legs on the energetics and biomechanics of walking," *Medicine & Science in Sports & Exercise,* vol. 39, no. 3, pp. 515-525, 2007.

[41] R. Soule and R. Goldman, "Energy cost of loads carried on the head, hands, or feet," *Journal of Applied Physiology,* vol. 27, pp. 687-690, 1969.

[42] Centers for Disease Control and Prevention, "Body Measurements," 10 September 2021. [Online]. Available: https://www.cdc.gov/nchs/fastats/body-measurements.htm. [Accessed 2022 March 18].

[43] F. Qian, T.-B. Xu and L. Zuo, "Design, optimization, modeling and testing of a piezoelectric footwear energy harvester," *Energy Conversion and Management,* vol. 171, pp. 1352-1364, 2018.

[44] R. D. Kornbluh, R. Pelrine, Q. Pei, R. Keydt, S. Stanford, S. Oh and J. Eckerle, "Electroelastomers: applications of dielectric elastomer transducers for actuation, generation, and smart structures," in *SPIE 4698, Smart Structures and Materials*

2002: Industrial and Commercial Applications of Smart Structures Technologies, 2002.

[45] Q. H. Ly, A. Alaoui, S. Erlicher and L. Baly, "Towards a footwear design tool: Influence of shoe midsole properties and ground stiffness on the impact force during running," *Journal of Biomechanics*, vol. 43, pp. 310-317, 2009.

[46] Q. H. Ly, A. Alaoui and L. Baly, "Influence of shoe midsoles dynamic properties and ground stiffness on the impact force during running," *Computer Methods in Biomechanics and Biomedical Engineering*, vol. 11, no. 1, pp. 150-159, 2008.

[47] K. Gerritsen, A. van den Bogert and B. Nigg, "Direct dynamics simulation of the impact phase in heel-toe running," *Journal of Biomechanics*, vol. 28, no. 6, pp. 661-668, 1995.

[48] D. Caroll and M. Duffy, "Modelling, design, and testing of an electromagnetic power generator optimized for integration into shoes," in *Proceedings of the Institution of Mechanical Engineers, Part 1: Journal of Systems and Control Engineering*, 2012.

[49] D. Zhu and S. Beeby, "Kinetic Energy Harvesting," in *Energy harvesting systems*, Springer, 2010, pp. 1-78.

[50] N. Sezer and M. Koç, "A comprehensive review on the state-of-the-art of piezoelectric energy harvesting," *Nano Energy*, vol. 80, no. 105567, 2021.

[51] T. J. Kazmierski and L. Wang, "Modelling, Performance Optimisation and Automated Design of Mixed-Technology Energy Harvester Systems," in *Energy Harvesting Systems*, Springer, 2010, pp. 79-201.

[52] D. Briand, E. Yeatman and S. Roundy, Micro Energy Harvesting, Wiley, 2015.

[53] Boston Piezo-Optics Inc., "CERAMIC MATERIALS - GENERAL CHACRACTERISTICS," [Online]. Available: bostonpiezooptics.com/ceramic-materials-pzt. [Accessed 15 3 2022].

[54] MEMS and Nanotechnology Clearinghouse, "Material: Lead Zirconate Titanate (PZT)," [Online]. Available: memsnet.org/material/leadzirconatetitanatepzt/. [Accessed 15 3 2022].

[55] L. Xie, G. Wang, C. Y. F. Jiang and X. Zhao, "Properties and Applications of Flexible Poly(Vinylidene Fluoride)-Based Piezoelectric Materials," *Crystals*, vol. 11, no. 644, 2021.

[56] M. K. Sappait and S. Bhardra, "Piezoelectric Polymer and Paper Substrates: A Review," *Sensors*, vol. 18, no. 11, p. 3505.

[57] P. Cahill, R. O'Keeffe, n. Jackson, A. Mathewson and V. Pakrashi, "Structural Health Monitoring of Reinforced Concrete Beam Using Piezoelectric Energy Harvesting System," in *7th European Workshop on Structural Health Monitoring*, Nantes, 2014.

[58] D. Isarakorn, A. Sambri, P. Janphuang, D. Briand, S. Gariglio, J.-M. Mriscone, J. W. Reiner and C. H. d. R. N. F. Ahn, "Epitaxial piezoelectric MEMS on silicon," *Journal of Micromechanics and Microengineering*, vol. 20, no. 5, 2010.

[59] A. M. Flynn and S. R. Sanders, "Fundamental limits on energy transfer and circuit considerations for piezoelectric transformers," *IEEE Transactions on Power Electronics,* vol. 17, no. 1, pp. 8-14, 2002.

[60] S. Priya, "Advances in energy harvesting using low profile piezoelectric transducers," *Journal of Electroceramics,* vol. 19, pp. 167-184, 2007.

[61] Piezo.com, "Materials Technical Data (Typical Values)," [Online]. Available: info.piezo.com/hubfs/Data-Sheets/piezo-material-properties-data-sheet-20201112.pdf. [Accessed 16 3 2022].

[62] H. S. Kim, J.-H. Kim and J. Kim, "A review of piezoelectric energy harvesting based on vibration," *International Journal of Precision Engineering and Manufacturing,* vol. 12, pp. 1129-1141, 2011.

[63] S. B. Lang and S. Muensit, "Review of some lesser-known applications of piezoelectric and pyroelectric polymers," *Applied Physics A,* vol. 85, pp. 125-134, 2006.

[64] H. Liu, J. Zhong and C. Lee, "A comprehensive review on piezoelectric energy harvesting technology: Materials, mechanisms, and applications," *Applied Physics Reviews,* vol. 5, no. 041306, 2018.

[65] B. S. Lee, S. C. Lin, W. J. Wu, X. Y. Wang, P. Z. Chang and C. K. Lee, "Piezoelectric MEMS generators fabricated with an aerosol deposition PZT thin film," *Journal of Micromechanics and Microengineering,* vol. 19, no. 065014, 2009.

[66] L. Mateu and F. Moll, "Optimum Piezoelectric Bending Beam Structures for Energy Harvesting using Shoe Inserts," *Journal fo Intelligent Material Systems and Structures,* vol. 16, pp. 835-845, 2005.

[67] S. B. Kim, H. Park, S.-H. Kim, H. C. Wilke, J.-H. Park and D.-J. Kim, "Comparison of MEMS PZT Cantilevers Based on d31 and d33 Modes for Vibration Energy Harvesting," *Journal of Microelectromechanical Systems,* vol. 22, no. 1, pp. 26-33, 2013.

[68] S. Roundy, "On the Effectiveness of Vibration-based Energy Harvesting," *Journal of Intelligent Material Systems and Structures,* vol. 16, 2006.

[69] M. Leinonen, J. Juuti, H. Jantunen and J. Palosaari, "Energy Harvesting with a Bimorph Type Piezoelectric Diaphragm Multilayer Structure and Mechanically Induced Pre-stress," *Energy Technology,* vol. 4, pp. 620-624, 2016.

[70] C. A. Howells, "Piezoelectric energy harvesting," *Energy Conversion and Management,* vol. 50, pp. 1847-1850, 2009.

[71] F. Qian, T.-B. Xu and L. Zuo, "Piezoelectric energy harvesting from human walking using a two-stage amplification mechanism," *Energy,* vol. 189, no. 116140, 2019.

[72] A. C. Turkmen and C. Calik, "Energy harvesting with the piezoelectric material integrated shoe," *Energy,* vol. 150, pp. 556-564, 2018.

[73] Y. Kuang, A. Daniels and M. Zhu, "A sandwiched piezoelectric transducer with flex end-caps for energy harvesting in large force environments," *Journal of Physics D; Applied Physics,* vol. 50, no. 345501, 2017.

[74] L. Luo, D. Lui, M. Zhu and J. Ye, "Metamodel-assisted design optimization of piezoelectric flex transducer for maximal bio-kinetic energy conversion," *Journal of Intelligent Material Systems and Structures,* vol. 28, no. 18, pp. 2528-2538, 2017.

[75] Z. Yin, S. Gao, L. Jin, S. Guo, Q. Wu and Z. Li, "A shoe-mounted frequency up-converted piezoelectric energy harvester," *Sensors and Actuators A: Physical,* vol. 318, no. 112530, 2021.

[76] L. Moro and D. Benasciutti, "Harvested power and sensitivity analysis of vibrating shoe-mounted piezoelectric cantilevers," *Smart Materials and Structures,* vol. 19, no. 115011, 2010.

[77] T. von Buren, P. Lukowicz and G. Troster, "Kinetic energy powered computing - an experimental feasibility study," in *Seventh IEEE International Symposium on Wearable Computers*, White Plains, 2003.

[78] T. von Buren, R. D. Mitcheson, T. C. Green, E. M. Yeatman, A. S. Holmes and G. Troster, "Optimization of inertial micropower Generators for human walking motion," *IEEE Sensors,* vol. 6, no. 1, pp. 28-38, 2006.

[79] K. Fan, Z. Liu, H. Liu, L. Wang, Y. Zhu and B. Yu, "Scavenging energy from human walking through a shoe-mounted piezoelectric energy harvester," *Applied Physics Letters,* vol. 110, no. 143902, 2017.

[80] D. Han and V. Kaajakari, "Microstructured Poluymer for Shoe Power Generation," in *IEEE Solid-State Sensors, Actuators and Microsystems Conference, Transducers*, Denver, 2009.

[81] J. Kymissis, C. Kendall, J. Paradiso and N. Gershenfeld, "Parasitic Power Harvesting in Shoes," in *Digest of Papers. Second International Symposium on Wearable Computers*, Pittsburgh, 1998.

[82] J. Zhao and Z. You, "A Shoe-Embedded Piezoelectric Energy Harvester for," *Sensors,* vol. 14, pp. 12497-12510, 2014.

[83] Y. Han, Y. Cao, J. Zhao, Y. Yin, L. Ye, X. Wang and Z. You, "A Self-Powered Insole for Human Motion Recognition," *Sensors,* vol. 16, no. 1502, 2016.

[84] D. Fourie, "Shoe-Mounted PVDF Piezoelectric Transducer for Energy Harvesting," *MITUG Research Journal,* vol. 19, pp. 66-70, 2010.

[85] W.-S. Jung, M.-J. Lee, M.-G. Kang, S.-J. Yoon, S.-H. Baek and C.-Y. Kang, "Powerful curved piezoelectric generator for wearable applications," *Nano Energy,* vol. 15, pp. 174-181, 2015.

[86] k. Ishida, T. C. Huang, K. Honda, Y. Shinozuka, H. Fuketa, T. Yokota, U. Zschieschang, H. Klauk, G. Tortissier, T. Sekitani, H. Toshiyoshi, M. Takamiya, T. Someya and T. Sakurai, "Insole pedometer with piezoelectric energy harvester and 2 V organic circuits," *IEEE Journal of Solid State Circuits,* vol. 48, no. 1, pp. 255-264, 2013.

[87] J. Y. Hayashida, "Unobtrusive Integration of Magnetic Generator Systems into Common Footwear," M.S. thesis, Dept. of Mech. Eng., Massachussets Institute of Technology, Cambridge, 2000.

[88] A. M. Purwadi, M. K. A. Ahamed Khan and I. Elamvazuthi, "Development of Biomechanical Energy Harvesting Device using Heel Strike," *Procedia Computer Science,* vol. 76, pp. 270-275, 2015.

[89] Y. Liu, W. Fu, W. Li and M. Sun, "Design and Analysis of a Shoe-Embeded Power Harvester Based on Magnetic Gear," *IEEE Transactions on Magnetics,* vol. 52, no. 7, 2016.

[90] P. Niu and P. Chapman, "Design and Performance of Linear Biomechanical Energy Conversion Devices," in *37th IEEE Power Electronics Specialists Conference,* Jeju, 2006.

[91] K. Ylli, D. Hoffmann, A. Willmann, P. Becker, B. Folkmer and Y. Manoli, "Energy harvesting from human motion: exploiting swing and shock excitations," *Smart Materials and Structures,* vol. 24, no. 025029, p. 12, 2015.

[92] S. Wu, P. C. K. Luk, C. Li, X. Zhao, Z. Jiao and Y. Shang, "An electromagnetic wearable 3-DoF resonance human body motion energy harvester using ferrofluid as a lubricant," *Applied Energy,* vol. 197, pp. 364-374, 2017.

[93] H. Fu, R. Xu, K. Seto, E. M. Yeatman and S. G. Kim, "Energy Harvesting from Human Motion Using Footstep-Induced Airflow," *Journal of Physics: Conference Series,* vol. 660, no. 012060, 2015.

[94] M. M. Rahman, R. Atkin and H. Kim, "Optimization of a microfluidic based electromagnetic energy harvester for shoe insoles," in *Power MEMS Journal of Physics: Conference Series 660,* 2015.

[95] R. Kornbluh, R. Pelrine, Q. Pei, R. Heydt, S. Stanford, S. Oh and J. Eckerle, "Electroelastomers: applications of dielectric elastomer transducers for acutation, generation, and smart structures," in *SPIE's 9th Annual International Symposium on Smart Structures and,* San Diego, 2002.

[96] R. D. Kornbluh, R. Pelrine, H. Prahlad, A. Wong-Foy, B. McCoy, S. Kim, J. Eckerle and T. Low, "From boots to buoys: promises and challenges of dielectric elastomer energy harvesting," in *Proceedings of SPIE,* San Diago, 2011.

[97] [Online].

[98] T. G. McKay, S. Rosset, I. A. Anderson and H. Shea, "Dielectric elastomer generators that stack up," *Smart Materials and Structures,* vol. 24, no. 1, 2014.

[99] Bimitech Inc., "Python Advanced Piezo Bending Actuator," [Online]. Available: bimitech.com/python/. [Accessed 4 April 2022].

[100] R. W. Schwartz, L. E. Cross and Q.-M. Wang, "Estimation of the Effective d31 Coefficients of the Piezoelectric Layer in Rainbow Actuators," *Journal of the American Ceramic Society,* vol. 84, no. 11, pp. 2563-2569, 2001.

[101] J. Paalosaari, M. Leinonen, J. Juuti, J. Hannu and H. Jantunen, "Piezoelectric circular diaphragm with mechanically induced pre-stress for energy harvesting," *Smart Materials and Structures,* vol. 23, no. 085025, 2014.

[102] THK Co., "Features of the Ball Screw," [Online]. Available: https://tech.thk.com/en/products/pdf/en_b15_006.pdf. [Accessed 8 April 2022].

[103] Misumi Corporation, "Technical Calculations: Selection of Ball Screws 1," [Online]. Available: https://us.misumi-ec.com/pdf/tech/mech/p2799.pdf. [Accessed 8 April 2022].

[104] U. Vats, "Dynamic Analysis of Engine Valvetrain and its Effects on Camshaft," *International Journal of Science and Research*, vol. 2, no. 6, pp. 225-229, 2013.

[105] Q. Hung Ly, A. Alaoui, S. Erlicher and L. Baly, "Towards a footwear design tool: Influence of shoe midsole properties and ground stiffness on the impack force during running," *Journal of Biomechanics*, vol. 43, no. 2, pp. 310-317, 2010.

[106] A. Jain, P. K. J., A. K. Sharma, A. Jain and R. P.M, "Dielectric and piezoelectric properties of PVDF/PZT composites: A review," *Polymer Engineering and Science*, vol. 55, no. 7, 2015.

[107] J. Song, G. Zhao, B. Li and J. Wang, "Design optimization of PVDF-based piezoelectric energy harvesters," *Heliyon*, vol. 3, 2017.

[108] A. M. Vinogradov, V. H. Schmidt, G. F. Tuthill and G. W. Bohannan, "Damping and electromechanical energy losses in the piezoelectric polymer PVDF," *Mechanics of Materials* , vol. 36, pp. 1007-1016, 2004.

[109] H. Shekhani, E. Gurdal, S. Ural and K. Uchino, "Analysis of High Power Behavior in Piezoelectric Ceramics from a Mechanical Energy Density Perspective," *arXiv*, 2016.

[110] J. Zou and G. Gu, "Modeling the Viscoelastic Hysteresis of Dielectric Elastomer Actuators with a Modified Rate-Dependent Prandtl–Ishlinskii Model," *Polymers*, vol. 10, no. 2, p. 525, 2018.